Influence of Molecular Conditioning Films on Microbial Colonization of Synthetic Membranes Determined by Internal Reflection Spectrometry

National Water Research Institute
Membrane and Research Development

NWRI Project No. MRDP 699-508-95

01 May 1995 through 30 April 1998

Kenneth P. Ishida
Richard M. Bold and
Harry F. Ridgway

Biotechnology Research Department
Orange County Water District
P. O. Box 8300
10500 Ellis Ave.
Fountain Valley, CA 92728-8300

Abstract

Under normal operating conditions, synthetic polymer separations membranes become fouled with suspended solids, dissolved organic and inorganic macromolecules and microorganisms. The result is a drop in membrane process efficiency, i.e., reduced water flux and salt rejection and increased differential pressure. These effects increase the costs of operation and maintenance and reduce membrane lifetime. Thus, control of membrane fouling is of great interest to the separations industry. In order to properly and effectively implement measures to alleviate or minimize fouling, a greater understanding of molecular interactions at the membrane surface is desired. This includes interactions between the membrane surface and dissolved organic macromolecules, chemical surfactants and extracellular polymeric substances of biological origin.

Adsorption phenomena at an aqueous-polymer interface were investigated by attenuated total reflection Fourier transform infrared (ATR/FT-IR) spectrometry. At first, adsorption of select organic compounds on bare germanium (Ge) was investigated to obtain reference spectra and identify unique infrared vibrational structure. Twelve (12) compounds were selected: ethylenediaminetetraacetic acid (EDTA), hexylglucopyranoside, deconoyl-N-methylglucamide (MEGA 10), polyoxyethylene(10)dodecyl ether (Genapol C-100), bovine serum albumin (BSA), dextran, alginic acid, gum arabic, dodecylbenzenesulfonic acid (DBSA), n-hexadecyl-N, N-dimethyl-3-ammoniuo-1-propanesulfate (Zwittergent 3-16), polyethylene glycol-p-isooctylphenyl ether (Triton X-100) and benzalkonium chloride. Later, thin films (1500-2000 Å) of cellulose acetate (CA) were cast on Ge and zinc selenide (ZnSe) internal reflection elements (IREs). Adsorption of albumin, alginic acid, gum arabic, dodecyl-benzenesulfonic acid, Triton X-100, benzalkonium chloride and Zwittergent 3-16 on CA were investigated. The CA film was rinsed with buffer, leaving a stable adsorbed organic layer. Subsequent application of DBSA resulted in the selective removal of adsorbed proteins and polysaccharides from the surface of the CA thin films. The DBSA treatment had little effect on the adsorbed film of benzalkonium chloride, as a very stable hemimicelle structure is believed to form on the CA surface.

Adsorption of dissolved organic material on CA from reverse osmosis feedwater at Water Factory 21 was investigated. The ATR/FT-IR spectrometric technique was not sensitive enough to detect any adsorbed organic material on the surface of the CA thin film. Adsorption of natural organic materials on CA from colored well water was also investigated. A small quantity of organic macromolecules was detected at the aqueous-polymer interface. Preliminary results suggest that this chemical species is aliphatic and aromatic in origin. Bubble contact angle measurements indicated a decrease in the surface hydrophobicity after 22-hr exposure to the colored well water.

Pretreatment of a CA film with the surfactant Zwittergent 3-16 resulted in a 3-fold reduction in the number of adherent *Mycobacterium* cells during the initial stage of bacterial attachment. Polysaccharide and material tentatively identified as protein were detected at the aqueous-polymer interface. A hemimicelle structure of Zwittergent 3-16 formed on the membrane surface, which actively prevented *Mycobacterium* cells from adhering to the CA film.

Efforts are currently under way to improve the detection limit of the ATR/FT-IR spectrometric technique. The recommended changes are to (1) reduce the CA film thickness

(from 1500 Å to 750 Å) cast on the IRE, thereby increasing the electric field intensity at the aqueous-polymer interface and (2) switch from a 3-mm thick ZnSe IRE to a 2-mm thick IRE, thereby increasing the number of internal reflections.

A system was developed to visualize bacterial cells attached to the same CA surface on which IR data is sampled. An ATR flow cell was designed with a window to accommodate a 40X microscope objective. The fluorescence microscope was designed and assembled in-house and will be mounted horizontal to the face of the ATR flow cell. This system will enable real-time in situ measurements of IR (molecular) data and fluorescent (visual) microscopic data from organic macromolecules and bacteria adsorbed or attached to CA thin films.

Table of Contents

Table of Contents (continued)

Table of Contents (continued)

Figures, Equations and Tables

Figures, Equations and Tables (continued)

Figures, Equations and Tables (continued)

Acknowledgments

This project was funded in part by the National Water Research Institute (Project No. MRDP 699-508-95), the U. S. Bureau of Reclamation and Orange County Water District. We thank Thomas Cormack for providing the contact angle measurements. Special thanks go to Bob Riley and Shui Wai Lin of Separation Systems Technology, San Diego, CA for providing all the assistance and expertise in casting thin films of cellulose acetate on the internal reflection elements.

Section 1.

Introduction

Fouling of synthetic polymer membranes used in reverse osmosis (RO), nanofiltration (NF), ultrafiltration (UF) and microfiltration (MF) applications is a major concern to the separations industry. Particles in the form of suspended solids, partially soluble inorganics, dissolved organic macromolecules and microbial cells deposit on the surface of these membranes, reducing process efficiency (i.e., reduced water flux and salt rejection) (Figure 1.1). This leads directly to an increase in operating costs by virtue of higher operating pressures, down time for chemical and physical cleaning and reduced membrane lifetime. Feedwater consisting of secondary and tertiary reclaimed wastewater often contains significant levels of dissolved organic macromolecules and microorganisms.[1,2,3] Bacteria normally transported in the feedwater have been shown to undergo rapid and stable attachment to membrane surfaces.[4,5,6] Once firmly attached, the sessile microorganisms grow and multiply, assimilating trace organic and inorganic nutrients dissolved in the bulk aqueous phase. During this process, the adherent bacteria typically produce copious amounts of extracellular polymeric substances (EPS), usually amphoteric heteropolysaccharides, that entrap and protect the cells in a gelatinous matrix.[7,8,9,10] The bacteria continue to grow and multiply, eventually forming a biofilm that covers the entire surface of the membrane. This series of events, termed "biological fouling," may be defined as the attachment and growth of microorganisms at an aqueous-solid interface resulting in a detectable effect on system performance.[11] These biofilms typically range in thickness from a cell monolayer to several tens of micrometers.

Microorganisms likely attach to a surface unlike the clean membrane, but adhere to a surface already fouled with low molecular weight dissolved organics, inorganics and suspended solids. These "conditioning films" precede bacterial adhesion by nature of the smaller size of the dissolved molecules and suspended solids. Though present at relatively low concentrations, the presence of these macromolecules is routinely reported.[1] The precise nature of the adsorbed macromolecules is generally unknown, although some common IR functional groups associated with proteins and proteoglycans have been detected in waters associated with heat exchange equipment.[12] In reclaimed wastewater and groundwater, nonvolatile dissolved organic carbon constitutes the majority of the total organic carbon.[1,3] Humic and fulvic acids are typically associated with colored water.[13,14] In any event, these macromolecules mask the original surface properties (e.g., electrostatic charge or hydrophobicity) which seem to influence both the rate[15] and extent of adhesion of cells.[16,17,18] Nonspecific adhesion to surfaces occurs by a variety of mechanisms. These non-covalent intermolecular forces include electrostatic, polar, nonpolar, hydrogen bonding and hydrophobic interactions. Attachment is known to be influenced by factors such as surface charge.[19,20] Adsorbed proteins have been shown to reduce subsequent bacterial attachment.[21,22,23] However, promotion of bacterial attachment by adsorbed proteins has also been shown.[24] The extent to which adsorbed macromolecules mask or alter the surface chemistry of a polymer separations membrane is still not clear. Understanding the nature of

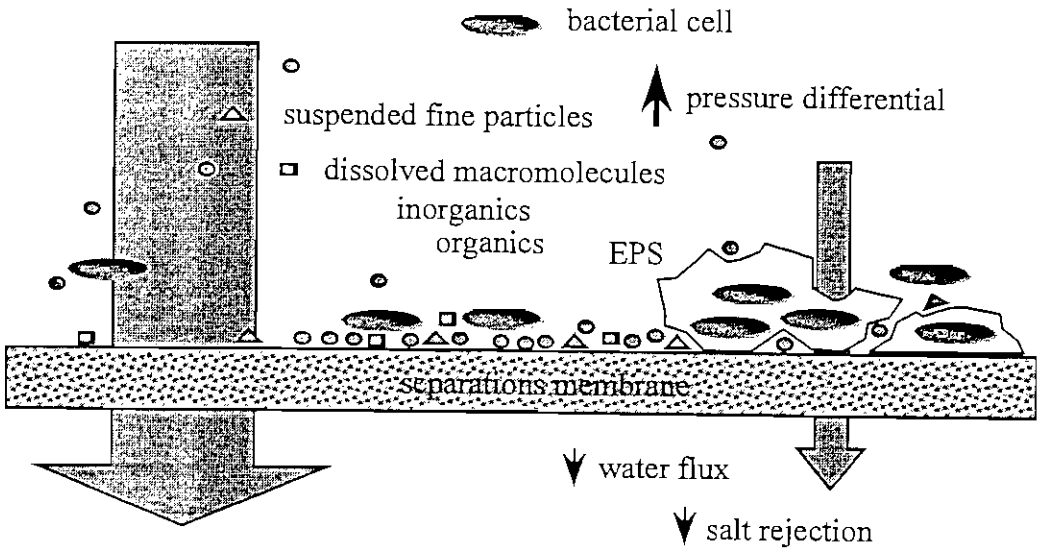

Figure 1.1 Diagram of separations membrane illustrating colloidal and biological fouling and some of the effects on membrane properties.

the chemical interactions and the dynamics of macromolecular adsorption at the aqueous-polymer interface is key to understanding membrane fouling. Thus, work has been directed toward understanding how organic materials interact with polymer surfaces and how adsorbed organics influence bacterial attachment.

Sensitive surface analytical techniques for in situ analysis of chemical components of adsorbed conditioning films have only recently become available. Hence the dynamics and physicochemical nature of the molecular conditioning films and how they might influence initial bacterial attachment and growth are not well understood. One very sensitive method for exploring organic conditioning films and bacterial attachment is attenuated total reflection Fourier transform infrared (ATR/FT-IR) spectrometry. Recently, ATR/FT-IR spectrometry has been used to study the in vitro formation of microbial biofilms on germanium (Ge) internal reflection elements (IREs)[24,25] and thin copper films.[26,27] ATR/FT-IR spectrometry has also been used to monitor the effect of a chemical biocide on biofilm growth[24] and biocide penetration into a mature biofilm.[28] A surface-sensitive analytical technique is needed to make these types of measurements, one that enables measurements to be made in situ and preferably in real time. The one method best suited for these studies of molecular adsorption at an aqueous-polymer interface is ATR/FT-IR spectrometry. In this project the analytical technique was applied to investigate macromolecular adsorption phenomena on thin films of cellulose acetate cast on internal reflection elements.

Section 2.

Project Goals and Objectives
Expected Outcomes and Benefits to the Separations Industry

Project Goals

The primary goals of the proposed research were to (1) determine the rate and extent of molecular conditioning film development on separations membranes, and (2) determine if artificial and natural conditioning films influence initial bacterial attachment to membranes, as modification of molecular conditioning films might be employed to inhibit or otherwise control bacterial attachment and biofilm formation on RO and related separations membranes.

Project Objectives

The above goals were to be accomplished by pursuing five project objectives:

Objective 1: Refine the current ATR/FT-IR spectrometry methodology to measure formation of artificial and natural molecular conditioning films on various polymer membranes. Optimize IRE coating with membrane polymers such as cellulose acetate, polyamide or polysulfone.

Objective 2: Use the ATR/FT-IR spectrometric method to screen the sorption of select organic compounds to various membrane polymers. The range of organics to be examined includes surfactants, chelating agents, biocides, proteins and polysaccharides. Examine sorption of specific organics as a function of pH, ionic strength, or other relevant physico-chemical parameters. Select strongly sorbing compounds for further analysis in bacterial attachment studies, as described below (see Objective 5).

Objective 3: Determine the kinetics and extent of organic conditioning film development on different synthetic membranes using (filter-sterilized) wastewater from Water Factory 21. If possible, correlate adsorption of naturally occurring trace organics on the membrane polymers with performance changes (flux, mineral rejection) or changes in bacterial adhesion.

Objective 4: Determine whether natural molecular conditioning films of wastewater origin can be replaced or otherwise modified via addition of selected organic substances, such as detergents, chaotropic agents or chelating compounds.

Objective 5: Compare the attachment of mycobacteria and other selected biofouling microorganisms to membranes with different types and amounts of molecular conditioning films. Both the kinetics of adhesion as well as the spatial distribution of the attached bacterial cells were to be measured using digital imaging techniques.

Expected Outcomes and Benefits to the Separations Industry

Expected outcomes from the research project include:

1) Determination of how strongly select organic macromolecules adsorb or bind to synthetic polymer membranes.

2) Identification of how artificially imposed surface treatments (i.e., applied biocides, surfactants, chelating agents, etc.) influence natural and artificial conditioning films.

3) Identification of how surface treatments influence initial microbial adhesion kinetics and growth rates.

A greater understanding of how organic foulants are partitioned at the aqueous-polymer interface and the exact nature of the molecular interactions between the organics/bacteria and the polymer membrane will result in the development of:

1) More effective treatments for membrane fouling, resulting in lower operations and maintenance costs.

2) New membranes that demonstrate a lower potential for colloidal and bacterial fouling, and

3) Possibly an in-line ATR/FT-IR spectrometry process monitor for membrane separation systems.

Section 3.

Conclusions

1. In general, adsorption on bare germanium, in terms of film thickness, was greatest for protein, followed by surfactants and polysaccharides.

2. Cellulose acetate did not adhere firmly to the surface of germanium IREs, making the infrared data very difficult to process and interpret.

3. Thin films of cellulose acetate cast on zinc selenide IREs demonstrated much greater stability as compared to films cast on germanium.

4. The surfactant dodecylbenzenesulfonic acid was very effective at removing organic macromolecules (protein and acidic polysaccharides) adsorbed on cellulose acetate thin films.

5. The detection limit of the ATR/FT-IR spectrometry technique was insufficient to observe organics adsorption on cellulose acetate thin films from reverse osmosis feedwater. (The limited exposure time of feedwater to the cellulose acetate thin film may also have contributed to the lack of detectable organics.)

6. Aliphatic aromatic trace organics from colored well water adsorbed to a thin film of cellulose acetate, resulting in reduced surface hydrophobicity.

7. Cellulose acetate pretreated with the surfactant Zwittergent 3-16 demonstrated less tendency to foul with *Mycobacterium* isolate BT12-100 compared to the untreated thin film.

Section 4.

Recommendations

1. Increase the sensitivity of the ATR/FT-IR spectrometry technique by making the following changes:

    a) Reduce the cellulose acetate film thickness (from 1500 Å to 750 Å) cast on the IRE, thereby increasing the electric field intensity at the aqueous/polymer interface.

    b) Switch from a 3-mm thick zinc selenide IRE to a 2-mm thick IRE, thereby increasing the number of internal reflections.

2. Continue development and implementation of simultaneous ATR/FT-IR spectrometry / Fluorescence Microscopy for studies of organics adsorption and bacterial attachment on thin polymer films.

Section 5.

Internal Reflection Spectrometry: Theory and Applications

ATR/FT-IR spectrometry provides a non-destructive method for monitoring molecular adsorption phenomena that occur at an aqueous-solid interface. The technique works by focusing radiation on the end of an infrared-transmitting crystal of high refractive index (n) at near normal angle of incidence. When IR radiation is transmitted into the crystal, light striking the interface between the optically dense (e.g. germanium, $n_1 = 4.0$) and optically rare medium (e.g., air, $n_2 = 1.0$) is totally internally reflected, provided that the angle of incidence of the radiation is greater than the critical angle (Figure 5.1). The critical angle is defined as

$$\theta_c = \sin^{-1} \frac{n_2}{n_1} \qquad \text{Eq. 5.1}$$

where n_1 and n_2 are the refractive indices of the IRE and the optically rare medium, respectively. At each point of internal reflection, the infrared radiation penetrates a short distance into the adjoining medium. The energy intensity of the radiation decays exponentially as a function of distance normal to the interface; thus, it is referred to as an "evanescent wave" (Figure 5.2). The depth of penetration of the evanescent wave is the distance at which the electric field intensity drops to $1/e$ (or 36.8%) of its magnitude at the interface and is defined by the equation,

$$d_p = \frac{\lambda}{2\pi n_1 \left[\sin^2 \theta - \left(\frac{n_2}{n_1} \right)^2 \right]^{1/2}} \qquad \text{Eq. 5.2}$$

where λ is the wavelength of the radiation.[29] For the most common IREs, Ge and ZnSe, the depth of penetration varies from ~300 to 1000 nm at an angle of incidence of 45°. Any chemical species within the depth of penetration of the evanescent wave can be detected, provided it absorbs light in the mid-infrared region of the spectrum. When the sample absorbs light, the beam is attenuated, and thus the name attenuated total reflectance (ATR) spectrometry. It is this unique physical property of internal reflection that enables one to observe adsorption phenomena at an aqueous-solid interface.

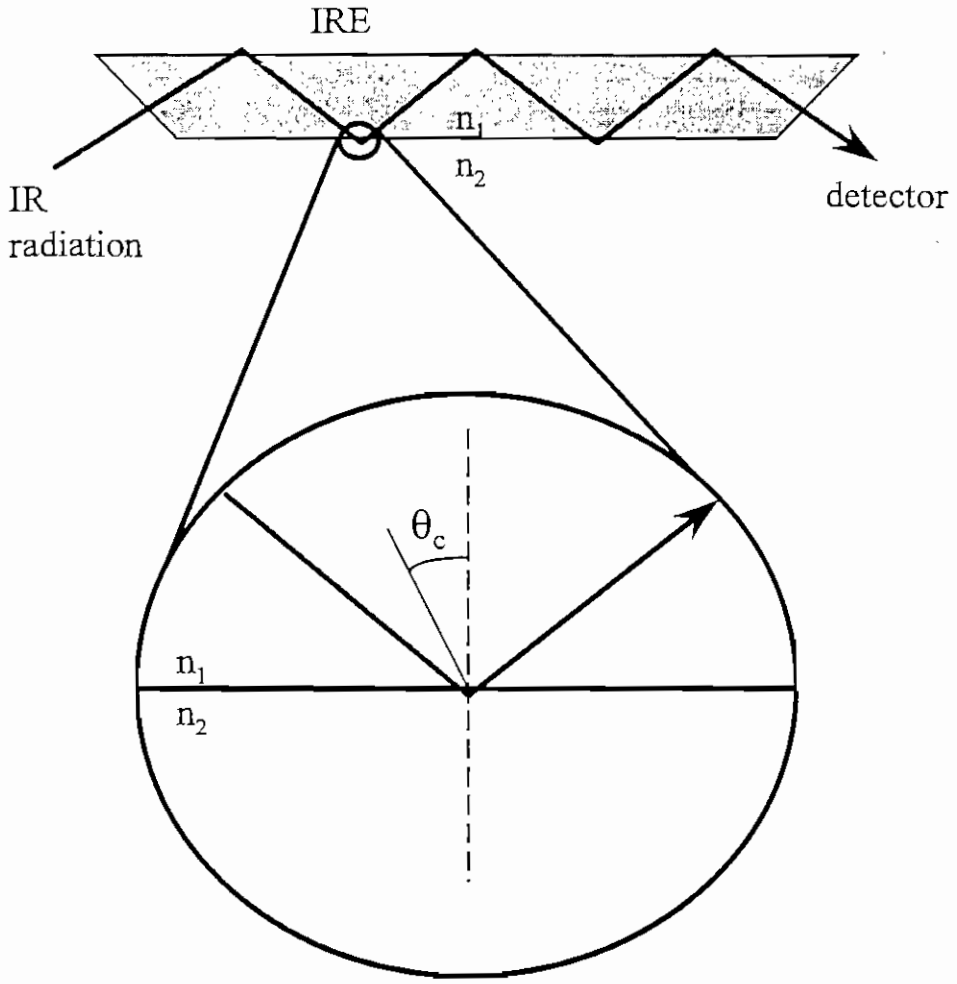

Figure 5.1 Internal reflection of light at an interface, where n_1 and n_2 are the refractive indices of the IRE and optically rare medium, and θ_c is the critical angle.

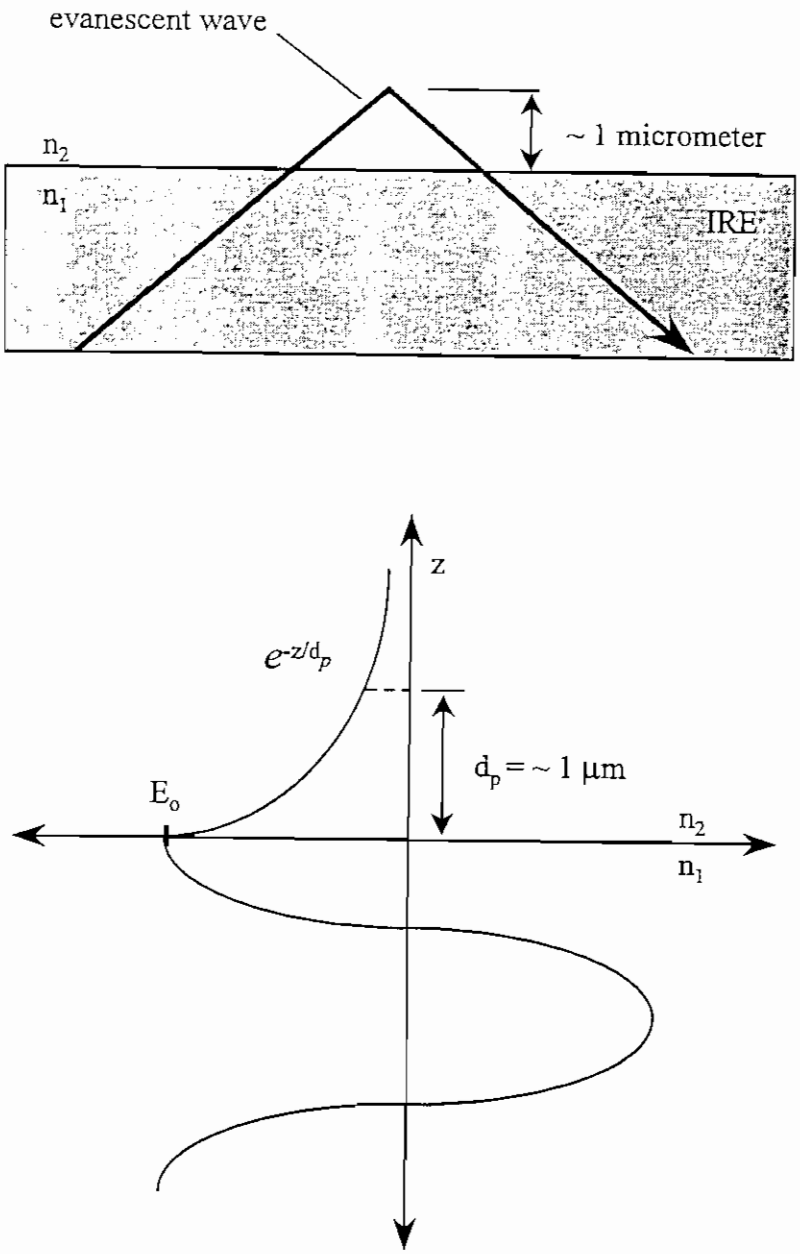

Figure 5.2 Internal reflection at a totally reflecting interface (top) and energy diagram of standing wave formed at the interface (bottom).

Studies of molecular adsorption can be extended to an aqueous-polymer surface. If a thin polymer film (500-2000 Å)[†] is cast on the surface of the IRE, infrared radiation will pass through the film and into the adjoining medium before reflecting back. The polymer film thickness must be carefully controlled. The magnitude of the electric field at the aqueous-polymer interface is altered by the thin polymer film that attenuates the IR beam. This effect is evident in the plots of electric field intensity (E_z) as a function of distance (D) from a Ge-polymer interface (Figure 5.3). Theoretical calculations of electric field intensity (E_z) for two polymer film thicknesses (500 and 2000 Å) were made at a 45° angle of incidence. The interface between Ge and polymer (Ge and water, in the case of bare Ge) is defined as D = 0 Å. In each case, there is a marked enhancement of E_z at this interface. The intensity drops as it passes through the polymer and the another enhancement of E_z occurs at the polymer-water interface. Finally, E_z decays exponentially as the radiation penetrates into the bulk aqueous phase. As the polymer film thickness is increased, the electric field intensity (E_o) at the polymer-water interface drops in magnitude. The effective thickness (d_e) of a thin film or an adsorbed molecular layer is given by

$$d_e = \frac{n_{21} E_o^2 d}{\cos\theta} \qquad \text{Eq. 5.3}$$

Where n_{21} is the ratio of the refractive index of the optically rare medium (water) to that of the IRE, d is the actual film thickness, and θ is the angle of incidence. This equation reveals four factors that determine the magnitude or strength of coupling of the evanescent wave to the absorbing rarer medium (e.g., adsorbed organic macromolecules). In the case where a layer of organics has adsorbed onto the thin polymer film, the angle of incidence and refractive indices are constant. However, the magnitude of E_0 at the interface where organics have adsorbed can vary significantly, as discussed above. In effect, the IR band intensities of the adsorbed species will drop as the polymer film thickness is increased due to the drop in electric field intensity at the aqueous-polymer interface. Therefore, the thickness of the polymer film cast on the IRE must be carefully controlled. If the film is cast too thick, insufficient radiation will pass into the bulk phase to enable measurements to be made (i.e., insufficient sensitivity to detect the adsorbed organic macromolecules). If the film is too thin, it will lack the physical strength to withstand handling and exposure to aqueous and ionic solutions. When the optimum film thickness is cast on the IRE, aqueous adsorption phenomena can be made in situ, void of artifacts associated with other methods of sample analysis involving dehydration, physical manipulation or chemical stains.

Corrections applied to the ATR spectra are required when measuring bulk samples due to the wavelength dependence of internal reflection spectrometry (see Equation 5.2). However, when the polymer film (or adsorbed organic layer) is much thinner than the penetration depth, i.e., $d \ll d_p$, the electric field can be assumed to be constant over the film thickness (d). Thus, no correction for the wavelength-dependent penetration depth is

[†] Angstroms will be used from here on to describe film thickness instead of nanometers.

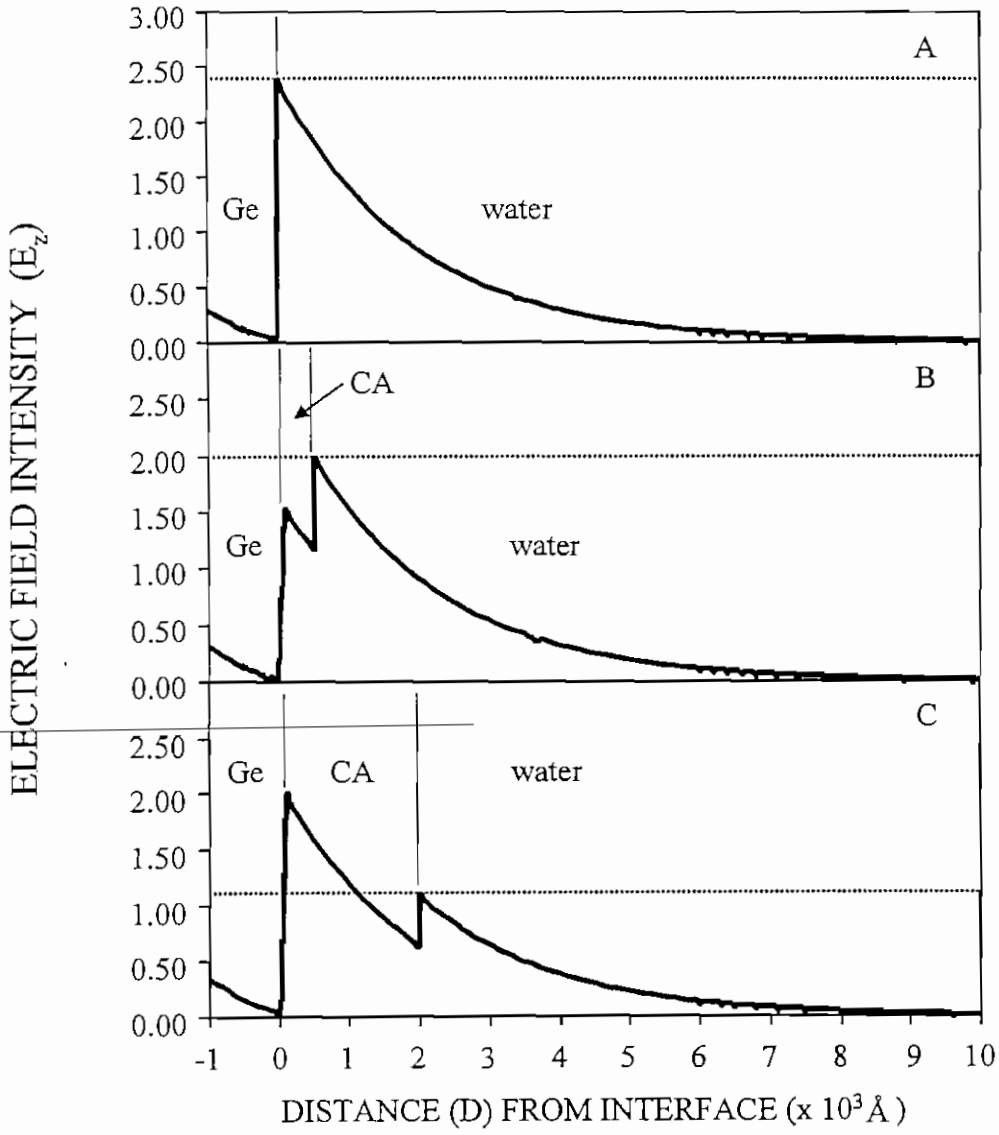

Figure 5.3 Plots of the electric field intensity as a function of distance from the interface of the IRE for (A) bare Ge, (B) 500 Å CA film and (C) 2000 Å CA film in contact with water.

necessary. More specifically, adsorption bands at longer wavelengths are no longer relatively stronger as they are for bulk materials, nor do the absorption bands become broadened on the long wavelength side. The internal reflection spectra of thin films actually resemble those obtained by transmission more closely than internal reflection spectra of bulk materials. Thus, if the polymer-coated IRE is placed in a flow cell and aqueous organic test solutions are pumped through the flow cell, it then becomes possible to measure the kinetics of macromolecular adsorption phenomena at the aqueous-polymer interface. Estimates of the film thickness of adsorbed organics can be made assuming a Beer-Lambert relationship.

Section 6.

Materials and Methods

Theoretical Calculations of Reflectance

A FORTAN program written by Richard Dluhy (University of Georgia, Athens, GA) was used to calculate theoretical values of reflectance and electric field intensities from stratified media.[30] The optical constants of water (refractive index and absorption index) were obtained from the literature.[31] The refractive index of CA was assumed to be 1.5, the absorption index at 1640 cm^{-1} equal to 0.01 and the angle of incidence 45°.

Cellulose Acetate (CA) Thin Film Cast on Internal Reflection Elements

Parallelepiped (50 x 10 x 2 mm) germanium (Ge) and (50 x 10 x 3 mm) zinc selenide (ZnSe) internal reflection elements were purchased from Harrick Scientific (Ossining, NY). Ge IREs were polished with 1.0 µm diamond paste (Buehler, Lake Bluff, IL), washed with detergent, rinsed with tap water and then rinsed with 18 Mohm-cm deionized water (E-pure, Barnstead/Thermolyne, Dubuque, IA). ZnSe IREs were washed but not polished.

Thin films of CA were cast on Ge IREs by Separations Systems Technology (SST) in San Diego, CA. The CA casting solution consisted of a blend of equal weights of 40.8% and 43.2% acetyl (by weight) CA that was dissolved in high purity dichloromethane. A strip of Teflon® adhesive tape was attached to the end of the IRE and the IRE dipped in chloroform to remove organic contaminants. After drying in a stream of nitrogen, the IRE was dipped into the polymer solution and then rapidly placed in the nitrogen stream to prevent water condensation on the thin film. IREs were dipped three times in a 0.088% solution of the blended CA(42% acetyl).

An estimate of the polymer film thickness was made by gravimetric analysis. Glass microscope slides (3 x 1 in.) were washed with detergent, rinsed with tap water and deionized water and allowed to air dry. Slides were dried to constant weight in a 105°C oven. Twelve slides were coated as described above. The CA-coated slides were dried to constant weight and reweighed. The coated area of each slide was measured. A CA film thickness of 1260 ± 80 Å was calculated, assuming a density equal to 1.3 g/cm^3. A similar thickness of CA was assumed to deposit on the Ge IREs.

In the second year of this project, the coating technology was transferred to the Biotechnology Research Department at Orange County Water District. Improvements to the casting process were made under the direction of SST. Polymers of cellulose acetate (100,000 MW) with varying levels of acetylation were obtained from SST. CA polymers were dissolved in high purity dichloromethane (B&JGC^2, Burdick & Jackson, Muskegon, MI). CA solutions with different acetyl content were made. The first consisted of an equal weight mix of 40.8% and 43.2% acetyl CA, average acetyl content 42%, and the second 43.9% acetyl CA. Solutions were mixed with a Teflon® stir bar and sonicated in a warm

water bath until the CA was completely dissolved. Solutions were filtered through lens paper to remove insoluble fibrous material.

A Pyrex cylinder (20 x 6 cm O.D.) was used in the coating process (Figure 6.1). Compressed air passed through a dryer (Balston Model 75-20), and a 0.2 μm polytetrafluoroethylene filter was used to purge the cylinder of water vapor. The CA solution (0.5% wt/vol) was mixed with a Teflon® stir bar. The stirring and air purge were turned off prior to casting of the film to eliminate turbulence at the air-solution interface. A peristaltic pump (Masterflex, Cole-Parmer Instrument Co.) was used to withdraw the IRE from the polymer solution. Nylon monofilament (2 lb test) was tied to the drive shaft of the pump. IREs were secured to a piece of fine copper wire with Teflon® adhesive tape, and the wire was attached to the nylon line with a small brass fishing swivel. IREs were dipped and then withdrawn from solution at a rate of 1 cm/sec (1.50 pump setting). The flow of air to the cylinder was turned on immediately after the IRE was withdrawn from solution. The ZnSe IREs were dipped once. CA was removed from the end of the IRE with a cotton swab saturated with chloroform. The film thickness was determined by gravimetric analysis. The CA-coated ZnSe IRE was weighed, stripped of CA, dried and then reweighed. The estimated film thickness on the ZnSe IRE dipped once in 0.5% CA solution was 1500 Å.

Bacterial Isolates and Culture Medium

Water Factory 21, located in Fountain Valley, CA, processes 15 million gallons of secondary treated municipal wastewater each day. Five million gallons of this water are treated by reverse osmosis. Two isolates of *Mycobacterium sp.* were recovered from a fouled cellulose acetate RO membrane. A recent (3-yr old) isolate of *Mycobacterium*, designated BT12-100, forms aggregates or flocs when grown as a broth culture. Another *Mycobacterium* isolate, BT2-4, is approximately 10 years old and has lost its ability to form aggregates due to repeated subculturing. *Mycobacterium* isolate BT2-4 has tentatively been identified as *Mycobacterium chelonae*. Both isolates were maintained on R2A agar plates and subcultured on a monthly basis.

The bacteria were grown on a defined mineral salts (MS) medium consisting of 0.75 g/L Na_2HPO_4, 0.75 g/L K_2HPO_4, 1.0 g/L NH_4Cl, 50 mg/L $MgSO_4 \cdot 7H_2O$, 11 mg/L $CaCl_2 \cdot 2H_2O$, 1.0 g/L mannitol and 600 μL of Wolfe's mineral salts solution per liter of water. The composition of Wolfe's mineral salts solution is as follows (per liter water): 1.5 g nitrilotriacetic acid (disodium salt), 3.0 g $MgSO_4 \cdot 7H_2O$, 0.5 g $MnSO_4 \cdot H_2O$, 1.0 g NaCl, 0.1 g $FeSO_4 \cdot 7H_2O$, 0.1 g $CoCl_2 \cdot 6H_2O$, 0.1 g $CaCl_2$, 0.1 g $ZnSO_4 \cdot 7H_2O$, 0.01g $CuSO_4 \cdot 7H_2O$, 0.01 g $AlK(SO_4)_2 \cdot 12H_2O$, 0.01 g H_3BO_3 and 0.01 g $Na_2MoO_4 \cdot 2H_2O$. Cultures were incubated at 28°C with shaking at 200 rpm. Cells were harvested in stationary phase (~60 hr) by centrifugation at 10,000 rpm for 15 min at 4°C, washed twice with MS buffer (no mannitol) and resuspended in buffer at pH 7. Cells were stained with 4',6-diamidino-2-phenylindole (DAPI), a DNA-binding fluorochrome, and viewed by epifluorescence microscopy to determine the cell surface coverage (% surface coverage or cells/cm^2).

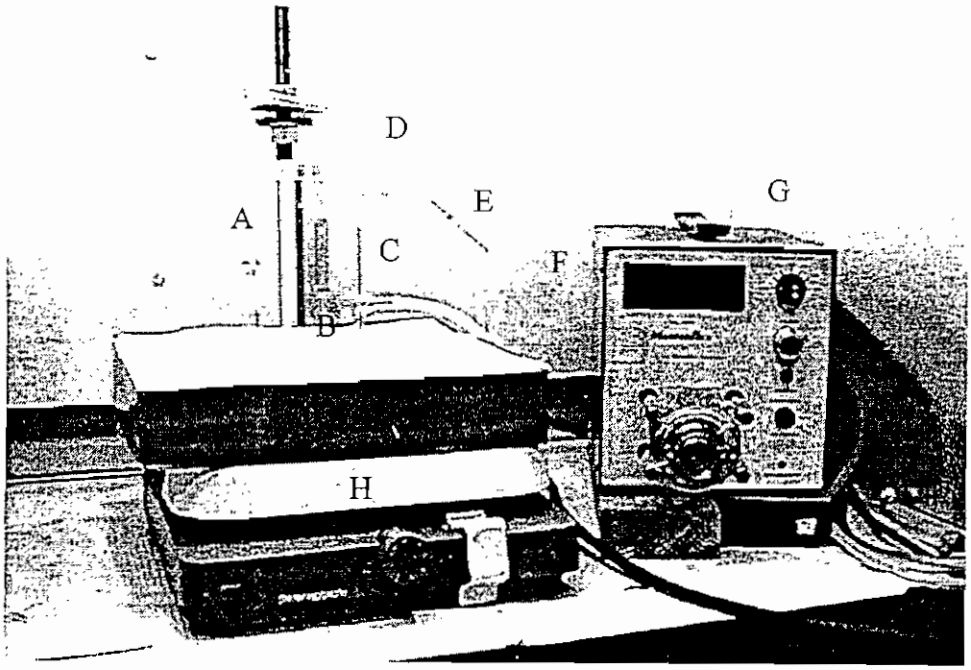

Figure 6.1 Apparatus for casting thin film of cellulose acetate on internal reflection elements including (A) coating cylinder, (B) ZnSe internal reflection element, (C) air inlet and outlet, (D) fine copper wire, (E) brass swivels, (F) nylon monofilament, (G) peristaltic pump and (H) stirring plate.

Growth Conditions for Bacterial Adhesion Studies (Circular Flow Cell / Nomarski Differential Interference Contrast Microscopy)

A 50-mL volume of MS medium was inoculated with *Mycobacterium* isolate BT12-100. The culture was incubated for 48 hr at 28°C with shaking at 200 rpm. The culture was centrifuged for 15 min at 10,000 rpm at 4°C. The cells were washed twice in 50 mL of MS buffer (pH 7) and then resuspended in buffer to a final volume of 150 mL. The cell suspension was split into three portions. One was used for the untreated CA control, one for exposure to the pretreated CA thin film and one to determine the total cell count in the suspension. The cell count, determined by DAPI staining, was 1.0×10^8 cells/mL.

Aqueous Organic Solutions

Bovine serum albumin (Fraction V), alginic acid (low viscosity), dextran (580,000 MW), gum arabic, Triton X-100 (polyethylene glycol-*p*-isooctylphenyl ether), ethylenediaminetetraacetic acid (EDTA) and benzalkonium chloride were purchased from Sigma Chemical Co., St. Louis, MO. Sodium dodecylbenzene-sulfonic acid (DBSA) was purchased from Aldrich Chemical Co., Milwaukee, WI. The surfactants Zwittergent 3-16 (n-hexadecyl-N, N-dimethyl-3-ammonio-1-propanesulfonate), Genapol C-100 (polyoxyethylene(10)isotridecyl ether), MEGA 10 (decanoyl-N-methylglucamide) and hexyl-β-D-glucopyranoside were purchased from CalBiochem, La Jolla, CA. Organic test solutions were made at a concentration of 0.5% (wt/vol) unless noted otherwise. Organic compounds were dissolved with MS buffer for experiments where bacterial cell suspensions were used; otherwise the organics were dissolved in E-pure deionized water. The pH was adjusted with dilute HCl or NaOH.

ATR / FT-IR Spectrometry

CA-coated Ge IREs were sterilized under ultraviolet light for 15 min on each side before being placed in a stainless steel multi-reflection edge-seal liquid cell (Harrick Scientific, Ossining, NY) (Figure 6.2). BUNA O-rings formed the seal. Both sides of the IRE were exposed to the aqueous test solutions. The flow cell volume was approximately 1 mL. The flow cell, O-rings and silicone tubing were autoclaved separately from the coated IREs. The flow cell was placed on a twin parallel-mirror reflection attachment (Harrick Scientific) installed in the sample compartment of a Nicolet Magna 550 FT-IR spectrometer (Nicolet Instrument Corp., Madison, WI) equipped with a medium-range mercury-cadmium-telluride detector (Figure 6.2). Experiments involved only with organics adsorption were not run under sterile conditions. Deionized water or aqueous organic test solution (0.5% wt/vol) was pumped through the flow cell at 8 mL/hr. Solutions (pH 7) were not recirculated. A macro program (OMNIC Macros\Basic Version 1.20) was used to collect infrared spectra at set intervals of time. A total of 80 scans (1-min acquisition time) at 4-cm^{-1} resolution were coadded and stored for spectral processing. Single-beam IR spectra were processed with GRAMS/32 (Version 4.0) spectroscopic software (Galactic Industries, Salem, NH). Macromolecule adsorption on CA was monitored by digitally subtracting a hydrated CA

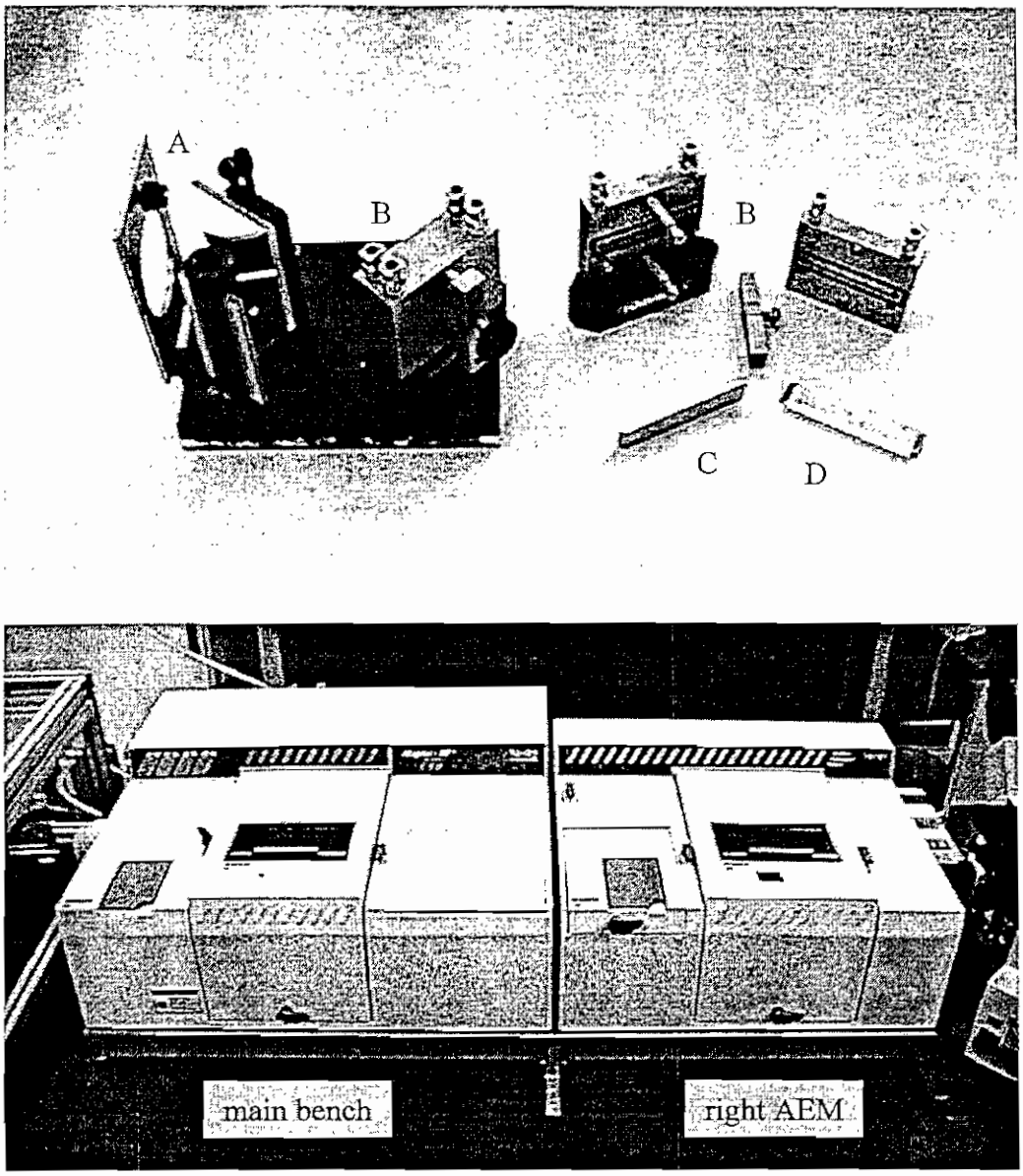

Figure 6.2 Attenuated total reflectance accessories (top) including (A) mirror assembly, (B) flow cell, (C) Ge IRE and (D) ZnSe IRE. FT-IR spectrometer (bottom) including main bench and right AEM.

reference spectrum from the sample absorbance spectrum, revealing the underlying spectrum of the adsorbed species.

The absorptivity of each compound was determined by measuring a transmission spectrum of a dilute aqueous solution, typically 0.5 to 1.0% wt/vol. Assuming a Beer-Lambert Law relationship ($A = a \cdot b \cdot c$) where concentration, c, was equal to the wt/vol% and pathlength, b, equal to 17 μm, the absorptivity, a, for each compound was calculated, having units of cm^{-1}. The film thickness of adsorbed macromolecules on Ge was calculated using the experimentally measured absorptivity. Macromolecular concentration was defined as unity for the adsorbed thin film.

Captive Bubble Contact Angle (Aspect Ratio) Measurement

The captive bubble contact angle apparatus was designed at OCWD and contracted to D. J. Engineering (Tustin, CA) for manufacture. The main components of the system consisted of a liquid reservoir, stage for sample support, charge-coupled device (CCD) camera, lens, x-y-z camera mount and illumination source (Figure 6.3). The major components mount on a flat sheet of aluminum (3/8 in.) equipped with threaded legs to maintain a level plane. The stage consisted of a 4 x 2 x 1 in. block of aluminum with a 1 cm slot cut 1.5 in. deep down the middle. A second stage was machined with a 0.5 cm wide slot. The stage was equipped with an aluminum plate to hold the samples flat. The sample stage was placed in a 4 x 4 x 4 in. plexiglass reservoir filled with 18 Mohm-cm deionized water. A thread feed syringe with Luerlock needle connection was mounted on the side of the reservoir. The syringe was equipped with a 3-in., 22-gauge, 90-degree bevel stainless steel needle (Hamilton Co.). Air bubbles discharged from the syringe were estimated at 7 - 10 μL. The syringe needle was reamed with 0.010-in. nickel wire prior to the day's measurements to insure needle diameter. A glass microscope slide was mounted in the wall of the reservoir, opposite the syringe, to enable capture of images. The CCD camera (COHU, Model 48155000 AL2D) was equipped with a 0.75X to 3.0X objective (Edmund Scientific) and mounted on the x-y-z positioning stage. Images were captured and processed using CUE2 Series Image Analysis software (Olympus). A Sobell filter was used to outline the bubble's circular perimeter and the contact baseline. The CUE2 program generated the bubble height and diameter data for calculation of the height:diameter (H:D) aspect ratio.

Differential Interference Contrast (DIC) Microscopy

Real-time observations of bacterial attachment on CA thin films were made by Nomarski DIC microscopy. An Olympus IX70 inverted microscope was equipped with a 40X objective and Optronics CCD camera. A frame grabber board (Media Cybernics, Silver Springs, MD) was installed in a Pentium 120 MHz PC. An 8" Sony Trinitron monitor was used to display live images. Digitized images were processed by Image-Pro Plus software (Version 3.0, Media Cybernetics). No fluorochromes were needed to visualize the bacterial cells.

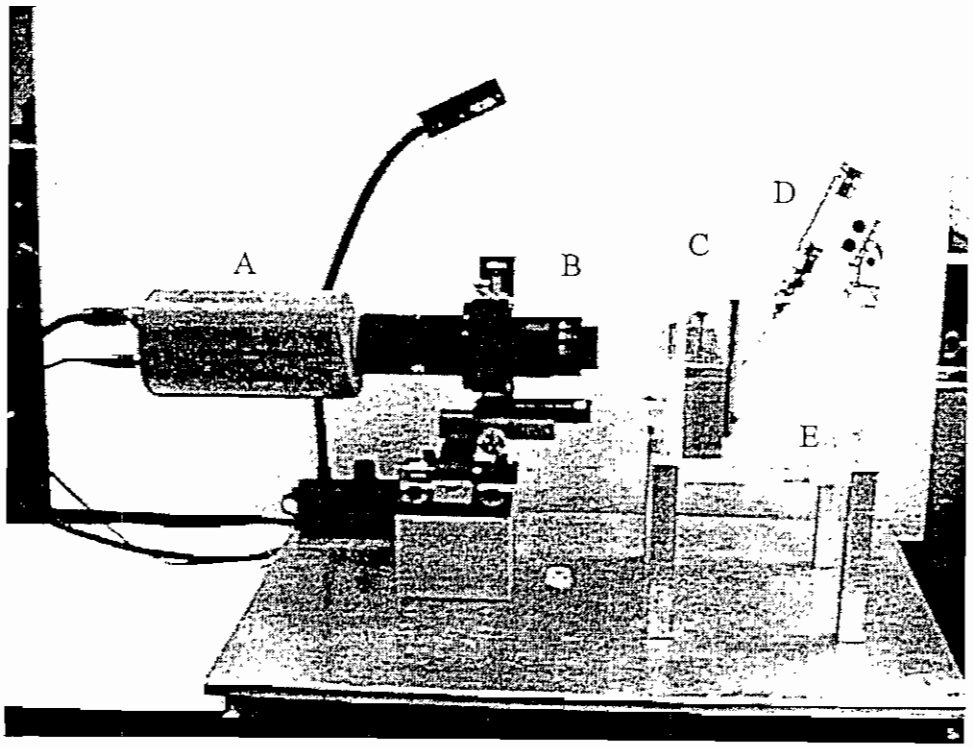

Figure 6.3 Captive bubble contact angle measurement device consisting of (A) CCD camera, (B) objective, (C) stage, (D) syringe and needle and (E) plexiglass reservoir.

Circular Flow Cell for Visual Microscopy of Bacterial Cells Attached to Cellulose Acetate Thin Films

Circular flow cells were manufactured from 316 stainless steel (D. J. Engineering) (Figure 6.4). The base of the flow cell was designed to fit on the stage of the Olympus IX70 inverted microscope. Circular coverslips were coated with CA as described above. Silicone spacers were placed over the CA-coated coverslips with channels (22 x 3.2 x 1.5 mm deep) cut to match the fluid dynamics of the ATR flow cell. The top plate of the flow cell contained a glass window and syringe needles (12 gauge) for inflow and outflow. Test solutions and bacterial cells were pumped from the ATR flow cell into the microscopic flow cell. Images of bacterial cells physically attached to the polymer surface were obtained periodically by the methodology described above.

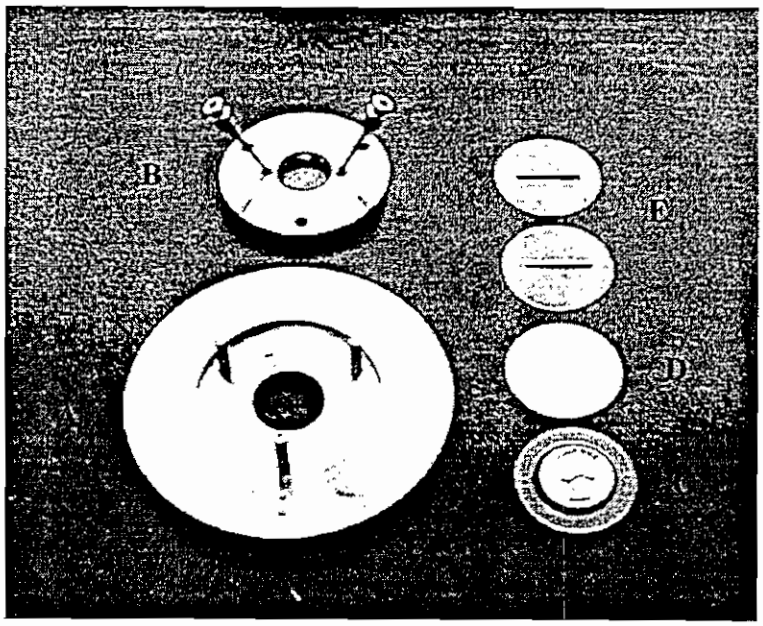

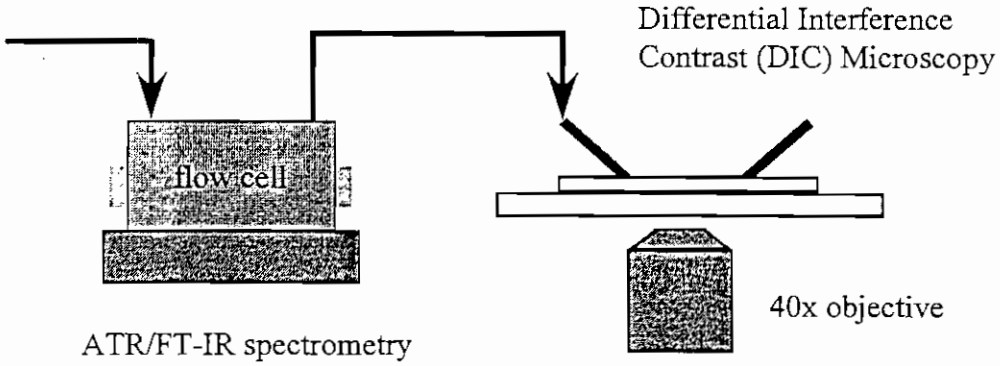

Figure 6.4 Circular flow cell (top) consisting of (A) base plate, (B) top plate with Luer lock syringe needles, (C) silicone gasket, (D) coverslip and (E) silicone spacers with 3.2 mm channel. Schematic diagram (bottom) of ATR/FT-IR spectrometry and differential interference contrast microscopy.

Section 7.

Results

Section 7.1 Adsorption of Organic Macromolecules on Ge IRE

Twelve different organic compounds were initially screened for use in sorption studies onto cellulose acetate thin films. The goal was to obtain reference spectra and find compounds with IR vibrational structure that did not overlap that of CA. Later these compounds were used in studies of organics adsorption on thin polymer films. As part of an American Water Works Research Foundation (AWWRF) grant conducted by OCWD, numerous chemical compounds and surfactants were screened for their ability to inhibit bacterial attachment. These compounds demonstrated varying abilities to affect bacterial attachment as determined by a radiolabeled adhesion assay (data not shown). Eight of these chemical agents from the AWWRF project were incorporated in the NWRI project, which included a nonionic, cationic, anionic and zwitterionic surfactant. The eight compounds were EDTA, hexaglucopyranoside, MEGA 10, Genapol C-100, DBSA, Zwittergent 3-16, Triton X-100 and benzalkonium chloride. A protein, two polysaccharides and a glycoprotein were selected as model compounds to represent EPS produced by bacteria. These four compounds were bovine serum albumin (BSA), alginic acid, dextran and gum arabic.

Aqueous organic solutions (0.5% wt/vol) were pumped through a flow cell containing a Ge IRE. After 4 hr, the CA thin film was rinsed by pumping water through the flow cell to the end of an 8-hr experiment. The kinetics of macromolecular adsorption and desorption on the Ge surface were investigated by plotting the vibrational band intensities as a function of time of flow. At the start of each experiment (T = 0 min), the flow cell was rapidly filled with sample solution. At this time, the IR spectrum represents primarily bulk solution phase sample since the IR radiation penetrates about 0.5 μm into the aqueous phase at each internal reflection. Any increase in the IR band intensities after T = 0 min was considered as adsorbed organic macromolecules. Therefore, all band intensities between T = 0 min and T = 4 hr were a combination of adsorbed and bulk aqueous phase organics. After the 4-hr adsorption period, the flow cell was rinsed with water or buffer. The turnover time for the flow cell was approximately 7.5 min at a flow rate of 8 mL/hr. During this time, the bulk phase solution organics were flushed from the flow cell, and loosely bound organics desorbed from the aqueous-polymer interface. Therefore, material remaining after 10 min of rinsing was defined as firmly bound. Desorption rate constants for the firmly bound material were determined by fitting the data points to a linear regression line.

Representative ATR/FT-IR spectra of EDTA, hexylglucopyranoside, Genapol C-100 and MEGA 10 are shown in Figure 7.1.1. Albumin, alginic acid, dextran and gum arabic are shown in Figure 7.1.2. DBSA, Zwittergent 3-16, Triton X-100 and benzalkonium chloride are shown in Figure 7.1.3. Each sample spectrum is one of many collected throughout the control study of adsorption and desorption on bare Ge surface. These spectra were obtained by digitally subtracting a water reference spectrum from each sample spectrum. In some cases, the water subtraction was not complete and a residual 1640 cm^{-1} water band remained.

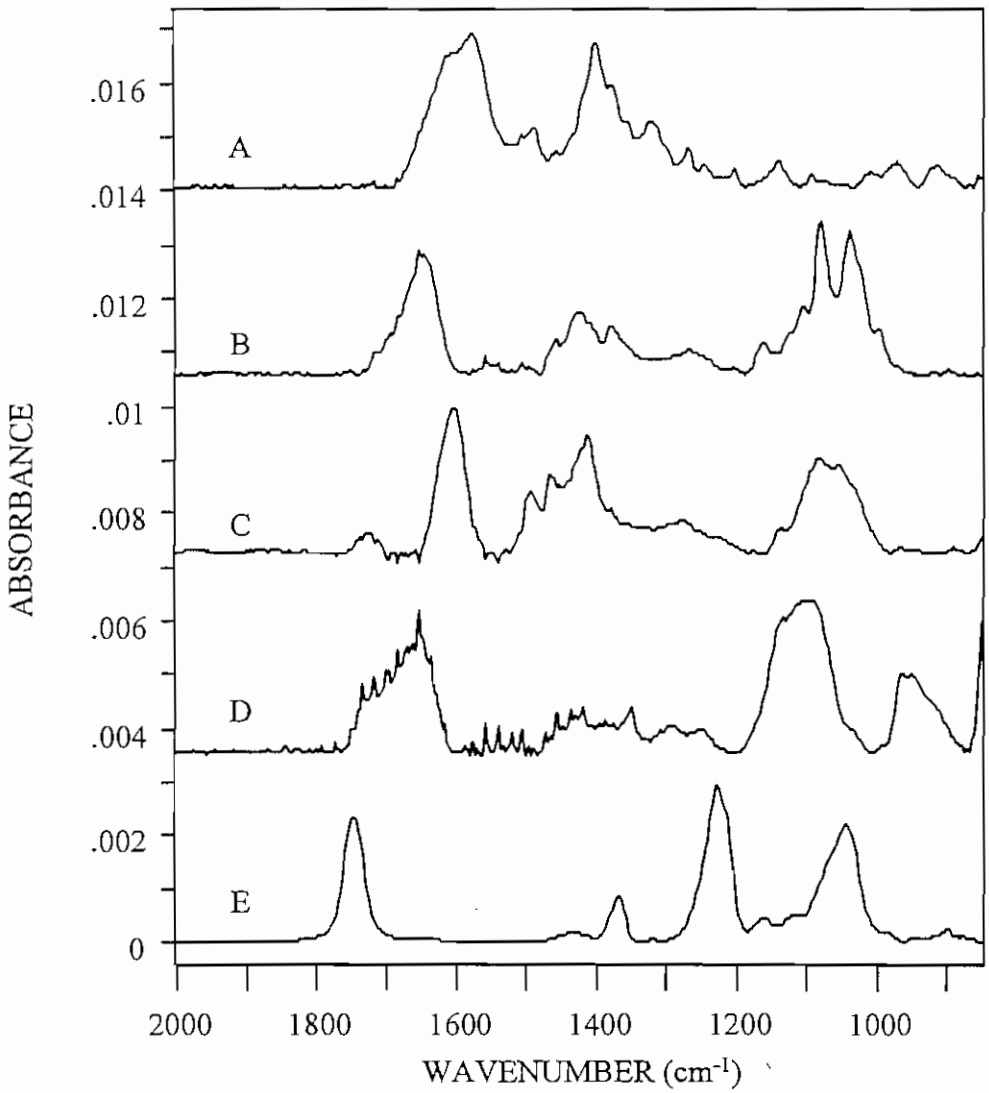

Figure 7.1.1 ATR/FT-IR spectra of (A) EDTA, (B) hexylglucopyranside, (C) MEGA 10 and (D) Genapol C-100 adsorbed on Ge IRE, and (E) thin film of CA cast on Ge IRE.

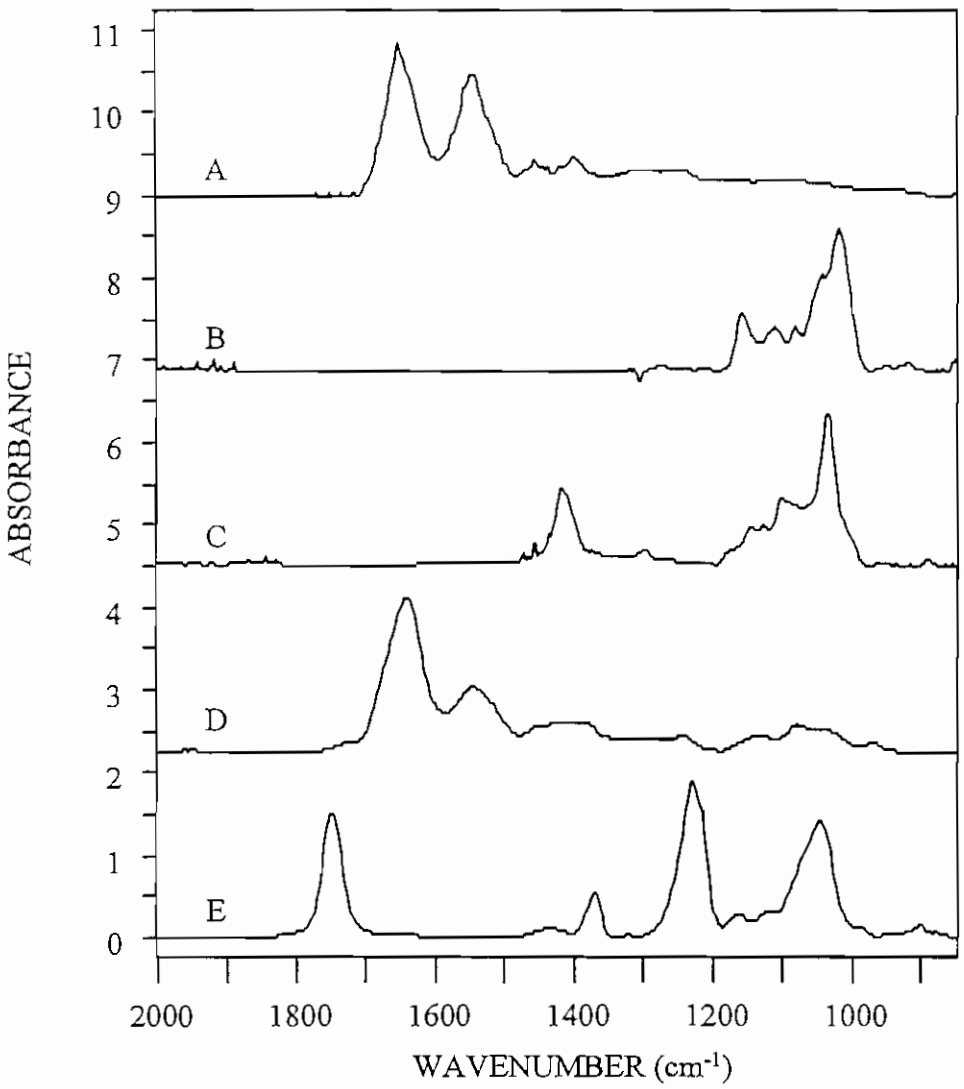

Figure 7.1.2 ATR/FT-IR spectra of (A) albumin, (B) dextran, (C) alginic acid and (D) gum arabic adsorbed on Ge IRE, and (E) thin film of CA cast on Ge IRE.

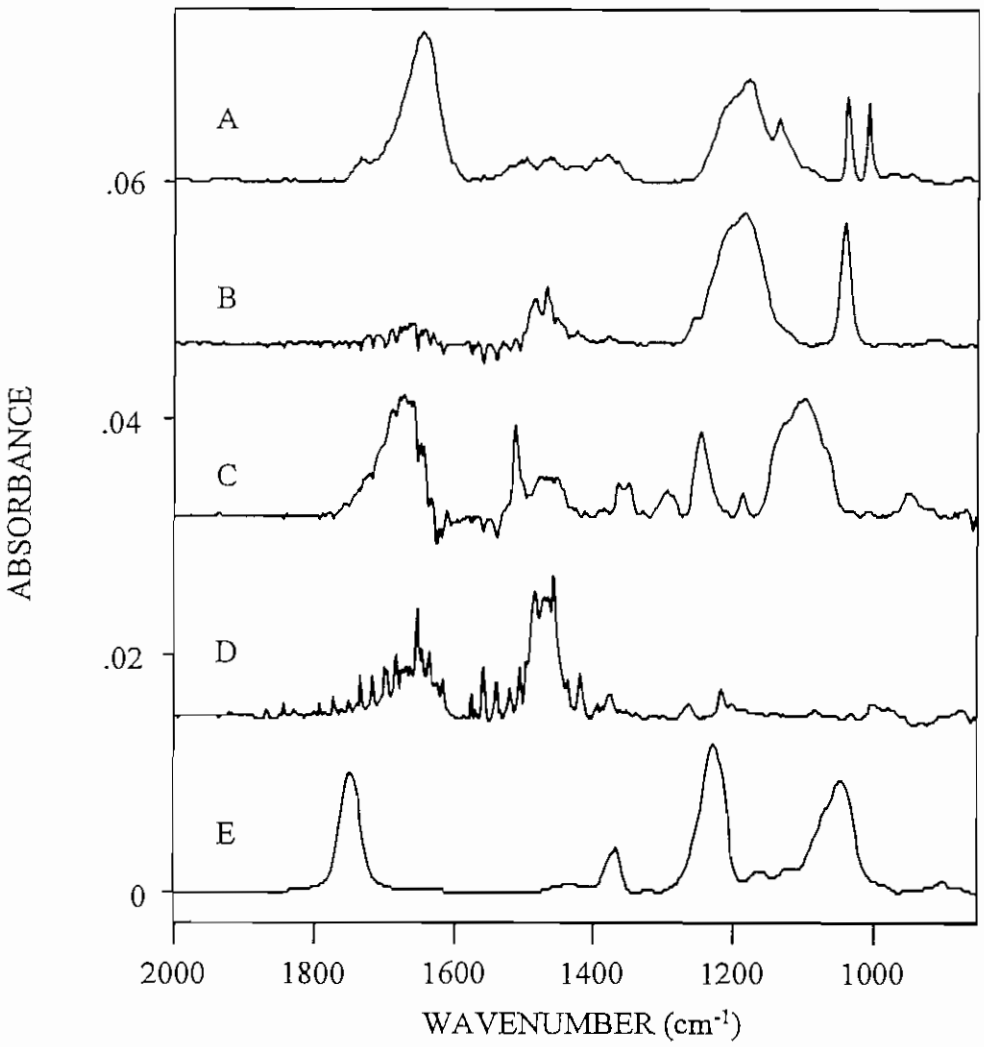

Figure 7.1.3 ATR/FT-IR spectra of (A) DBSA, (B) Zwittergent 3-16, (C) Triton X-100 and(D) benzalkonium chloride adsorbed on Ge IRE, and (E) CA thin film cast on Ge IRE.

An infrared ATR spectrum of CA cast on a Ge IRE is displayed at the bottom of each set of spectra. No correction for the wavelength dependence of ATR measurements was made, as the adsorbed films were much thinner than the depth of penetration of the evanescent wave.

Ethylenediaminetetraacetic Acid

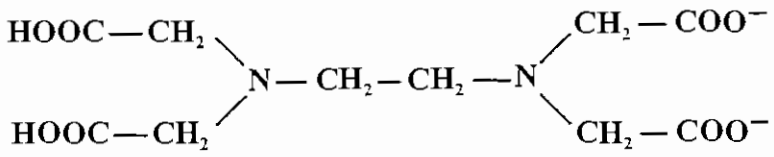

EDTA, a metal chelating agent, was initially run with a stainless steel flow cell. The 1400 cm^{-1} symmetric carboxylate band and the 1321 cm^{-1} C-H deformation band intensities both reached a plateau after 60 min (Figure 7.1.4A). Both band intensities dropped rapidly at the start of the rinse, due to the loss of sample from the bulk aqueous phase and desorption of loosely bound material. Very little of the material that adsorbed was firmly bound, as the band intensities dropped to near zero absorbance after the 4-hr rinse. As time passed, the solution in the waste reservoir turned light blue in color. Analysis of this solution by inductively coupled plasma atomic emission spectroscopy revealed the presence of mostly copper, nickel and aluminum ions. The desorption rate constant of firmly adsorbed material was -4.8 x 10^{-3} min^{-1}. An EDTA film <1 Å remaining after the rinse.

A Teflon® flow cell was purchased, and the experiment was repeated. The 1400 cm^{-1} and 1321 cm^{-1} bands appeared to plateau approximately 40 min into the experiment (Figure 7.1.4B). However, both 1400 cm^{-1} and 1321 cm^{-1} bands continued to increase, reaching a maximum intensity of 15.2 and 6.0 mAU, respectively, by the end of the initial 4-hr period. More EDTA remained firmly bound to the Ge IRE as compared to the experiment run with the stainless steel flow cell. These results suggest that the uncomplexed molecule demonstrated a greater affinity for the Ge substrate. Free carbonyl and carboxylate groups may play a role in sorption to the surface of the IRE. The estimated film thickness of EDTA left firmly bound to the Ge surface was 13 Å.

Hexylglucopyranoside

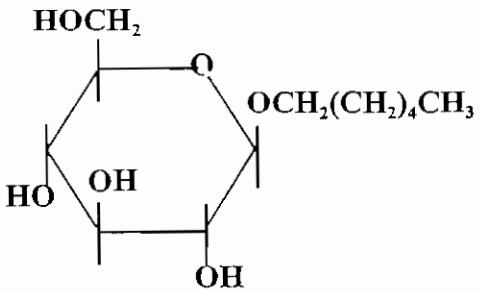

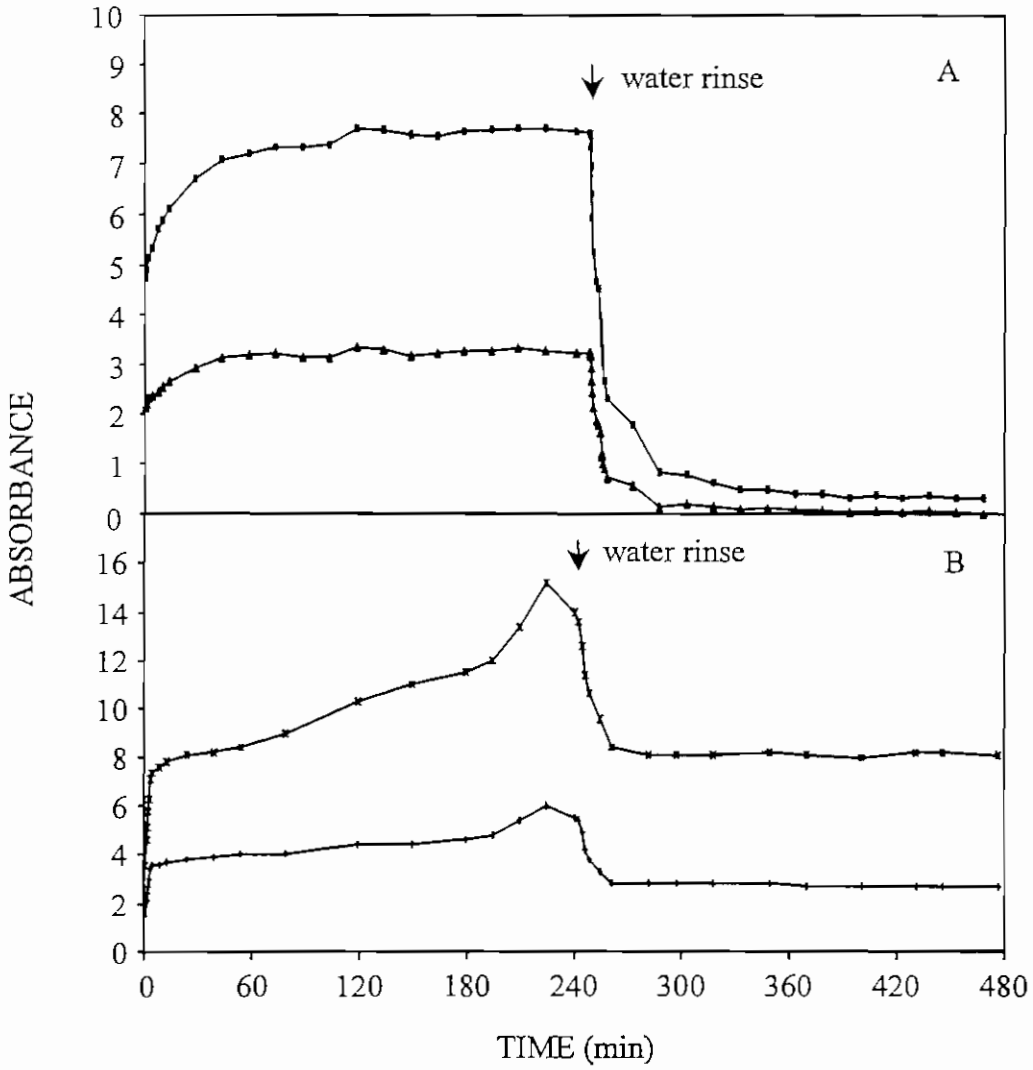

Figure 7.1.4 Plot of 1400 cm^{-1} (▪,×) and 1321 cm^{-1} (▲,•) band intensities of EDTA as a function of time of flow (A) stainless steel and (B) Teflon® flow cell.

Hexyl-β-D-glucopyranoside is a nonionic surfactant consisting of glucose and a 6-carbon aliphatic tail. The surfactant accumulated at the surface of the Ge IRE, reaching a plateau after 60 min, as indicated by the rise in the 1080 cm^{-1} and 1040 cm^{-1} bands attributed to a C-O-H and C-O ring stretch, respectively (Figure 7.1.5). The 1379 cm^{-1} C-H deformation band intensity increased gradually throughout the 4-hr period, indicating that the hydrocarbon tail of the surfactant continued to accumulate at the interface. All three bands dropped rapidly at the start of the rinse period, indicating the loss of bulk phase organics and loosely bound surfactant from the surface of the IRE. Between T = 250 min and the end of the rinse, the 1080 cm^{-1} and 1040 cm^{-1} bands dropped 60% and 50%, respectively. The C-H deformation band remained unchanged, suggesting that the hydrocarbon tail remained firmly bound to the Ge surface. No desorption rate constant or film thickness was calculated for this compound.

MEGA 10

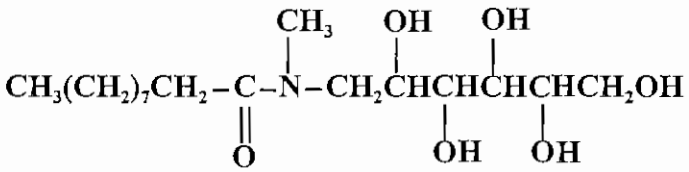

MEGA 10 is a nonionic surfactant, decanoyl-N-methylglucamide. The molecule can exist in a configuration with a negative charge on the oxygen and positive charge on the nitrogen. Thus, the carbonyl band is shifted down to 1603 cm^{-1}, and there is a C-O^- band located near 1412 cm^{-1}. The 1603 cm^{-1} and 1412 cm^{-1} bands and 1082 cm^{-1} C-O-H band all rose gradually and plateaued at approximately T = 150 min (Figure 7.1.6). Very little of the material appeared to be firmly bound to the surface of the IRE, as all three bands dropped between 82 and 90% between T = 250 min and the end of the 4-hr rinse. The desorption rate constant for the firmly bound material was -1.7×10^{-3} min^{-1}. An estimated film thickness of 5.8 Å remained following the rinse.

Genapol C-100

Genapol C-100 is a nonionic surfactant, polyoxyethylene(10)dodecyl ether (or polyethylene glycol lauryl ether). The C-O-C antisymmetric stretching band near 1097 cm^{-1} increased 1.5 mAU following the addition of Genapol C-100 to the flow cell (Figure 7.1.7). The 1350 cm^{-1} C-H deformation band increased less than 1 mAU over the initial 4-hr period. The 1350 cm^{-1} band dropped 12% during the rinse period, while the 1097 cm^{-1} band

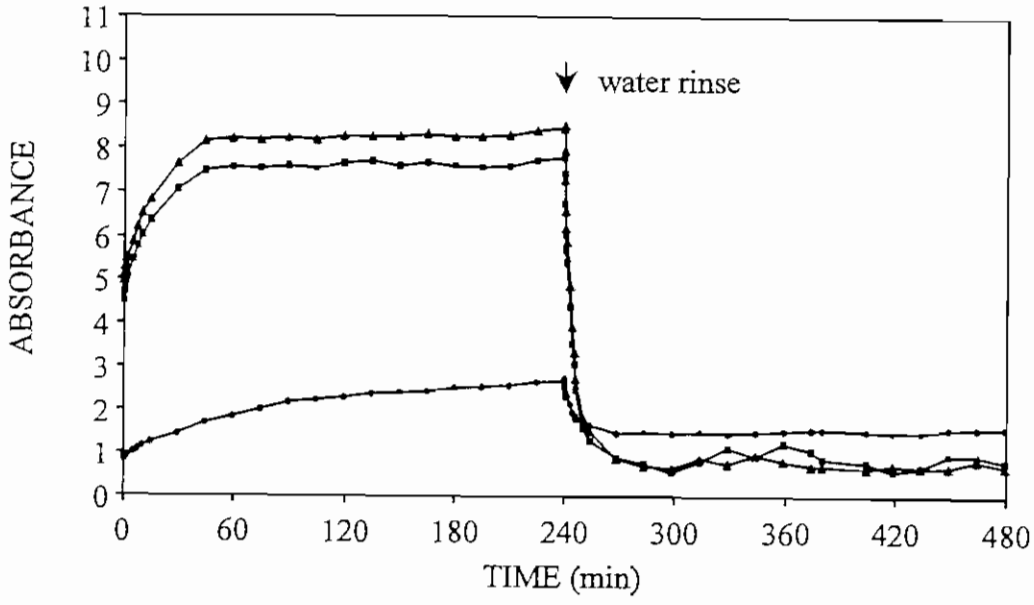

Figure 7.1.5 Plot of the (▲) 1080, (•) 1040 and (•) 1379 cm^{-1} band intensities of hexylglucopyranoside as a function of time of flow.

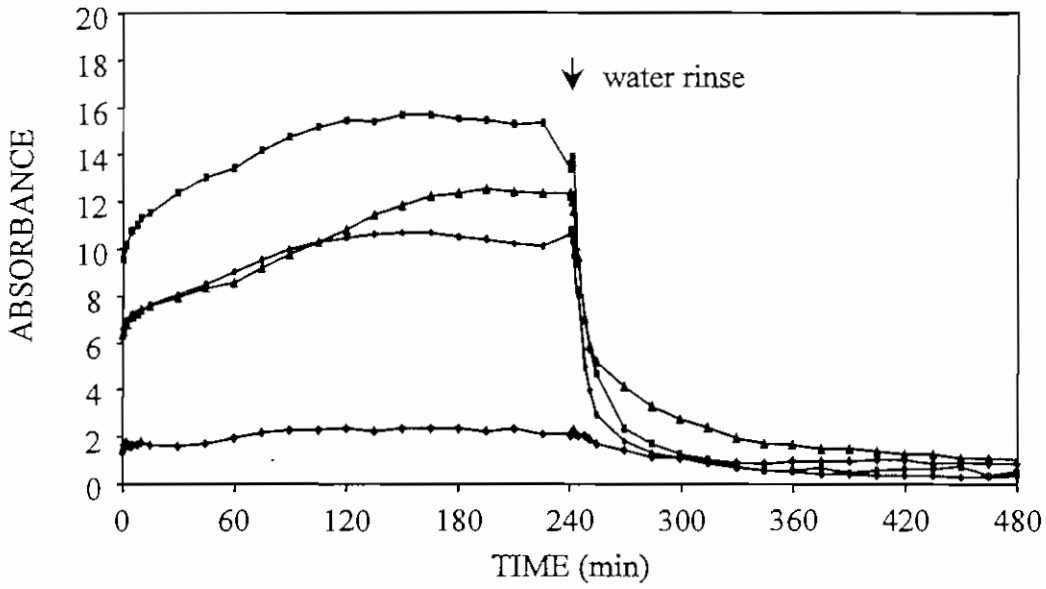

Figure 7.1.6 Plot of the (▲) 1726, (•) (1603, (•) 1412 and (▪) 1082 cm^{-1} band intenities of MEGA 10 as a function of time of flow.

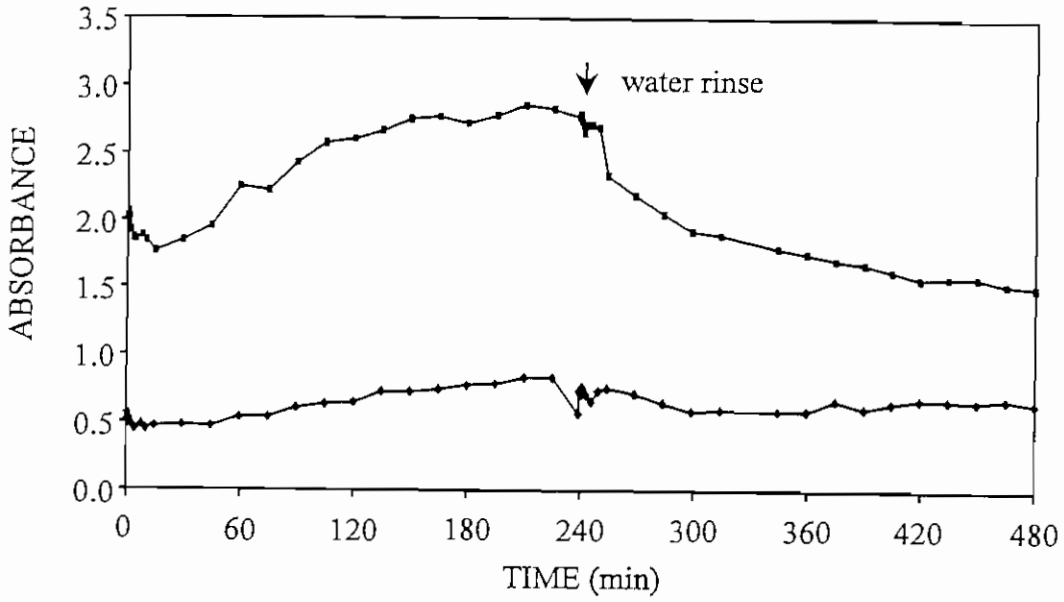

Figure 7.1.7 Plot of the (•) 1350 cm^{-1} and (•) 1097 cm^{-1} band intensities of Genapol C-100 as a function of time of flow.

dropped 44%. These results suggest that the aliphatic tail of the surfactant is more firmly bound to the Ge surface than the ethoxy substituents. A desorption rate constant of -3.0×10^{-3} min^{-1} was calculated. An estimated film thickness of 33 Å remained following the rinse.

Bovine Serum Albumin

Bovine serum albumin (40 x 140 Å) is an acidic protein with an isoelectric pH of 4.8. At pH 7 the protein has a net negative charge. BSA initially adsorbed rapidly onto the Ge surface, then gradually tapered off (Figure 7.1.8). Adsorption of BSA on Ge did not plateau. The 1546 cm^{-1} Amide II band intensity reached a maximum of 47 mAU by the end of the initial 4-hr period. Most of this protein was firmly adsorbed to the Ge surface, as the Amide II band dropped only 21.8% during the 4-hr rinse period. The desorption rate of BSA from the interface was -10×10^{-3} min^{-1}. The estimated film thickness of BSA on the IRE was 61 Å—approximately a monolayer, assuming the molecule lies flat on the surface of the Ge surface.

Dextran

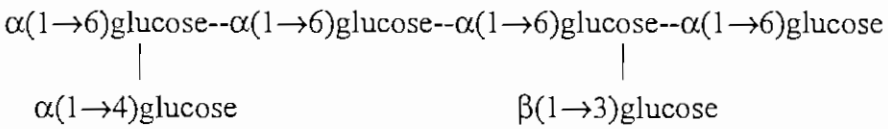

Dextran is a branched homopolysaccharide composed entirely of glucose and is classified as neutral. The glucose subunits are linked α(1→6) with branches at β(1→3) and β(1→4).[32] Dextran rapidly accumulated at the aqueous-polymer interface, as indicated by the rapid rise in the 1019 cm^{-1} band intensity after the start of the experiment (Figure 7.1.9). The C-O stretching band intensity appeared to plateau after approximately 60 min but continued to increase slowly to the end of the 4-hr period. This band dropped rapidly (60% in the first 20 min of the rinse), suggesting that much of the polysaccharide was only loosely bound to the Ge IRE. The firmly bound dextran desorbed at a rate of -15×10^{-3} min^{-1}, and the estimated film thickness of polymer left in contact with the IRE was 2.2 Å.

Alginic Acid

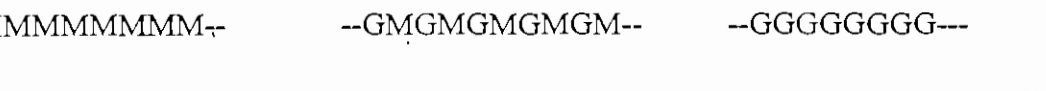

Alginic acid is composed of β-D-mannuronic acid (M) and α-L-guluronic acid (G).[33,34,35] This polysaccharide is linear with homopolymeric sequences of each monomer

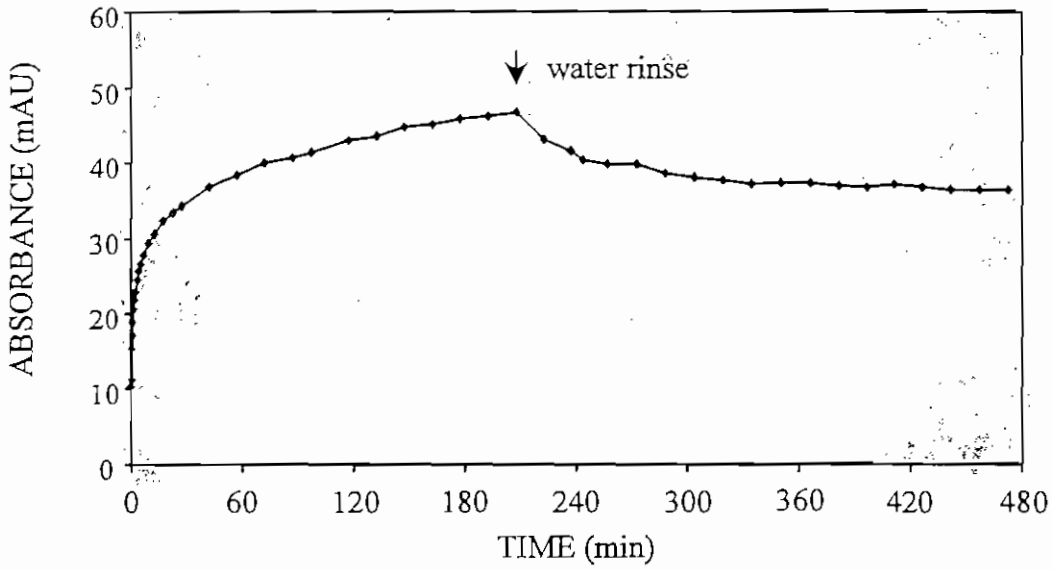

Figure 7.1.8 Plot of the (•) 1546 cm^{-1} Amide II band intensity of bovine serum albumin as a function of time of flow.

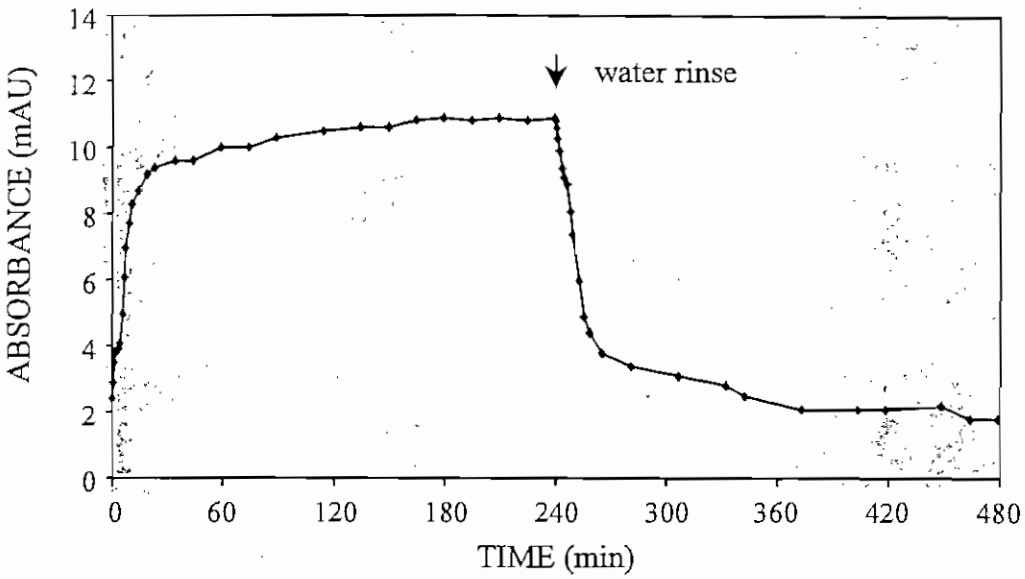

Figure 7.1.9 Plot of the (•) 1019 cm^{-1} band intensity of dextran as a function of time of flow.

interspersed with series of alternating sequences. Each sugar subunit has a free carboxylic acid that has a pK_a near 3.3 at an ionic strength of 0.15 M.[36] At pH 7.0, the polysaccharide exists almost entirely in the ionized (carboxlyate) form and thus has a net negative charge. As with dextran, the polysaccharide rapidly accumulated at the surface of the IRE. The 1034 cm^{-1} band plateaued near 9 mAU after 60 min (Figure 7.1.10). The C-O band intensity dropped 84% in the first 20 min, indicating that most of the polysaccharide was not firmly bound. A desorption rate of -1.9×10^{-3} min^{-1} was calculated, and a film 2.2 Å thick was left remaining on the IRE after the rinse.

Gum Arabic

L-arabinose L-rhamnose D-galactose D-glucuronic acid protein

Gum arabic is a plant polysaccharide composed of the sugars arabinose, rhamnose, galactose and glucuronic acid. A protein component has been reported to be closely associated with this polysaccharide, possibly covalently linked.[37] When exposed to the bare Ge IRE, the 1080 cm^{-1} C-O band intensity of the polysaccharide plateaued in 60 min, reaching an intensity near 7 mAU (Figure 7.1.11). Protein adsorption (1547 cm^{-1}) did not plateau by the end of the initial 4-hr period, but did reach a maximum of 18 mAU. Virtually all the protein remained firmly bound to the surface of the IRE, as the Amide II band intensity only dropped 1 mAU during the rinse. The protein layer remaining on the IRE after the rinse was estimated at 34 Å (assuming an absorptivity similar to albumin). The desorption rate of the protein component was -2.9×10^{-3} min^{-1}. The polysaccharide component was less firmly bound. The 1080 cm^{-1} band dropped 78% during the initial phase of the 4-hr water rinse. However, some polysaccharide did remain firmly bound to the IRE. The desorption rate of the firmly bound polysaccharide component of gum arabic was -2.3×10^{-3} min^{-1}. The film thickness of the remaining gum arabic was 5 Å (assuming an absorptivity similar to alginic acid).

Dodecylbenzenesulfonic Acid (DBSA)

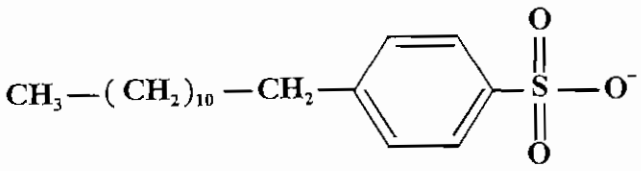

DBSA is an anionic surfactant with a negatively charged, para-substituted, sulfonate group on the benzene ring and a 12-carbon aliphatic tail. It was initially screened at a

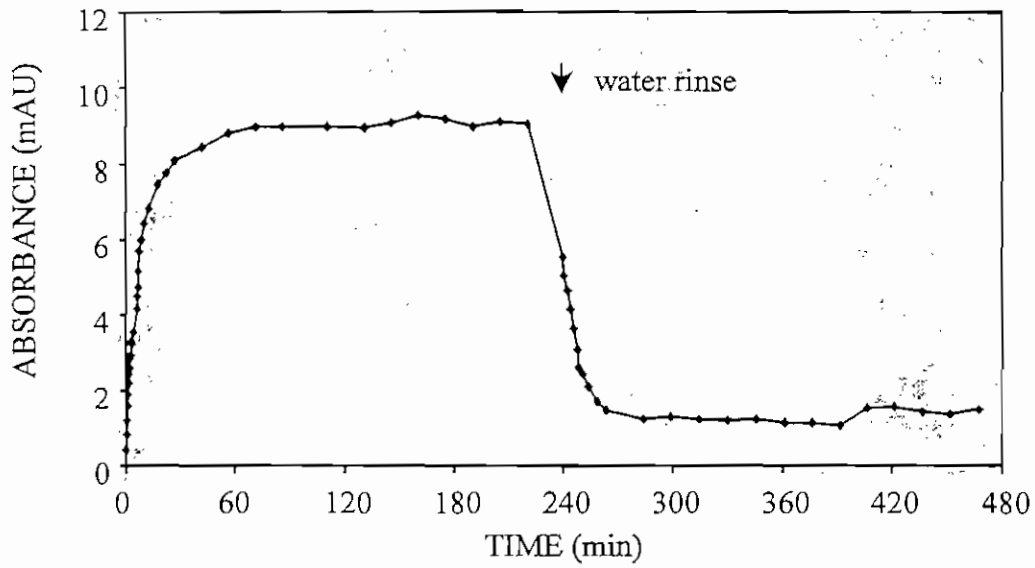

Figure 7.1.10 Plot of the (•) 1034 cm^{-1} band intensity of alginic acid as a function of time of flow.

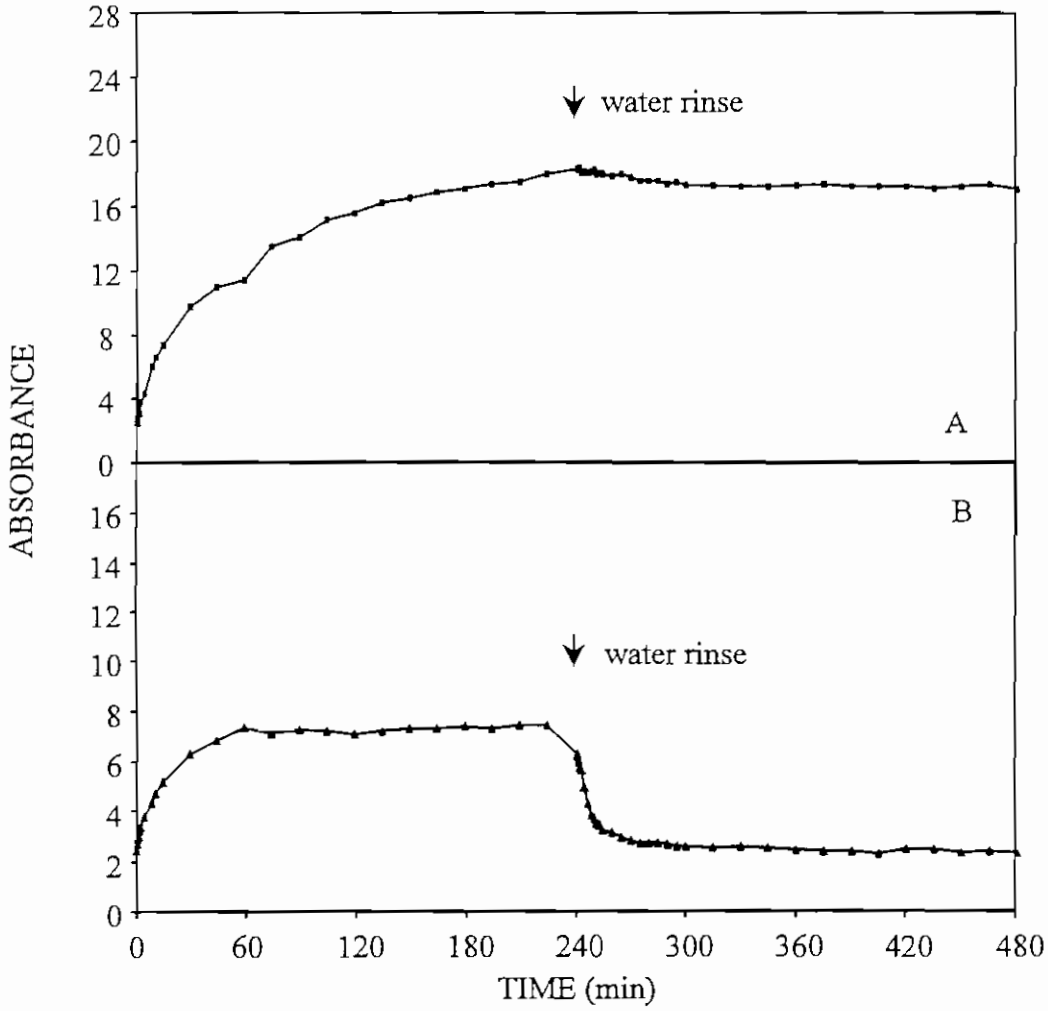

Figure 7.1.11 Plots of the (A) 1547 cm^{-1} Amide II and (B) 1080 cm^{-1} C-O stretching band intensities of gum arabic as a function of time of flow.

concentration of 0.25% and later at 0.5%. A significant amount of DBSA adsorbed to the Ge surface at 0.25%, as indicated by the increase in the 1178 cm^{-1} antisymmetric S-O stretching band and the 1136 cm^{-1} and 1009 cm^{-1} ring vibrations (Figure 7.1.12). The surfactant slowly desorbed from the IRE throughout the 4-hr rinse. A desorption rate of -12×10^{-3} min^{-1} was calculated, and a film thickness of 3.1 Å remained after the rinse.

When the concentration of DBSA was increased to 0.5%, similar adsorption kinetics were observed. However, more surfactant adsorbed to the Ge substrate at the higher concentration. The 1009 cm^{-1} band intensity neared a plateau at 8.4 mAU. The desorption rate kinetics were also very similar. A desorption rate constant of -8.5×10^{-3} min^{-1} was calculated based on the 1009 cm^{-1} band intensity. A film thickness of 5.7 Å remained after the rinse. At both concentrations, the intensity of the 1136 cm^{-1} ring mode leveled off during the rinse, while the other band intensities continued to drop. These results suggest that the benzene ring is more closely associated with the IRE surface than the other parts of the molecule.

Zwittergent 3-16

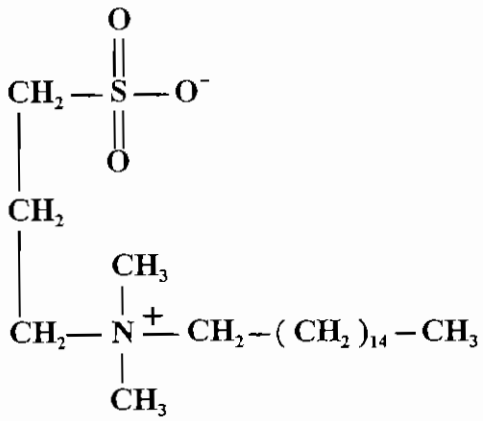

Zwittergent 3-16 (n-hexadecyl-N, N-dimethyl-3-ammonio-1-propanesulfonate) is a zwitterionic surfactant with a terminal sulfonate group and a quaternary amine. After filling the flow cell with sample solution (T = 0 min), there was a 15-min delay before a significant change in the band intensities associated with Zwittergent 3-16 adsorption was observed (Figure 7.1.13). After this brief lag period, surfactant began to accumulate on the surface of the IRE, as indicated by the increase in intensity of the 1468 cm^{-1}, $-CH_2$, $-CH_3$ deformation band and the 1186 cm^{-1}/1041 cm^{-1} antisymmetric/symmetric S-O stretching bands. None of the absorption bands plateaued before the end of the 4-hr period. Desorption of surfactant from the surface occurred in two phases which were defined as loosely bound and firmly bound Zwittergent 3-16. The three major band intensities dropped 52% between T = 250 min and the end of the experiment. The desorption rate of the most firmly bound Zwittergent 3-16 was -5.5×10^{-3} min^{-1}, and an estimated film thickness of 9.8 Å remained at the end of the rinse.

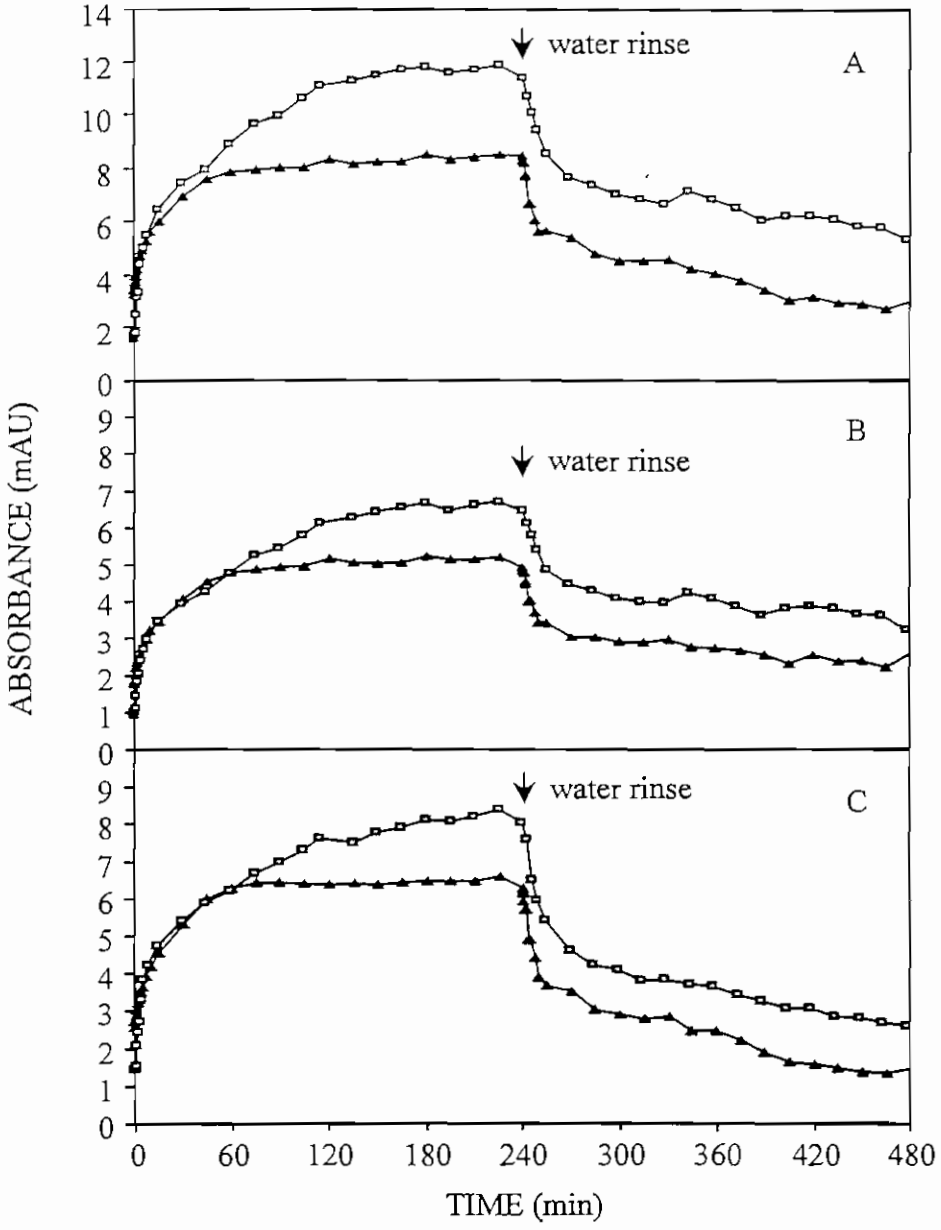

Figure 7.1.12 Plots of the (A) 1178 cm^{-1}, (B) 1136 cm^{-1} and C) 1009 cm^{-1} band intensities of DBSA as a function of time of flow at concentrations of (▲) 0.25% and (▫) 0.5% wt/vol.

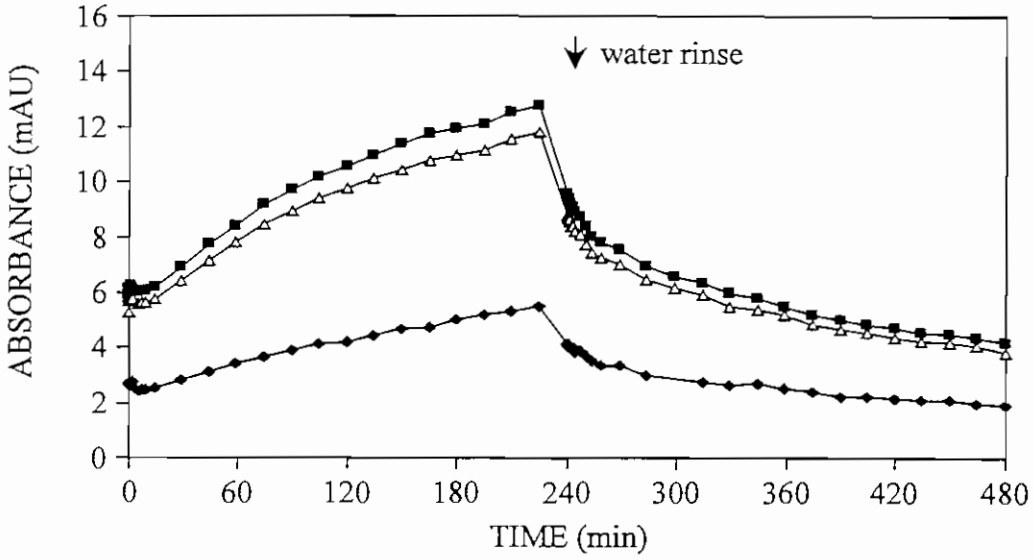

Figure 7.1.13 Plot of the (◆) 1468, (■) 1186 and (▲) 1041 cm^{-1} band intensities of Zwittergent 3-16 as a function of time of flow.

Triton X-100

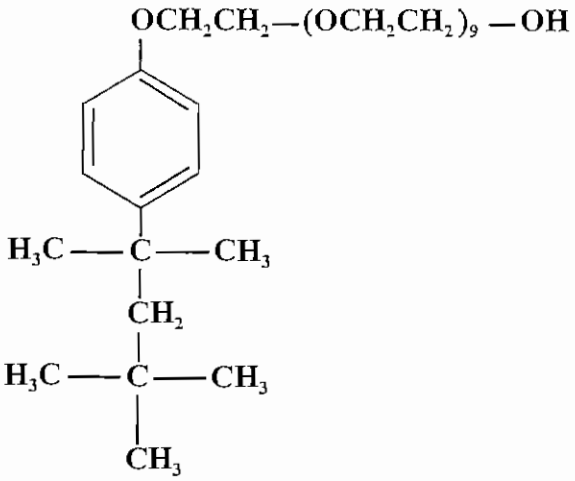

Triton X-100 (polyethylene glycol-*p*-isooctylphenyl ether) is a nonionic surfactant. As with Zwittergent 3-16, there was a delay (30 min at 0.1% and 60 min at 0.5%) before a detectable quantity of Triton X-100 began to accumulate at the surface of the IRE. At a concentration of 0.1%, the 1512 cm^{-1} semicircle stretching band of benzene reached a maximum of 1.6 mAU at the end of the initial 4-hr period (Figure 7.1.14A). The 1512 cm^{-1} band dropped rapidly at the start of the rinse. However, this was primarily due to the loss of bulk phase Triton X-100 from the flow cell. Some surfactant did remain adsorbed to the Ge surface following the rinse. The film thickness was estimated at 2.6 Å. At 0.5% the 1512 cm^{-1} band plateaued near 18 mAU after 210 min (Figure 7.1.14B). Very little material desorbed from the Ge surface, as the 1512 cm^{-1} band only dropped 14% following the 4-hr rinse. A desorption rate of -3.2 x 10^{-3} min^{-1} was calculated for the firmly bound material. The thickness of the film remaining on the IRE after the rinse was estimate at 80 Å.

Benzalkonium Chloride

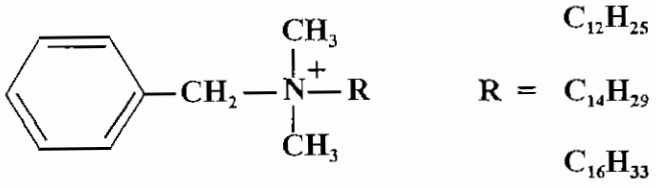

Benzalkonium chloride is a cationic quaternary amine with a methyl benzene group and a mixture of 12-, 14- and 16-carbon aliphatic chains. Benzalkonium chloride rapidly adsorbed to the Ge surface, approaching near-maximum levels after approximately 30 min (Figure 7.1.15). Both 1487 cm^{-1} and 1473 cm^{-1} C-H deformation bands pleateaued near

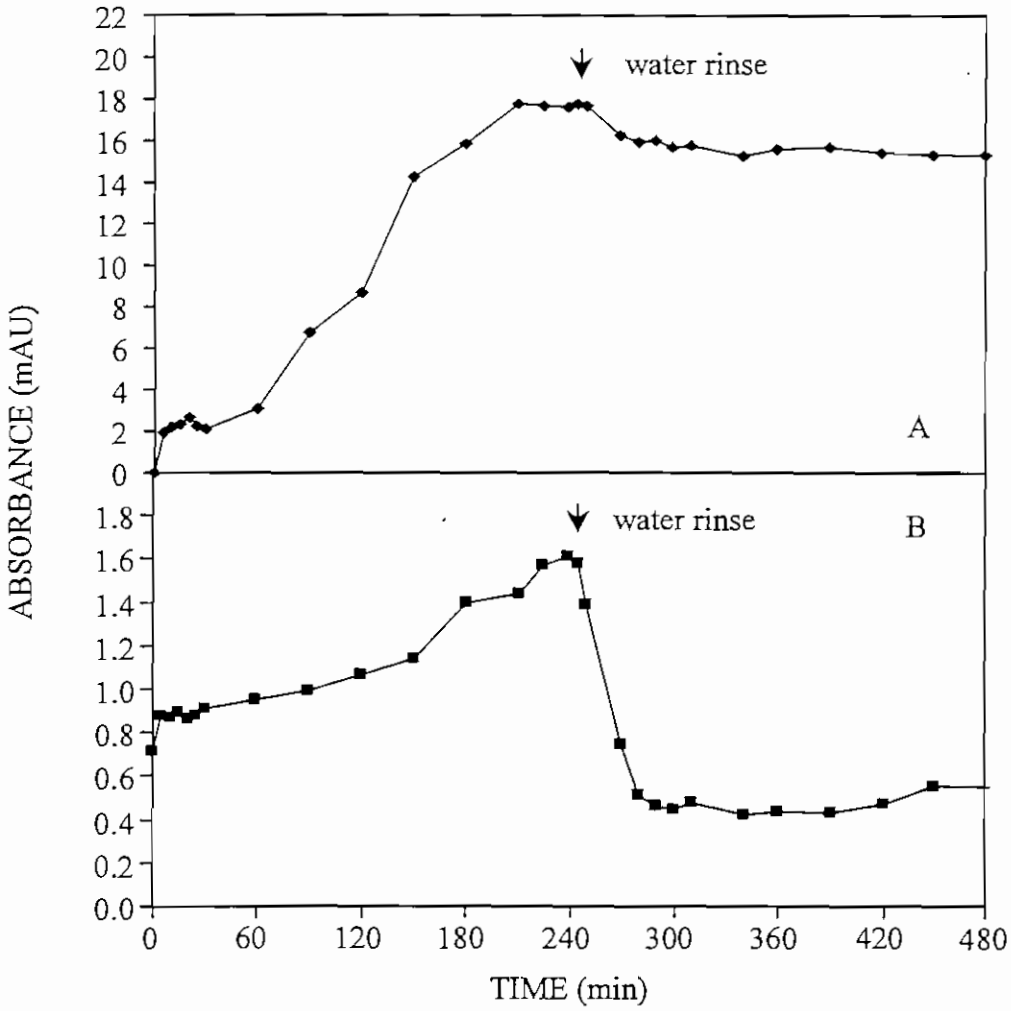

Figure 7.1.14 Plots of the 1512 cm^{-1} band intensity of Triton X-100 as a function of time of flow at (A) 0.5% and (B) 0.1%.

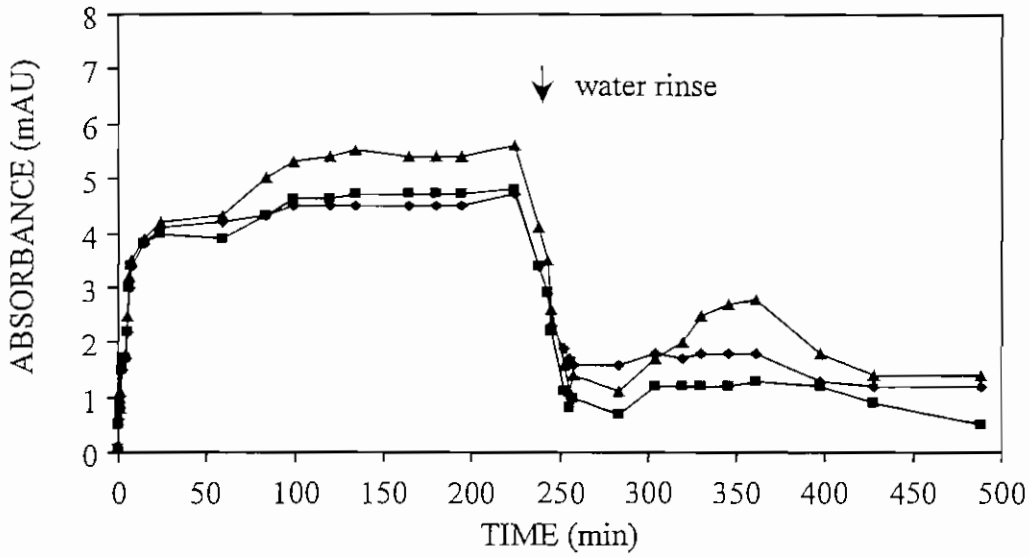

Figure 7.1.15 Plot of the (◆) 1487, (■) 1473 and (▲) 1457 cm^{-1} band intensities of benzalkonium chloride as a function of time of flow.

4.5 mAU. These bands dropped rapidly at the start of the water rinse; however, a measurable quantity of material remained at the Ge surface at the end of the 4-hr rinse. The estimated film thickness was 5.9 Å. The IR data from the rinse was too noisy to calculate a desorption rate constant.

Summary

Each of the compounds had at least one IR vibrational band that could be used to monitor molecular adsorption onto CA thin films. A list of these vibrational bands is shown in Table 7.1.1. Desorption rate constants were calculated by fitting the data to a linear regression line. Data from the first 15 min of the rinse was not included as the flow cell took approximately 10 min to turn over one volume. During this time loosely bound organics and organics in the bulk phase were flushed from the flow cell. The thickness of the organic film left on the IRE surface was calculated. The desorption rate constants and thickness of the adsorbed films are summarized in Table 7.1.2. Proteins and Triton X-100 adhered to the greatest extent based on the calculated thickness of the adsorbed film. The remaining surfactants fell in the middle, and the polysaccharides were grouped at the end. There was no adsorption trend with respect to the net charge on the surfactants, i.e., nonionic surfactants didn't adsorb to a greater extent than all cationic or anionic surfactants.

Table 7.1.1

Infrared Vibrational Bands of Organic Compounds
for Use in Adsorption Studies on Thin Films of Cellulose Acetate

Organic Compound	**Vibrational Band (cm^{-1})**
EDTA	1400
Hexylglucopyranoside	1040, 1379
MEGA 10	1412
Genapol C-100	1350
Albumin	1547
Dextran	1159
Alginic Acid	1416
Gum Arabic	1547, 1080
Dodecylbenzenesulfonic Acid	1009
Zwittergent 3-16	1468
Triton X-100	1512
Benzalkonium Chloride	1487, 1473, 1457

Table 7.1.2

Desorption Rate Constants and Film Thickness of Organic Molecules on Germanium Internal Reflection Element

Organic Compound	**Properties**	**Desorption Rate Constant x 10^{-3} (min^{-1})**	**Film Thickness After Rinse (Å)**
Triton X-100 (0.5% w/v)	nonionic surfactant	-3.3	80
Bovine Serum Albumin	acidic protein $pK_a = 4.8$	-10	61
Gum Arabic (protein component)	polysaccharide (w/ protein)	-2.9	34
Genapol C-100	nonionic surfactant	-3.0	33
EDTA (Teflon® flow cell)	anionic / metal chelating agent	NA	13
Zwittergent 3-16	zwitterionic surfactant	-5.5	9.4
Benzalkonium Chloride	cationic surfactant	-2.0	5.9
MEGA 10	nonionic surfactant	-1.7	5.8
DBSA	anionic surfactant	-8.5	5.7
Gum Arabic (polysaccharide component)	polysaccharide (w/ protein)	-2.3	5.0
DBSA	anionic surfactant	-12	3.1
Triton X-100 (0.1% w/v)	nonionic surfactant	NA	2.6
Alginic Acid	acidic polysaccharide	-1.9	2.2
Dextran	neutral polysaccharide	-1.5	2.2
EDTA (stainless steel flow cell)	anionic metal chelating agent	-4.8	<1

NA—not available

Section 7.2 Cellulose Acetate Mid-Infrared Spectrum

Cellulose acetate is a linear polysaccharide composed of β(1→4) linked glucose subunits. The hydroxyl groups on each subunit may be acetylated to form di- or triacetates. Commercial RO membranes are typically made of a blend of polymers with an average acetyl content of 42% by weight. The molecular structure of a dissacharide subunit of CA with a triacetate and a diacetate of glucose is shown in Figure 7.2.1. A mid-IR (4000 – 800 cm^{-1}) spectrum of cellulose acetate (42% acetyl) cast on a Ge IRE is shown in Figure 7.2.2. The baseline was offset to zero absorbance at 4000, 1338, 1306 and 964 cm^{-1}. No correction for the wavelength dependence of internal reflection was made since the film thickness was significantly less than the depth of penetration of the evanescent wave. The IR spectrum was very similar to those reported by other labs.[38,39] An enlarged region of the spectrum between 4000 cm^{-1} and 2600 cm^{-1} is shown in Figure 7.2.2 (inset). The broad band centered near 3500 cm^{-1} represents the O-H stretching band, and the 2900 cm^{-1} and 2850 cm^{-1} bands represent the CH_2 antisymmetric and symmetric stretching bands. The area of most interest to this study lies between 2000 and 800 cm^{-1}, the fingerprint region of the spectrum (Figure 7.2.3). The four major vibrational bands in this region are the 1749 cm^{-1} C=O carbonyl band, the 1369 cm^{-1} C-H deformation band, the 1230 cm^{-1} C-O-C acetate ester band and the 1049 cm^{-1} C-O sugar backbone band. The thin film spectrum was very similar to the ATR (contact mode) spectrum of a standard CA membrane measured in the lab.

Section 7.3 Stability of CA Thin Films Cast on Ge IRE

The effect of long-term exposure to water and the effect of changing ionic strength on the physical integrity and vibrational structure were investigated. Thin films of CA dip-cast onto Ge IREs were exposed to deionized water and NaCl solutions of increasing (1, 5 and 10%) concentration.

Hydration of CA Thin Film

Deionized water (pH 7) was pumped through a flow cell containing a CA(42% acetyl)-coated IRE. IR spectra were collected over a 22 hr period and are shown in Figure 7.3.1. The four major IR band intensities of CA are plotted as a function of time of flow in Figure 7.3.2A. Upon exposure to deionized water, all four CA band intensities dropped rapidly. After 30 min, a much slower rate of change was observed. Between T = 6 hr and T = 10 hr, the rate of change of all CA band intensities dropped again and then a slightly lower desorption rate was recorded to the end of the 22-hr experiment. The four bands dropped concurrently between 77 - 79% over the 22-hr period (Table 7.3.1). These results indicate that the dry film swelled and physically separated from the Ge substrate upon hydration. A typical CA membrane only expands about 10% upon hydration.[40] Therefore, something other than normal polymer expansion from hydration must have occurred. Essentially all of the CA in contact with the aqueous solution appeared to physically separate from the IRE, as 70% of the CA-coated surface area is in contact with water.

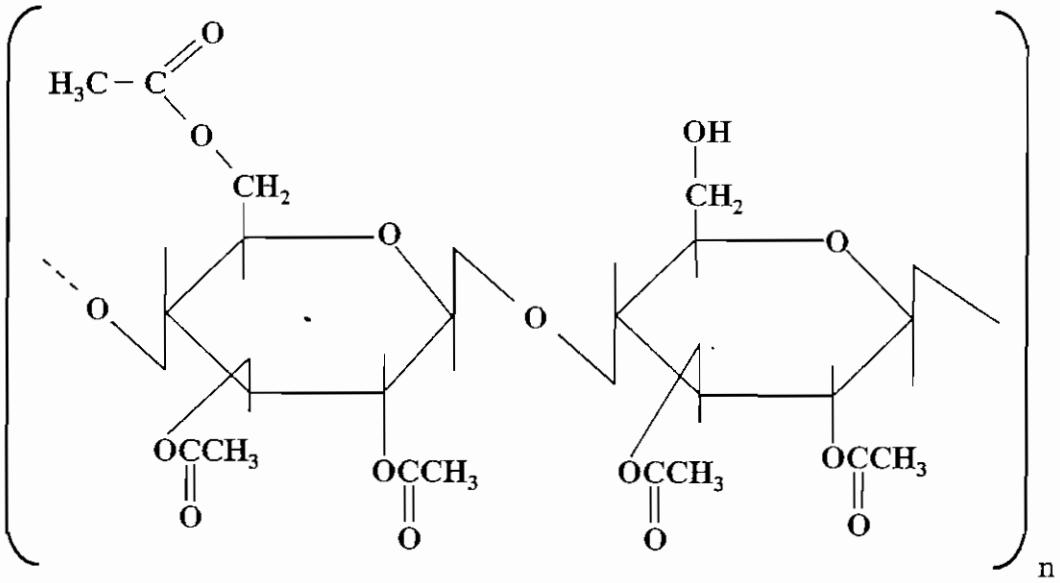

Figure 7.2.1 Disaccharide subunit of cellulose acetate polymer with triacetate (left) and diacetate (right).

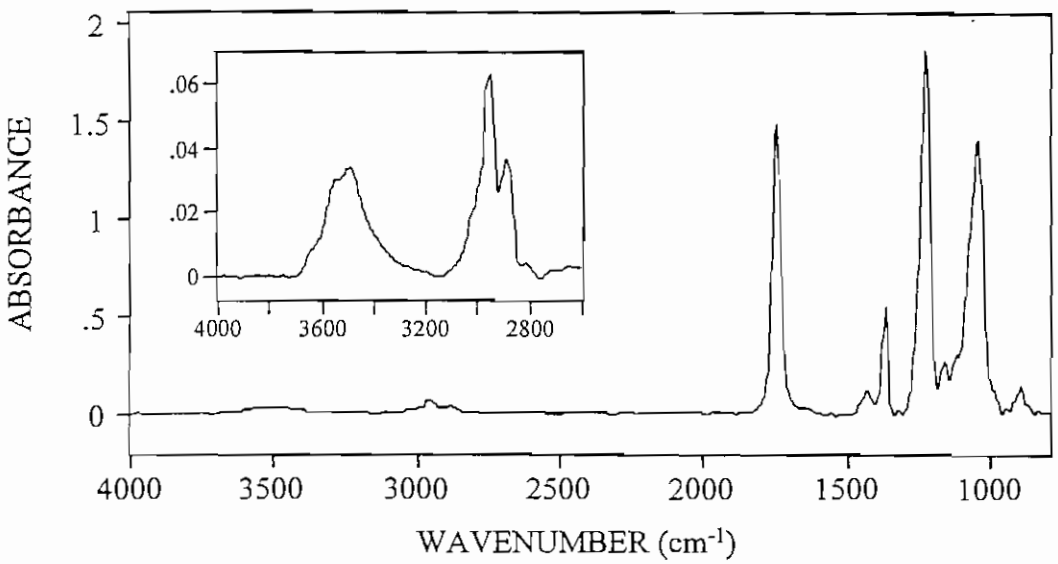

Figure 7.2.2 Mid-infrared ATR spectrum (4000 - 800 cm^{-1}) of a thin film of CA(42% acetyl) cast on a Ge IRE.

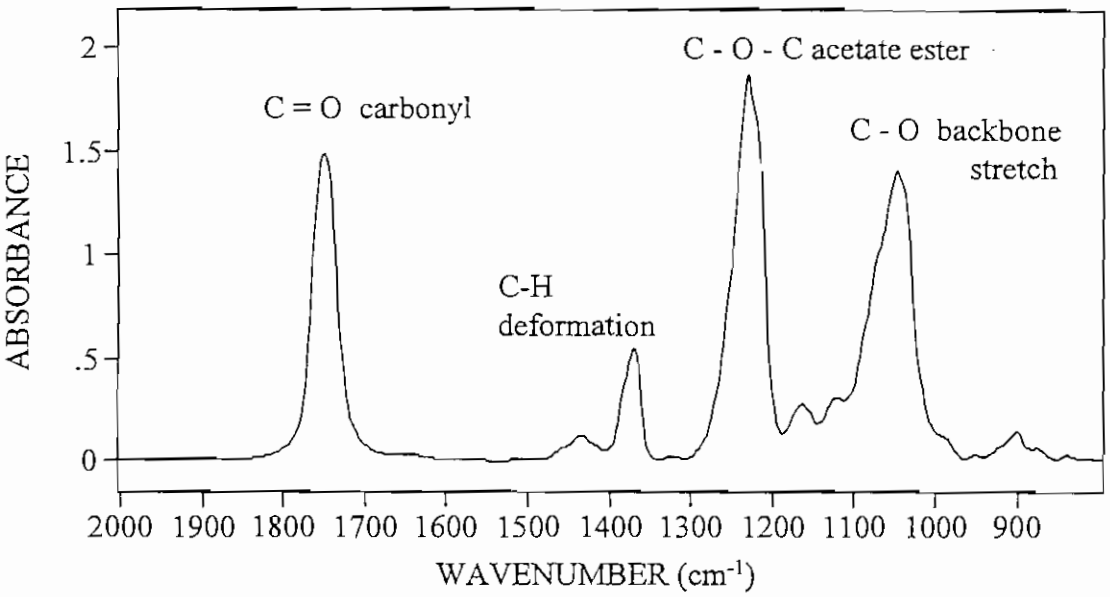

Figure 7.2.3 Mid-infrared ATR spectrum (2000 - 800 cm^{-1}) of a thin film of CA(42% acetyl) cast on a Ge IRE.

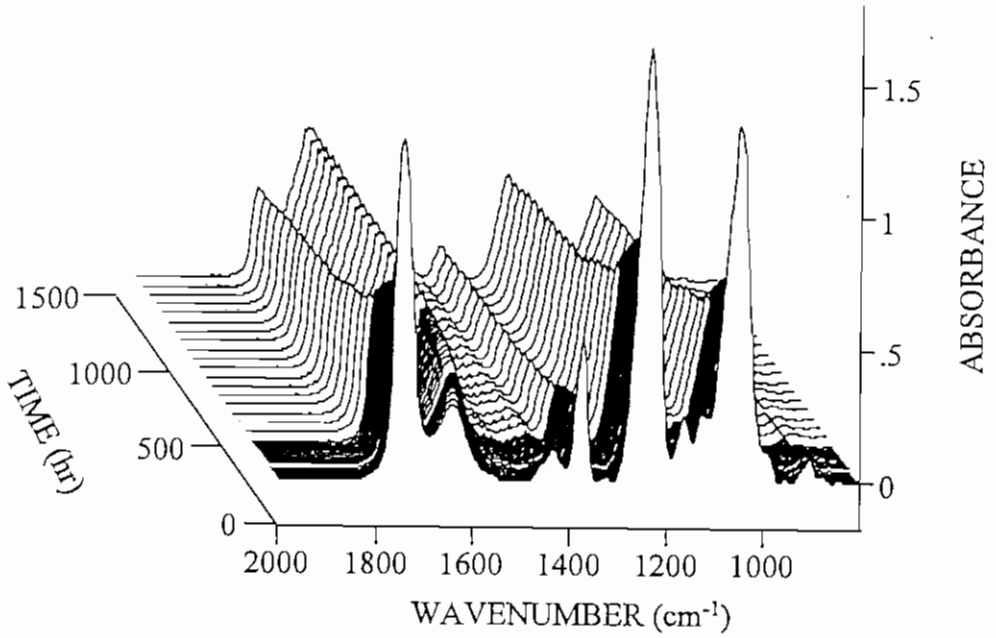

Figure 7.3.1 ATR spectra of CA(42% acetyl) thin film cast on a Ge IRE and exposed to deionized water at pH 7.

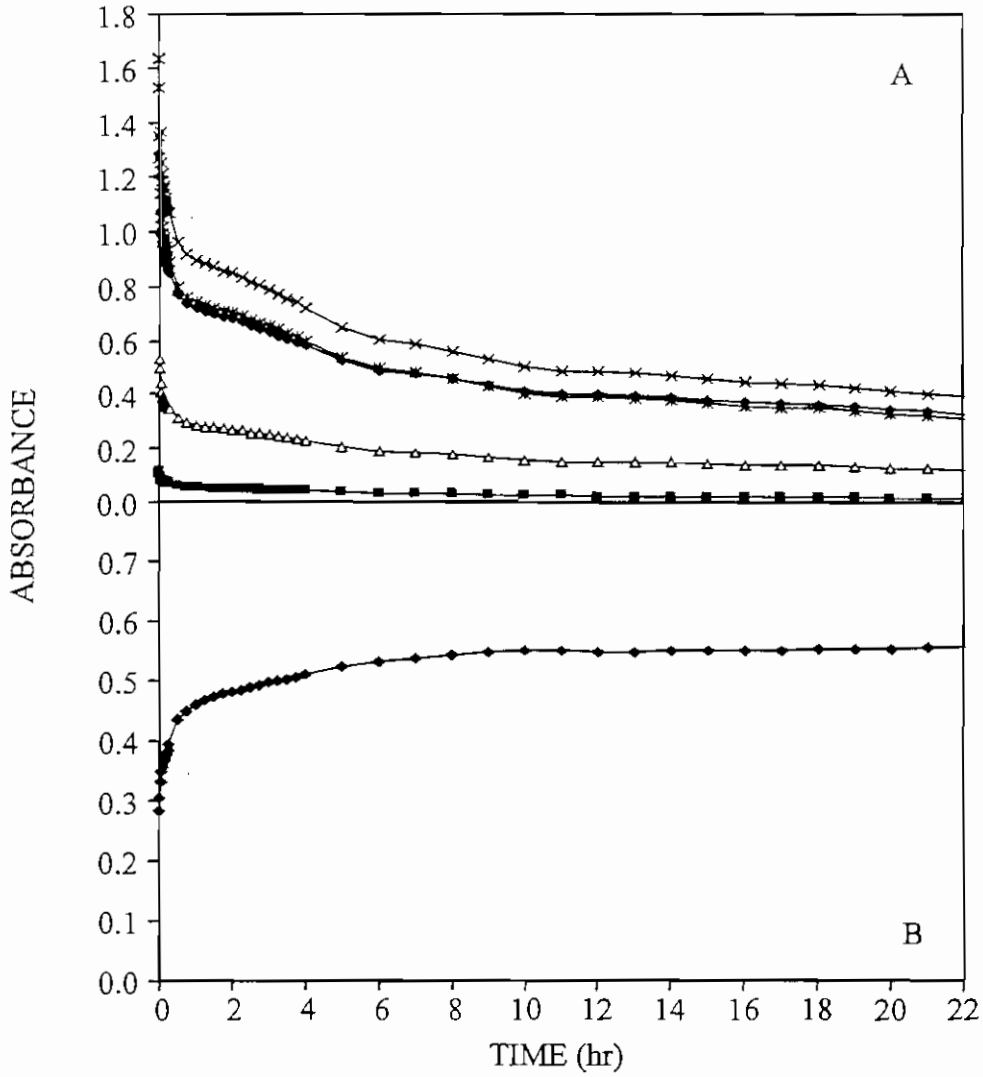

Figure 7.3.2 Plots of the (◆) 1744, (■) 1433, (▲) 1369, (×) 1232 and (✱)1049 cm^{-1} band intensities of (A) cellulose acetate (42% acetyl) and (B) the 1639 cm^{-1} water band intensity as a function of time of flow.

The intensity of the 1639 cm^{-1} water band intensity is plotted as a function of time of flow in Figure 7.3.2B. At T = 0 min, a water band intensity of 0.284 AU was measured. The 1639 cm^{-1} band intensity increased rapidly during the first 45 min. Between T = 60 hr and T = 10 hr, the rate of increase dropped, and the 1639 cm^{-1} band eventually stabilized near 0.56 AU. The water band intensity measured with a bare Ge IRE (50 x 10 x 2 mm) is typically 0.698 ± 0.038 AU (± std. dev., n = 17). The greatest water band intensity measured with the CA-coated Ge IRE was 0.558 AU, 80% of the maximum possible value. Therefore, some CA was still in contact with the IRE or, at the least, still within the depth of penetration of the evanescent wave.

Table 7.3.1

Effect of Hydration on Cellulose Acetate Thin Film
Cast on Ge IRE

Sample	**1747 cm^{-1}**	**1369 cm^{-1}**	**1234 cm^{-1}**	**1049 cm^{-1}**	**1639 cm^{-1}**
Dry CA	1.484 AU	0.542 AU	1.870 AU	1.399 AU	---
Wet CA (T = 0 hr)	---	---	---	---	0.284 AU
Wet CA (T = 22 hr)	0.336	0.124	0.395	0.314	0.558
% Change (after hydration)	-77%	-77%	-79%	-76%	+96%
CA (Dried)	1.439	0.530	1.786	1.329	---
% Change (after drying)	-3%	-2%	-4%	-5%	---

The kinetic plot of the water band intensity is inversely related to the plot of the CA bands, i.e., at every point where the water band intensity increased, the CA band intensities decreased. These results indicate that the polymer was displaced from the surface of the IRE and immediately replaced by water. As discussed in Section 5, the electric field intensity drops as a function of distance from the interface, and the measured band intensities are proportional to the electric field intensity. Thus, the CA film moved farther from the surface of the IRE, and the CA band intensities dropped. In turn, water passed through the film

occupying the void space left by the CA, and the water band intensity increased (see Figure 7.3.2B). If the CA film is displaced by water and distends from the Ge surface beyond d_p, then a water band of approximately 0.7 AU should be observed.

Significant changes in the vibrational spectrum of CA were observed upon hydration. The carbonyl band shifted to lower wavenumber, moving 2 cm^{-1} from 1749 cm^{-1} to 1747 cm^{-1}. The C-O-C acetate ester band shifted to higher wavenumber, moving 2 cm^{-1} from 1230 cm^{-1} to 1232 cm^{-1}. Similar shifts in frequency have been reported by Toprak and coworkers.[41] These frequency shifts occur as a result of hydrogen bond formation with the carbonyl group on CA. When the wet CA film was dried by purging the flow cell with dry air, both bands shifted back to their higher wavenumber position. All CA bands returned to within 2 to 5% of their pre-hydrated intensities (Table 7.3.1). Several more experiments were run with similar results (data not shown). The CA-coated IREs were examined after each control experiment to determine if the thin film was still intact. The polymer-coated IREs were removed from the flow cell and placed in a petri dish of water. A Pasteur pipet was used to manipulate the CA film. In most cases, the thin films were still physically intact, i.e., void of rips or tears. There were usually small areas of the film not in direct contact with the surface of the IRE. However, areas on the CA film typically had to be peeled from the IRE surface. Since the films were intact, work with the CA-coated Ge IREs continued.

Effect of Changing Ionic Strength on CA Thin Films

A thin film of CA was exposed to sodium chloride solutions of varying concentration to determine its stability in solutions of varying ionic strength. A CA(42% acetyl)-coated IRE was placed in a flow cell and hydrated with deionized water (pH 7). All CA band intensities dropped immediately upon exposure to water. The rate and the extent to which each band dropped (Figure 7.3.3A) were greater than previously observed (see Figure 7.3.2). The CA film appeared to stabilize after 11 hr. The changes in the water band intensity were inversely related to the changes in CA band intensities. The 1639 cm^{-1} band intensity rose rapidly over the first 1 hr, tapered off and plateaued near 0.61 AU after approximately 11 hr (Figure 7.3.3B).

1% NaCl Addition. After 24-hr exposure to deionized water, a 1% NaCl solution was pumped through the flow cell. The four major CA band intensities increased between 61 and 143% upon addition of the salt solution (Figure 7.3.4A), while the water band intensity dropped 4% from 0.616 to 0.592 AU (see Figure 7.3.4B and Table 7.3.2). As time passed, the CA band intensities returned to levels recorded prior to the NaCl addition.

These results indicate that the film of CA does not remain physically attached to the Ge surface but exists in a dynamic state and responds to changes in ionic strength. If the thin film is viewed as a free-floating membrane where water is allowed to pass through the film into an area between the film and the IRE, the data is more easily interpreted. When water in the flow cell is displaced by the salt solution, water diffuses from within the space between the IRE and the film, back through the film and into the bulk aqueous phase. As a result, the film collapses onto the IRE, where the electric field intensity is much greater, and thus the CA band intensities increase. As time passes, the water and Na^+ and Cl^- ions in the bulk

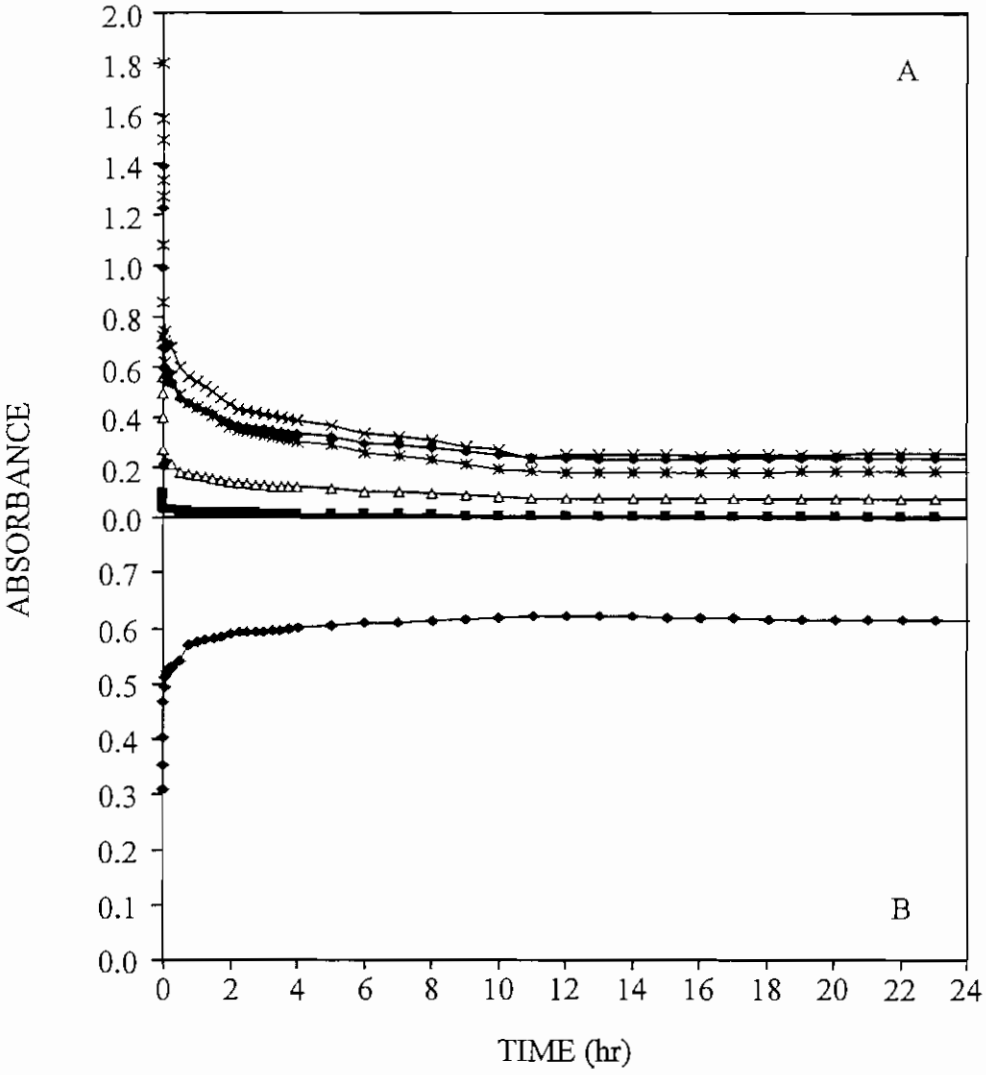

Figure 7.3.3 Hydration of cellulose acetate. Plots of the (◆) 1747, (■) 1433, (▲) 1369, (×) 1232 and (×) 1049 cm^{-1} band intensities of (A) cellulose acetate (42% acetyl) and (B) the 1639 cm^{-1} water band intensity as a function of time of flow.

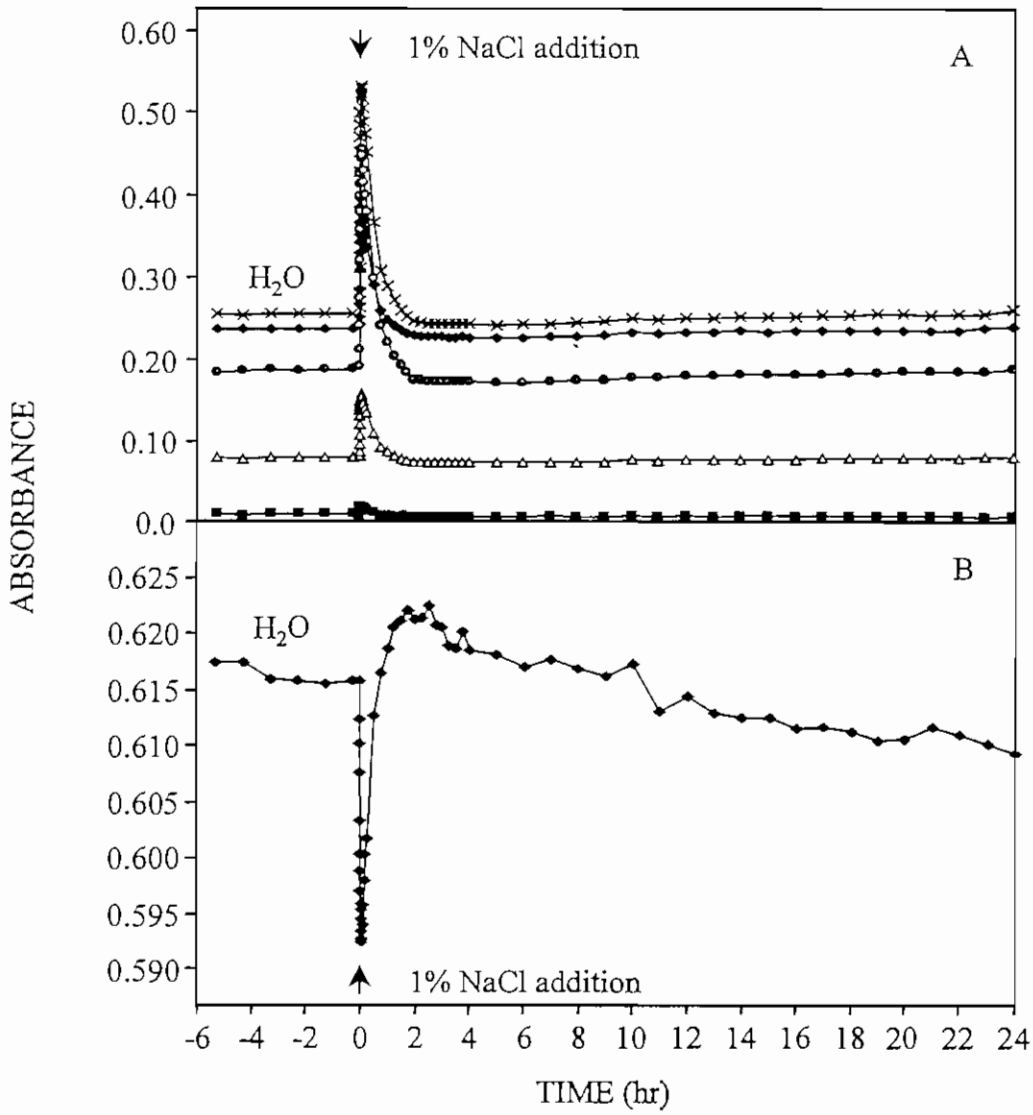

Figure 7.3.4 1% NaCl Addition. Plots of the (•) 1747, (▪) 1433, (▵) 1369, (×) 1232 and (•) 1049 cm^{-1} band intensities of (A) cellulose acetate (42% acetyl) and (B) the 1639 cm^{-1} water band intensity as a function of time of flow.

Table 7.3.2

Percent Change in Cellulose Acetate IR Band Intensities
as a Result of Exposure to NaCl Solutions and Water Rinses

Treatment	1747 cm^{-1} C=O	1369 cm^{-1} CH_2	1234 cm^{-1} C-O-C	1049 cm^{-1} C-O	1639 cm^{-1} H_2O
Hydration	-85%	-86%	-88%	-88%	NA
1% NaCl	+61	+97	+108	+143	-4%
1st H_2O rinse	-4.0	-7.0	-6.7	-8.4	NC
3.5% NaCl	+234	+331	+328	+470	-16
2nd H_2O rinse	-1.6	-2.9	-3.8	-6.3	-3.6
10% NaCl	+289	+384	+378	+470	-19
3rd H_2O rinse	-18	-25	-24	-29	-6.4

NC—no change
NA—not applicable

phase slowly diffuse through the polymer film into the space between the film and IRE, reestablishing a new equilibrium state. The drop of CA band intensities back to values observed prior to NaCl addition might be related to physical or mechanical constraints placed on the film by the O-ring seal. The polymer's inherent tendency to attain the most relaxed conformation may also be a factor in the observed changes.

First Water Rinse. After 24-hr exposure to 1% NaCl, the CA film was rinsed with deionized water. Water was rapidly siphoned through until one cell volume was displaced and then pumped at 8 mL/hr. The four major CA band intensities are plotted as a function of time of flow in Figure 7.3.5A. Data from 5.25 hr before the switch from 1% NaCl to deionized water are shown. The time of T = 0 hr represents the start of the water rinse. The CA bands dropped between 4 and 8% after the start of the water rinse but remained unchanged throughout the remaining 6-hr period (Table 7.3.2). The 1639 cm^{-1} band increased 1.3% from 0.609 to 0.617 AU at T = 0 hr but returned to an intensity near 0.609 AU 15 min later (Figure 7.3.5B).

When NaCl was displaced from the flow cell during the water rinse, the equilibrium conditions were altered. Water diffused through the thin film from the bulk phase, causing it to distend farther from the IRE. As the film moved farther from the IRE surface, it became positioned where the electric field was less intense. Therefore, the CA bands dropped in intensity. Once equilibrium was reestablished, the band intensities remained unchanged.

3.5% NaCl Addition. After the first rinse, a 3.5% NaCl solution was pumped through the flow cell. Within 3 min of exposure to the salt solution, a 2- to 4- fold increase

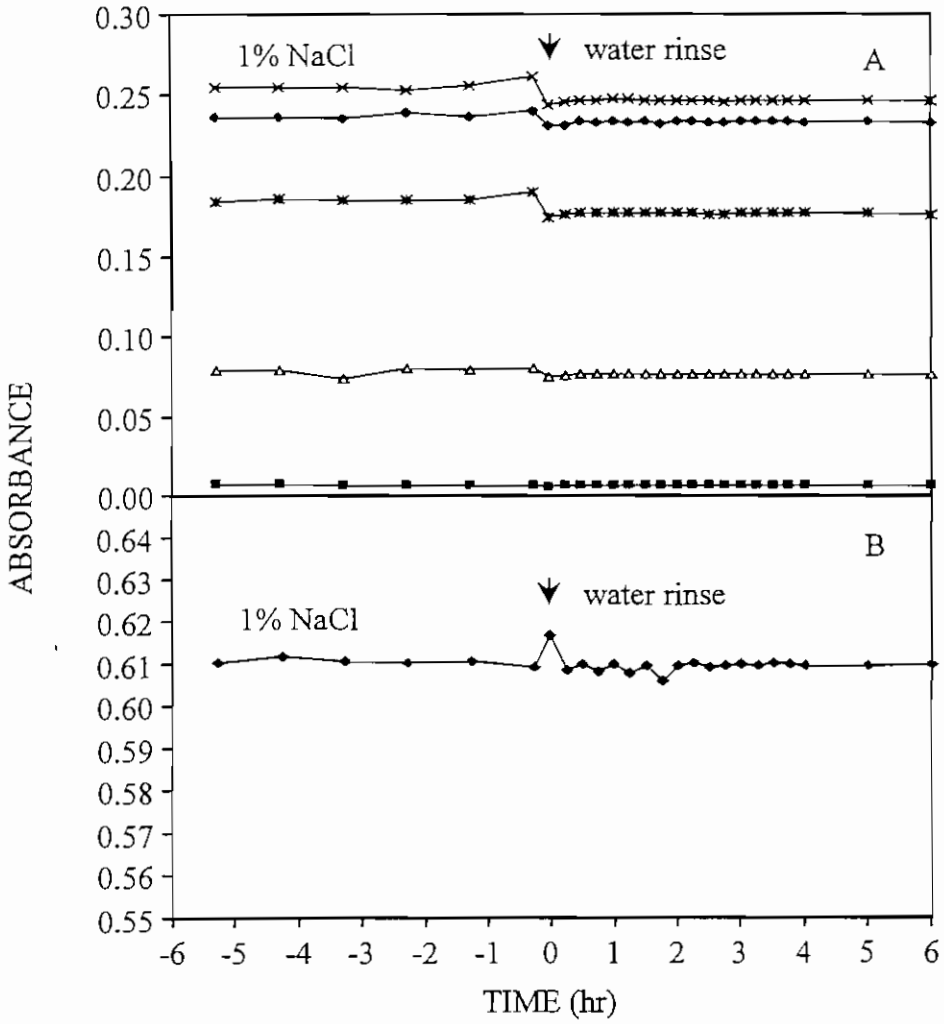

Figure 7.3.5 First water rinse. Plots of the (◆) 1747, (■) 1433, (▲) 1369, (×) 1232 and (✱) 1049 cm^{-1} band intensities of (A) cellulose acetate (42% acetyl) and (B) the 1639 cm^{-1} water band intensity as a function of time of flow.

in all CA band intensities was observed, with greater changes occurring at lower frequencies (see Figure 7.3.6A and Table 7.3.2). All CA bands slowly dropped in intensity, eventually returning to the levels recorded prior to the NaCl addition. The rate at which the band intensities dropped was significantly slower at 3.5% NaCl as compared to 1%. While the CA band intensities increased, the 1639 cm^{-1} band intensity decreased, dropping 16% from 0.610 to 0.509 AU in 1.77 min (Figure 7.3.6B). The water band gradually returned to an intensity that fluctuated near 0.627 AU.

The same series of events occurred when the deionized water was replaced by 3.5% NaCl. Water trapped between the thin film and the IRE diffused through the CA into the bulk phase, causing the polymer film to collapse onto the IRE. As a result, the intensities of the CA bands increased. With time, water and Na^+ and Cl^- ions slowly diffused through the thin film, reestablishing an equilibrium condition while the CA bands dropped in intensity.

Second Water Rinse. After 24-hr exposure to the salt solution, water was siphoned through, displacing one flow cell volume, then pumped through at 8 mL/hr. All four CA bands dropped sharply between 2 and 12 mAU, then rapidly increased in intensity, approximately 5 mAU above those measured before the water addition (Figure 7.3.7A). The water band dropped 3.6% after approximately 15 min and remained unchanged for the remainder of the 6-hr rinse period (Figure 7.3.7B). These changes in the water band intensity were consistent with the observed increase in the CA band intensities, which indicates that the film collapsed onto the IRE displacing water at the interface.

10% NaCl Addition. Following the second water rinse, a 10% NaCl solution was pumped through the flow cell. Again, there was a rapid increase in all the CA band intensities (Figure 7.3.8A). The four major CA bands increased 3- to 4-fold within 2.5 min (Table 7.3.2.). These bands immediately began to drop in intensity, at first quite rapidly and then more gradually up to T = 6 hr. The CA band intensities appeared to stabilize between T = 6 hr and T = 24 hr but actually dropped at a rate of 0.7 - 2.0 mAU/hr during this time (Table 7.3.3). After 24 hr exposure to 10% NaCl, the CA bands were 9 to 20% above the intensity recorded at the end of the second rinse. The water band intensity increased at a rate of 0.4 mAU/hr and was 7% above the intensity prior to NaCl addition (Figure 7.3.8B).

Third Water Rinse. After exposure to the salt solution, the CA film was rinsed a final time with deionized water. All CA band intensities dropped between 18 and 29% (Table 7.3.2) and remained stable throughout the 6-hr rinse (Figure 7.3.9A). The 1639 cm^{-1} water band dropped 6.4% after the start of the water rinse, which was unexpected since the CA band intensities all dropped (Figure 7.3.9B). The water band should have increased in response to the drop in CA band intensities.

Summary

The thin CA film cast on the Ge IRE appears to act as an osmotic pressure cell. At the start of the experiment, the dry CA film absorbed water and physically separated from the surface of the IRE. The magnitude of the changes in band intensities was too great to be associated solely with polymer swelling upon hydration (see Table 7.3.2). Therefore, it is believed that the thin film detaches from the surface, forming an osmotic cell. When the CA

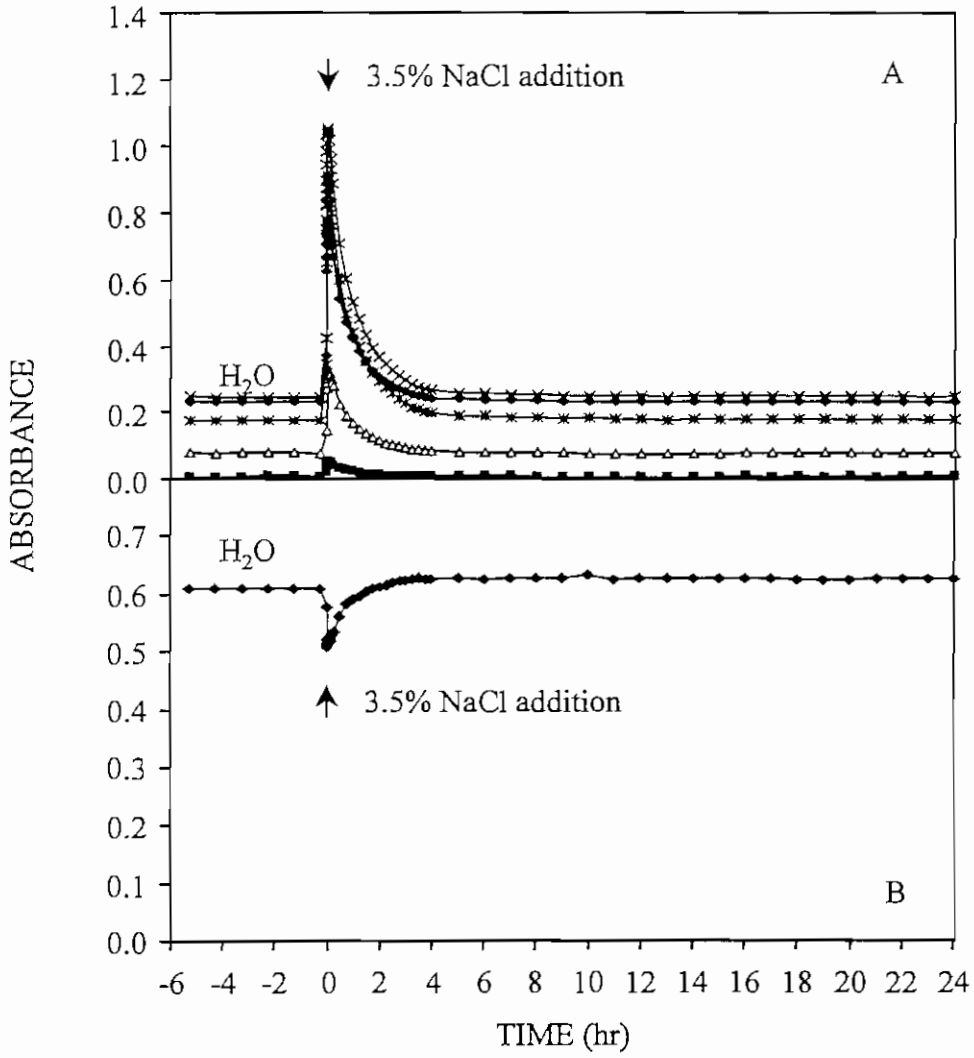

Figure 7.3.6 3.5% NaCl Addition. Plots of the (◆) 1747, (■) 1433, (▲) 1369, (×) 1234 and (✱) 1049 cm^{-1} band intensities of (A) cellulose acetate (42% acetyl) and (B) the 1639 cm^{-1} water band intensity as a function of time of flow.

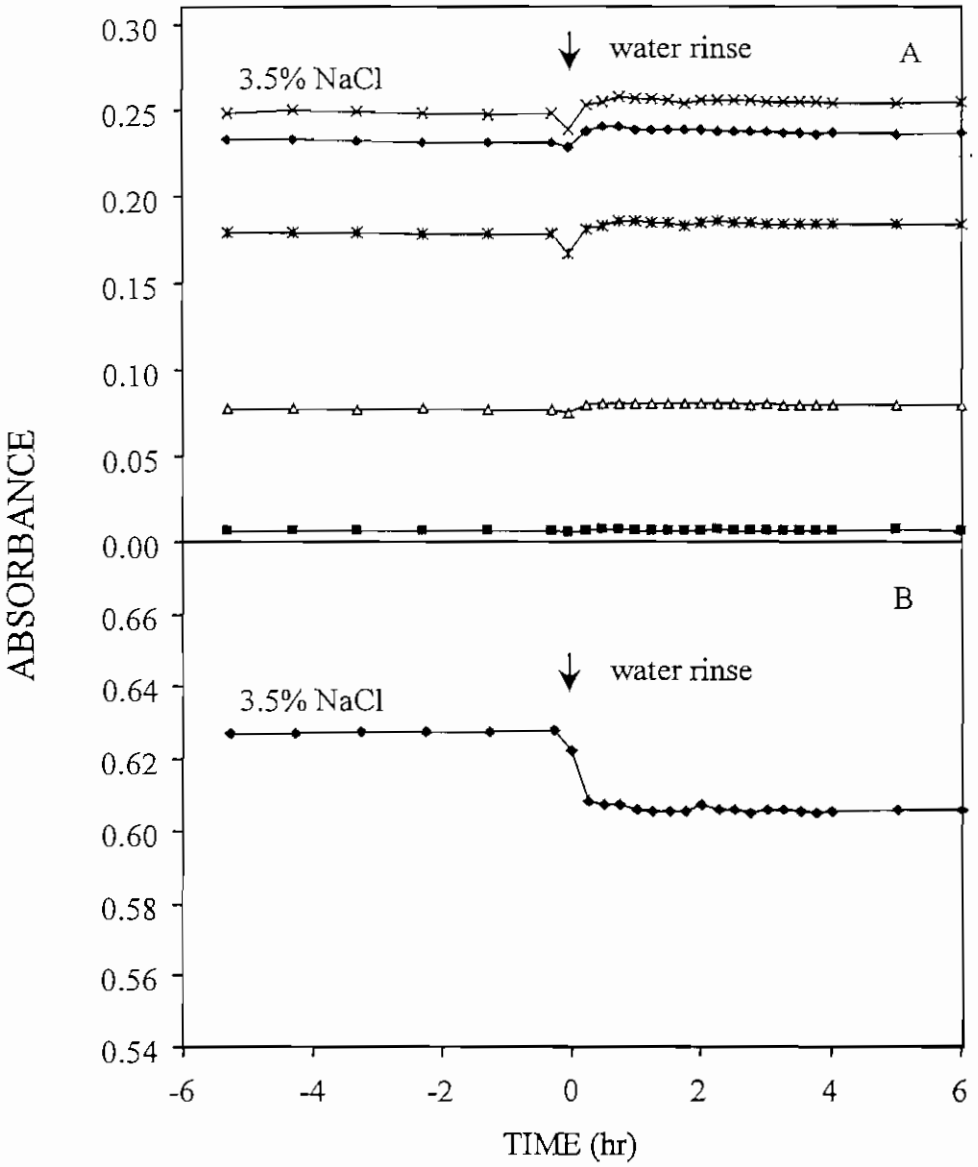

Figure 7.3.7 Second water rinse. Plots of the (◆) 1747, (■) 1433, (▲) 1369, (×) 1234, and (✱) 1049 cm^{-1} band intensities of (A) cellulose acetate (42% acetyl) and (B) the 1639 cm^{-1} water band intensity as a function of time of flow.

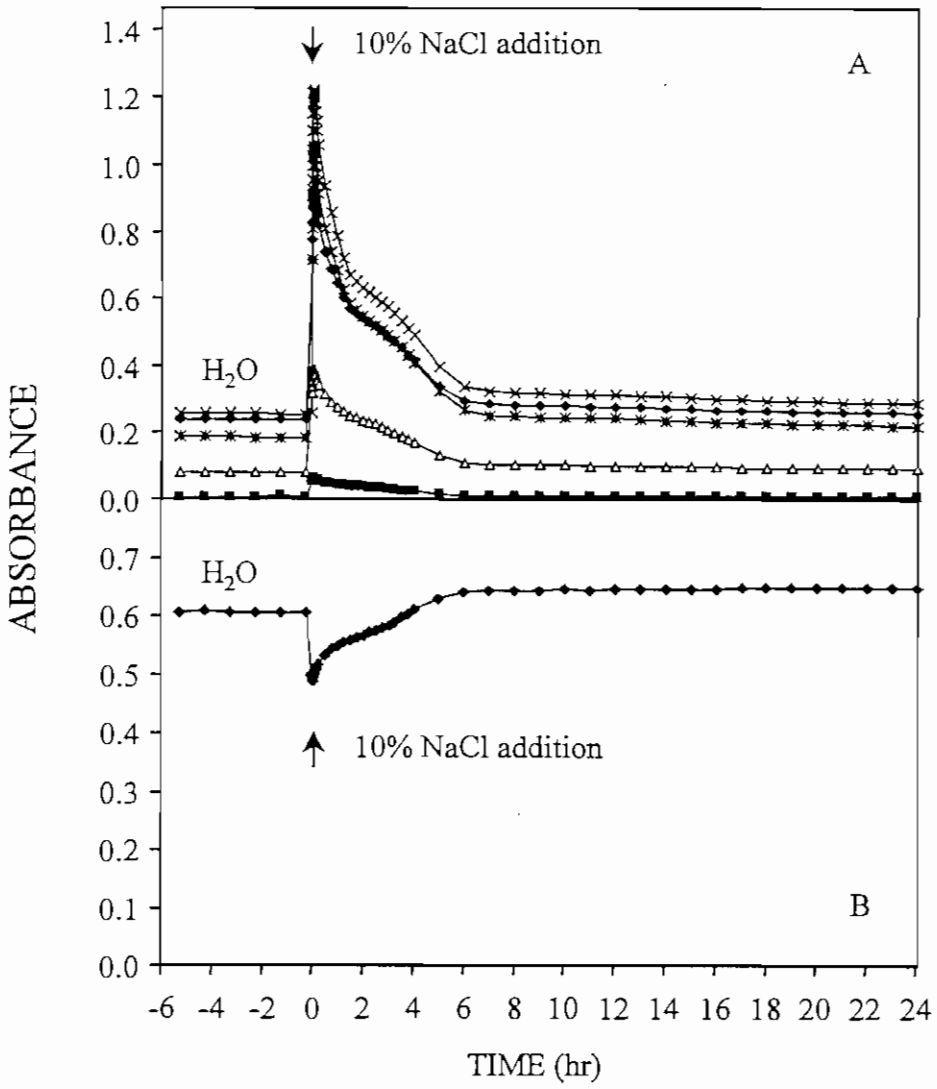

Figure 7.3.8 10% NaCl Addition. Plots of the (◆) 1747, (■) 1433, (▲) 1369, (×) 1234, and (✱) 1049 cm^{-1} band intensities of (A) cellulose acetate(42% acetyl) and (B) the 1639 cm^{-1} water band intensity as a function of time of flow.

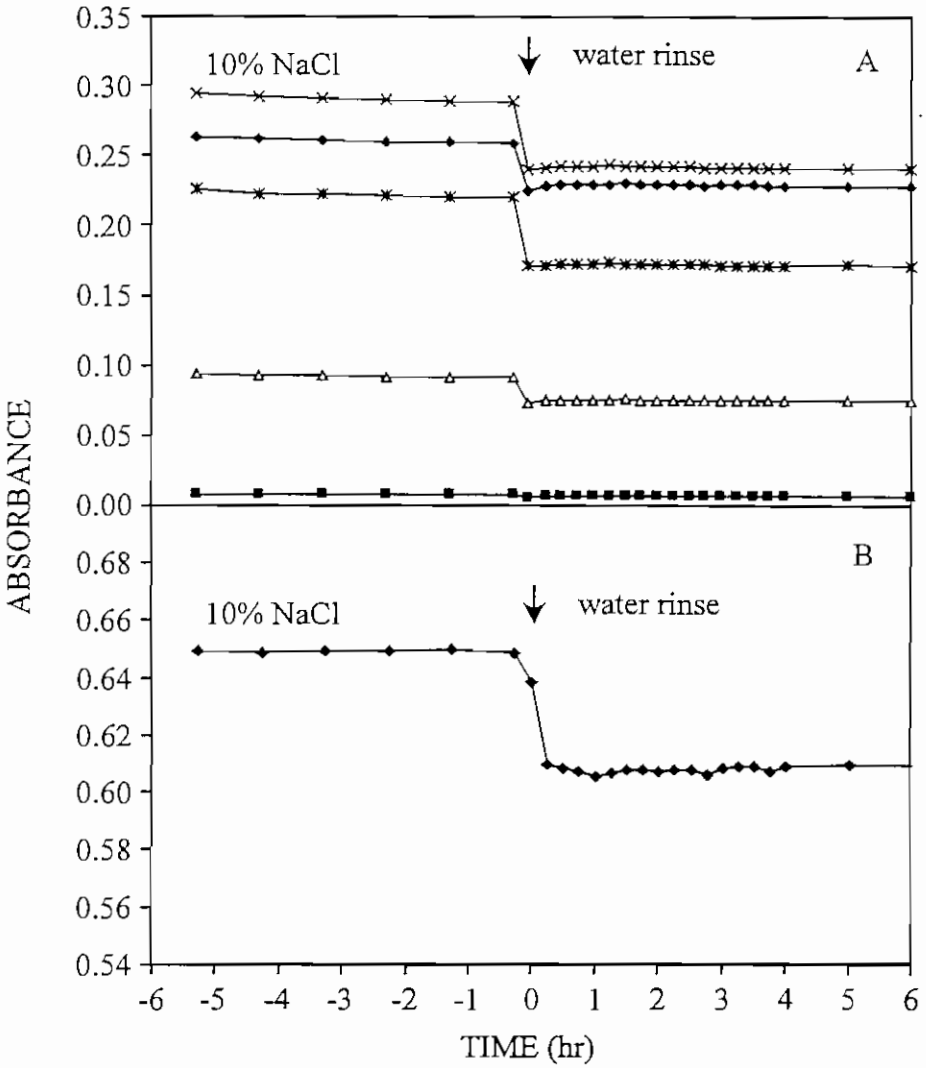

Figure 7.3.9 Third water rinse. Plots of the (◆) 1747, (■) 1433, (▲) 1369, (×) 1234, and (*) 1049 cm^{-1} band intensities of (A) cellulose acetate(42% acetyl) and (B) the 1639 cm^{-1} water band intensity as a function of time of flow.

film is exposed to the NaCl solution, water diffuses across the film into the bulk phase, causing the film to collapse back onto the IRE. As a result, the film is positioned in an area where the electric field is more intense, and thus the CA band intensities increase. This theory would account for the simultaneous drop of all four major CA band intensities and the subsequent increase in the water band intensity. Eventually, Na^+ and Cl^- ions (and water) diffuse back through the CA film into the osmotic cell. This cycle is repeated each time the salt solution and rinse are applied to the CA film. As the concentration of NaCl is increased from 3.5% to 10%, the magnitude of the changes increases, and the relaxation rates decrease, i.e., the equilibration time increases. These changes are evident in Figures 7.3.10A and 7.3.1B, where the 1232 cm^{-1} and 1639 cm^{-1} band intensities are plotted as a function of time of flow for the entire experiment.

Table 7.3.3

Effect of 10% NaCl Solution on
Cellulose Acetate and Water Band Intensities

CA Bands And Water Band	T = -15 min (AU)	T = 24 hr (AU)	Change (%)	Rate of Change Between T = 6 & T = 24 hr (mAU/hr)
1747 cm^{-1}	0.2365	0.2584	+9	-2.0
1369 cm^{-1}	0.0796	0.0921	+16	-1.6
1234 cm^{-1}	0.2542	0.2889	+14	-1.8
1049 cm^{-1}	0.1841	0.2203	+20	-0.7
1639 cm^{-1}	0.6060	0.6491	+7	+0.4

Section 7.4 *Mycobacterium* Isolate BT2-4 Adhesion on CA Thin Film

Mycobacterium Isolate BT2-4 Culture

Adhesion of bacterial cells on CA was investigated by pumping a culture of *Mycobacterium* isolate BT2-4 through a flow cell containing a CA(42% acetyl)-coated Ge IRE. Isolate BT2-4 was recovered from a fouled RO membrane operated at Water Factory 21. Its ability to produce aggregates of cells has been lost due to extensive subculturing, and thus the culture grows as a turbid cell suspension. A stationary phase culture (60 hr) was pumped through the flow cell at 8 mL/hr. After 2 hr, MS medium was substituted for the bacterial culture. A series of ATR spectra collected throughout the 28-hr

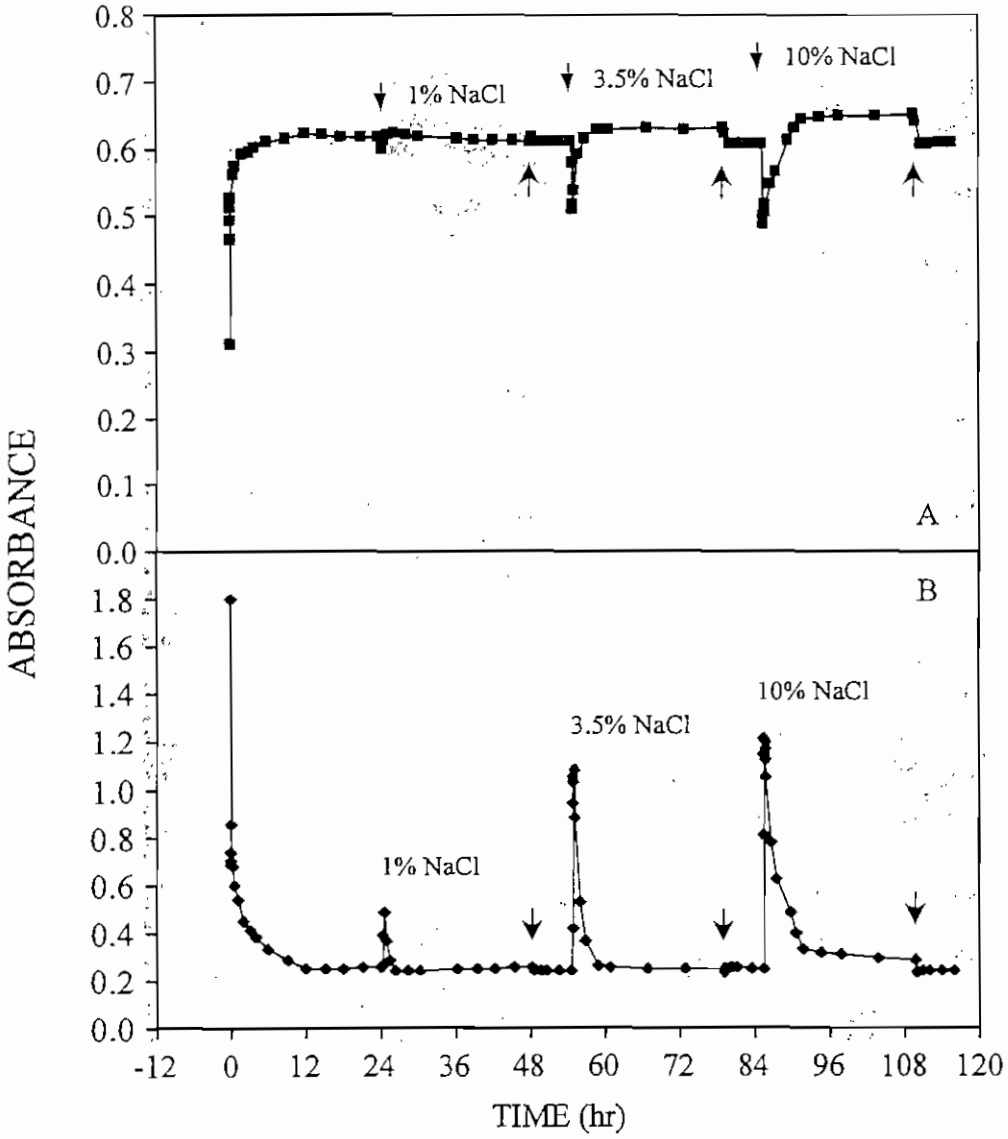

Figure 7.3.10 Plot of the (A) 1639 cm^{-1} and (B) 1232 cm^{-1} band intensity of cellulose acetate (42% acetyl) as a function of time of flow. Unlabeled arrows indicate start of water rinse.

experiment are shown in Figure 7.4.1. The 1547 cm^{-1} Amide II band intensity, indicative of protein, is plotted as a function of time flow in Figure 7.4.2. The onset of what was initially believed to be bacterial attachment occurred 20 min after the introduction of the culture into the flow cell. Bacterial adhesion was indicated by the rapid rise in the Amide II band intensity after the short (20 min) delay. A cellular adhesion rate of 7.38 x 10^{-4} hr^{-1} was calculated based on the rate of change of the Amide II band intensity. Since the whole culture was pumped into the flow cell, the first 2 hr more than likely represent the adsorption of bacterial cells and proteinaeous EPS dissolved in the culture. After 2 hr, when the flow of bacterial culture was terminated, the rate dropped to 1.47 x 10^{-4} hr^{-1}. No source of protein was introduced into the flow cell after 2 hr, only MS medium that provided a source of nutrients for the bacteria. The IR spectrum of MS medium does not contribute to the Amide II region of the spectrum. Therefore, the rate of change in the Amide II band intensity after T = 2 hr can be defined as the bacterial growth rate at the surface of the CA thin film. At the end of the experiment, the IRE was removed from the flow cell, the surface of the CA film stained with DAPI and adherent cells enumerated. Cell surface coverage was estimated at 10^7 - 10^8 cells/cm^2 after 28-hr exposure to *Mycobacterium* isolate BT2-4 fed with MS medium pH 7.

The *Mycobacterium* culture consists of a complex mixture of whole cells, EPS and other cellular products. The 1547 cm^{-1} band is indicative of protein—protein that may represent either EPS that was released into solution or was physically bound to the bacterial cells. Since it was not possible to distinguish between protein suspended in solution and protein directly bound to whole cells, the protein and other dissolved components in the bulk solution phase were removed. Whole cells were centrifuged, washed twice and resuspended in buffer. This cell suspension was then substituted for the bacterial culture and the experiment repeated.

Mycobacterium Isolate BT2-4 Cell Suspension

A dual flow cell experiment was set up with one flow cell in the main sample compartment of the spectrometer and the other in the right auxiliary experimental module (AEM). Each CA(42% acetyl) thin film (1 mm Ge IRE) was hydrated with deionized water (11 hr), "conditioned" with 0.5% DBSA (4 hr) and rinsed with water (4 hr). The 1009 cm^{-1} band intensity of DBSA is plotted as a function of time of flow in Figure 7.4.3. The kinetic plot of DBSA adsorption onto CA (right AEM) was similar to results previously observed where DBSA was exposed to a 2-mm Ge IRE coated with CA(42% acetyl). The magnitude of the 1009 cm^{-1} band intensity was 2-fold greater as expected since there were twice as many internal reflections. Adsorption of DBSA on CA in the main bench flow cell was significantly different. The rate of adsorption on CA was much slower; however, the 1009 cm^{-1} band intensity from both flow cells peaked near 12 mAU after the initial 4-hr period. Data beyond T = 4 hr (main bench) was not completely processed due to complications associated with the spectral subtractions. Changes in band shape and the presence of anomalous bands prevented complete subtraction of the hydrated CA reference spectrum from the sample spectra. The differences in the adsorption rate observed in the main and right AEM flow cells were attributed to experimental error.

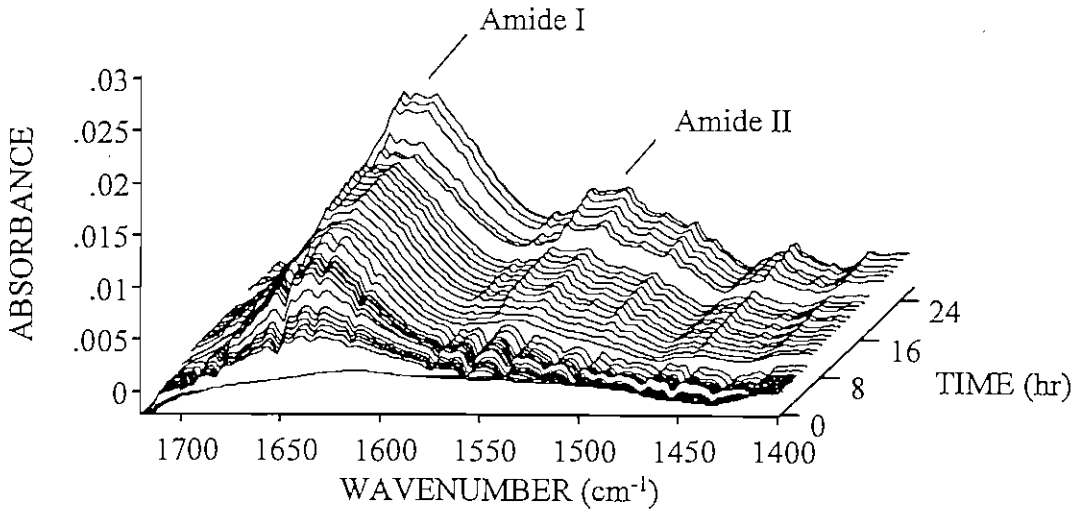

Figure 7.4.1 ATR spectra of *Mycobacterium* isolate BT2-4 adsorbed on a cellulose acetate (43.9% acetyl) thin film from flowing solution at pH 7.

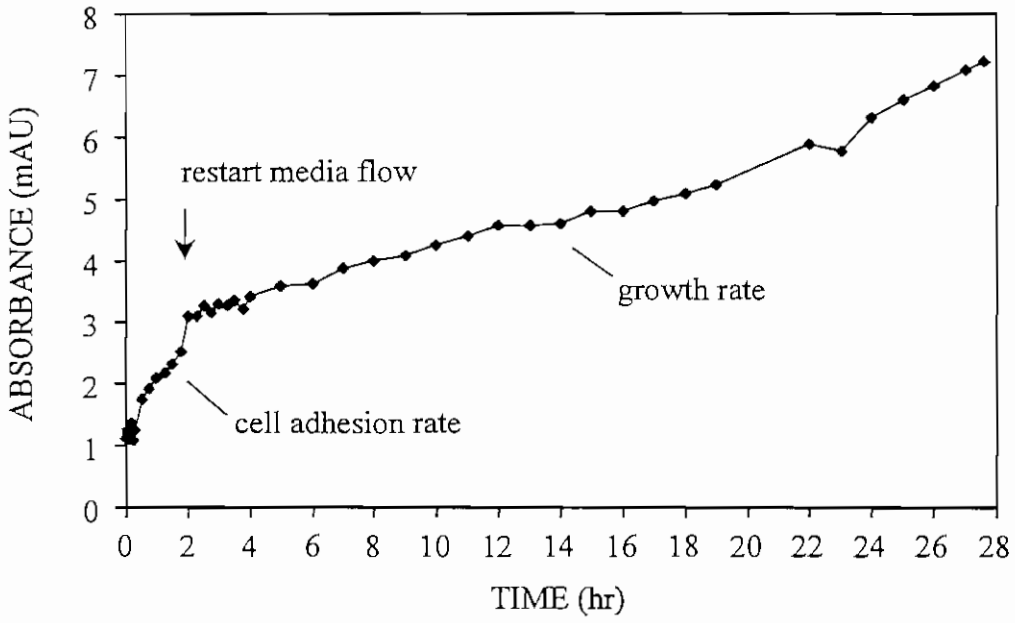

Figure 7.4.2 Plot of the 1547 cm^{-1} Amide II band intensity as function of time of flow.

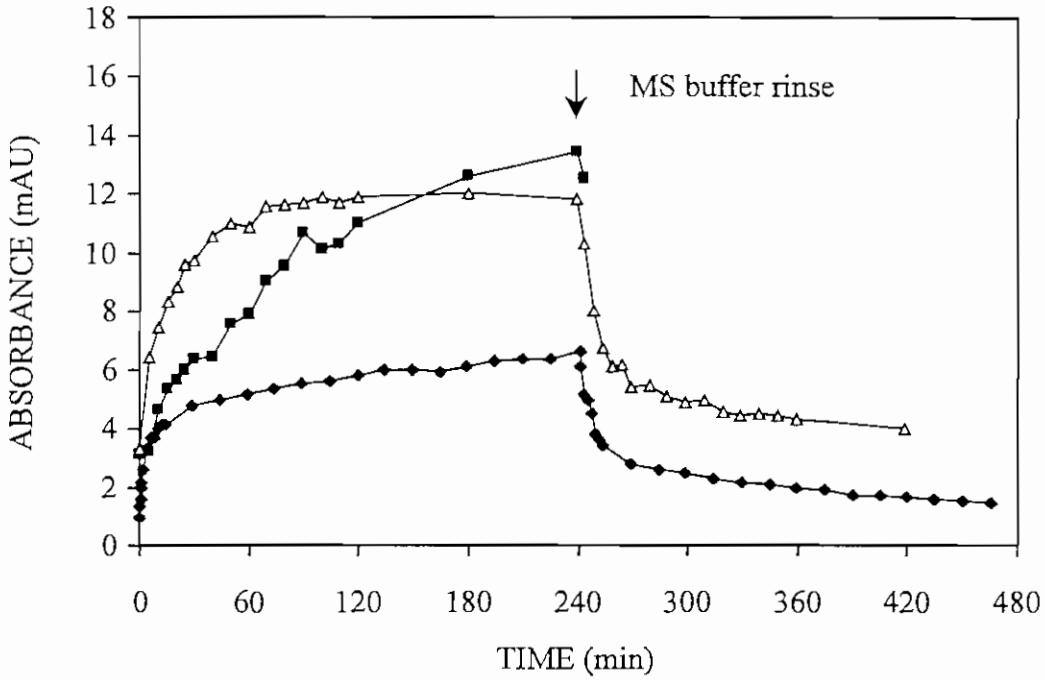

Figure 7.4.3 Plot of the 1009 cm^{-1} band intensity of 0.5% DBSA adsorbed on cellulose acetate (42% acetyl) thin film (▪ , right AEM and ▵ , main bench) and (◆) CA-coated Ge (2mm) IRE as function of time of flow.

After both CA films were preconditioned with 0.5% DBSA, a cell suspension of *Mycobacterium* isolate BT2-4 was pumped (8 mL/hr) into each flow cell to determine the influence adsorbed organics have on bacterial adhesion. The stationary phase culture was harvested by centrifugation, washed twice with MS buffer (pH 7) and resuspended in buffer to a concentration of 4.3×10^8 cells/mL. The last DBSA-treated CA spectrum (T = 8 hr) was subtracted from the sample spectra to reveal the underlying vibrational bands associated with the adherent cells. The Amide II band intensities were normalized to the 1234 cm^{-1} band intensity to take into account the differences in the CA film thickness. ATR spectra collected over the 4-hr period are shown in Figure 7.4.4 (main bench) and in Figure 7.4.5 (right AEM). Changes in the intensity of the Amide II protein band indicate that bacterial cells adsorbed onto the DBSA-conditioned CA film. A detectable increase in the Amide II band was first observed at 25 min (right AEM) as compared to 180 min (main bench) (Figure 6.4.6). The adsorption of bacterial protein on the CA film in the right AEM occurred at a greater rate. However, after approximately 4 hr, the adsorption rate of bacteria on both CA films was virtually identical—4.02×10^{-1} hr^{-1} (main bench) versus 4.26×10^{-1} hr^{-1} (right AEM). Both CA thin films were inspected by epifluorescence microscopy. Areas of heavy bacterial coverage were visible on both IREs, while other areas were only sparsely covered. In general, similar patterns of bacterial coverage were observed on both CA-coated IREs.

Quantitation of Bacteria Attached to Cellulose Acetate Thin Films

Our original intent was to use epifluorescence microscopy to visually quantitate the cell surface coverage and determine how adsorbed organics influence bacterial attachment in conjunction with ATR/FT-IR spectrometry. The experimental setup consisted of CA-coated microscope slides in flow cells placed in series with the ATR flow cell (Figure 7.4.7). Periodically slides were removed, stained with DAPI and cell surface coverage determined as a function of time flow. Since the Research Advisory Board expressed concern that quantitation of cell coverage was made on a surface removed from where the IR single was collected, another method for enumerating cells was proposed. A new flow cell was designed and an epifluorescence microscope built to capture images of adherent bacteria on the CA film in the same area where the IR data was sampled. This system, simultaneous ATR/FT-IR spectrometry / fluorescence microscopy, is in the process of being built (see discussion below, Section 7.10). In the meantime, another method to make in situ measurements of adherent bacteria was implemented. A specially designed flow cell capable of visualizing native bacteria by Nomarski differential interference contrast microscopy was utilized. These flow cells were used in another NWRI research project[‡] conducted at OCWD and were incorporated into this ATR/FT-IR project. Delays associated with the purchase of an inverted microscope and imaging software led us to focus more on organics adsorption on CA and post-treatment of organic conditioning films with chemical surfactants. A small amount of bacterial attachment data was collected; however, it is best presented following the organics adsorption data (see Section 7.9).

[‡] NWRI Final Report Project No. MRDP 669-507-95 Fouling Composition During Membrane Treatment of Secondary Effluent: Microscale Characterization Leading to Fouling Prevention of the Pilot Scale.

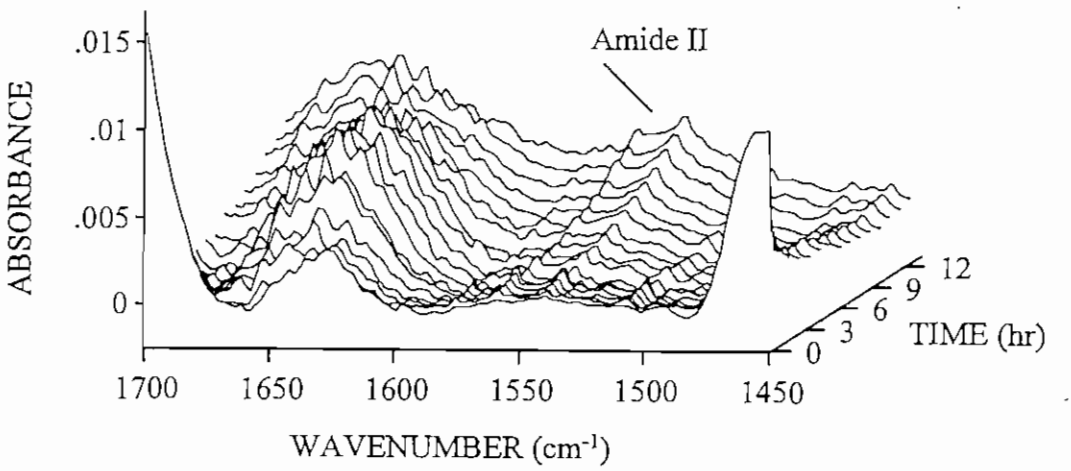

Figure 7.4.4 ATR spectra of *Mycobacterium* isolate BT2-4 adsorbed on a cellulose acetate (42% acetyl) thin film from flowing solution. CA film was pretreated with 0.5% DBSA pH 7 (main bench).

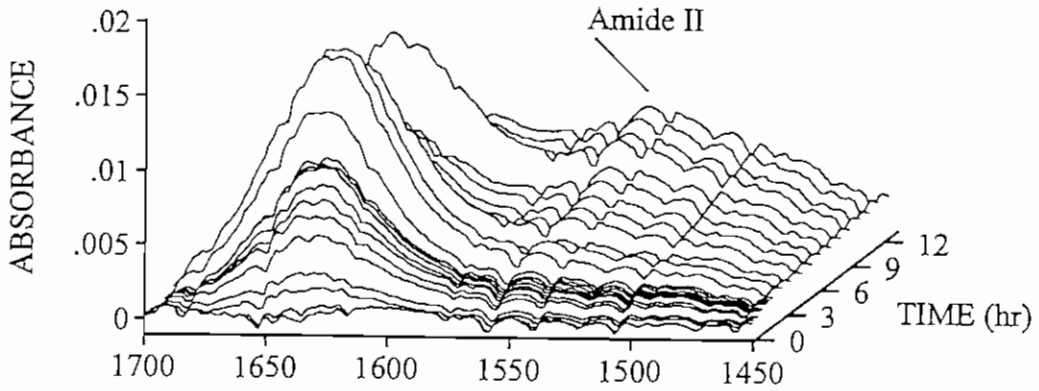

Figure 7.4.5 ATR spectra of *Mycobacterium* isolate BT2-4 adhesion on a cellulose acetate (42% acetyl) thin film from flowing solution. CA film was pretreated with 0.5% DBSA (right AEM).

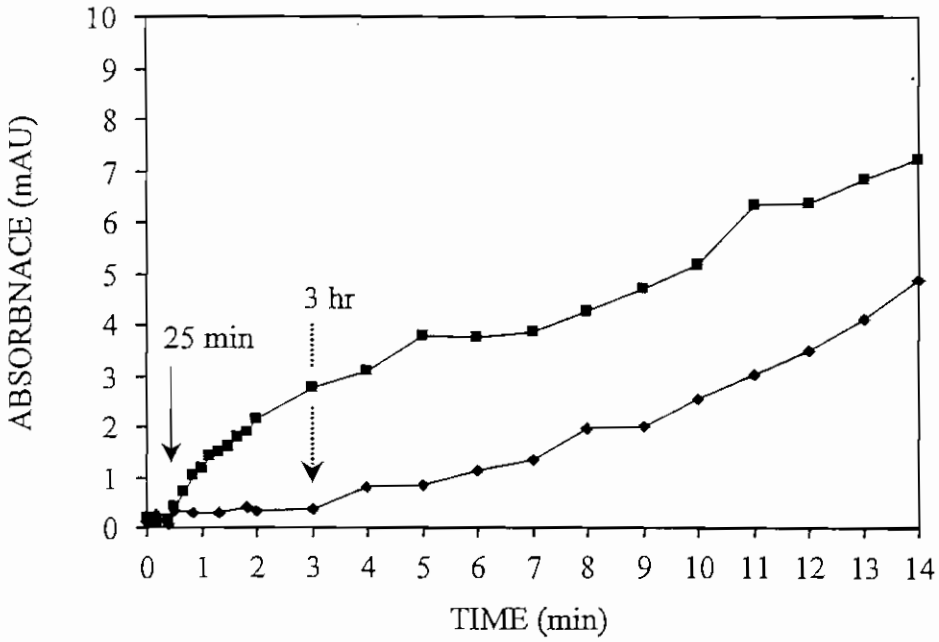

Figure 7.4.6 Plot of the 1549 cm^{-1} Amide II band intensity of *Mycobacterium* isolate BT2-4 adhesion on cellulose acetate (42% acetyl) film as a function of time of flow (◆) main bench and (■) right AEM flow cell.

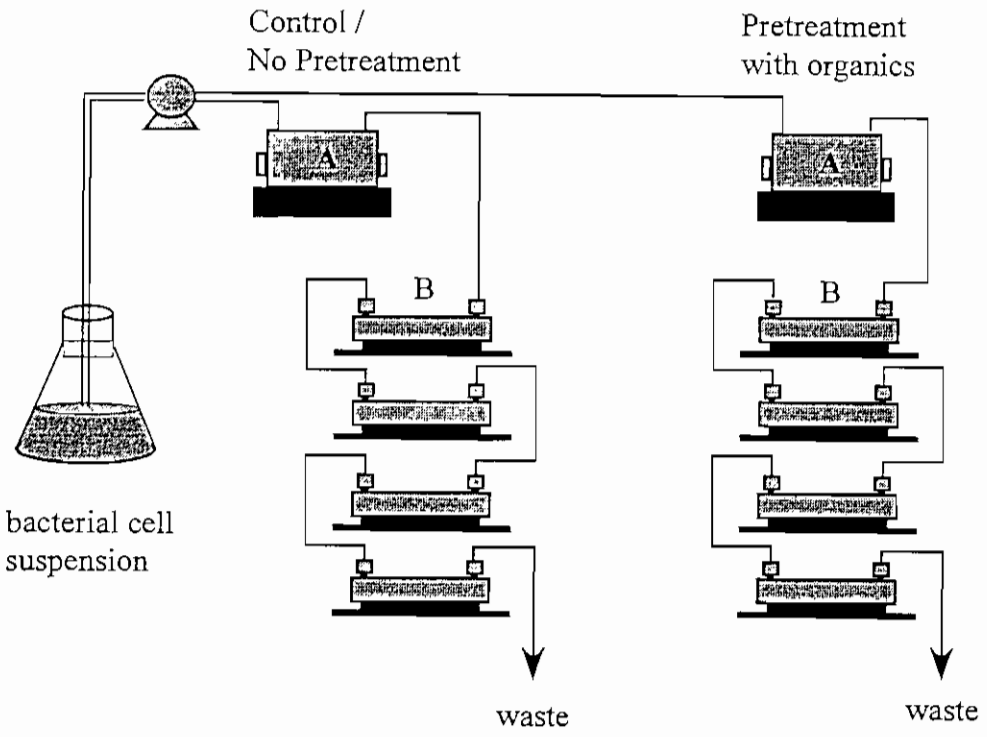

Figure 7.4.7 Experimental setup for epifluorescence quantitation of cell surface coverage on CA-coated coupons, (A) ATR flow cell and (B) stainless steel flow cell with CA-coated microscope slides.

Section 7.5 Stability of CA Thin Films Cast on ZnSe IRE

After running several experiments with CA-coated Ge IREs, investigations into a new IRE material were initiated. While use of CA-coated Ge IREs was demonstrated to be feasible for studies of organics adsorption and bacterial adhesion, data generated from these experiments were difficult to process. Physical separation and movement of the thin film near the surface of the IRE necessitated the inclusion of correction factors for each data point. A thin CA film that adhered firmly to the IRE was desired. Two other IRE materials were available for these studies, zinc selenide and KRS-5 (thalium-bromide-iodide). KRS-5 was ruled out because it deforms under pressure, is toxic and is easily attacked by complexing agents. ZnSe is also attacked by complexing agents. However, it is a harder material and less toxic, and was therefore selected.

The stability of a CA(42% acetyl) film was tested by pumping deionized water through a flow cell containing the polymer-coated IRE. The four major CA band intensities dropped between 1 and 1.5% after 2 min of exposure to water (Figure 7.5.1) as compared to the >50% drop in intensity typically observed with CA-coated Ge IREs (Figure 7.3.2 and 7.3.3). In the same 2-min period, the water band intensity plateaued near 0.1 AU. The water band intensity measured with a bare ZnSe IRE (50 x 10 x 3 mm, 45°) is typically around 1.7 AU. Thus, the low water band intensity also indicated that the film remained in good contact with the surface of the IRE. The 1 - 2% drop in intensities of the four major CA bands was more indicative of polymer swelling that occurs upon hydration of CA. The carbonyl and C-O-C acetate ester bands shifted in frequency upon hydration as previously observed, i.e., the carbonyl band shifted to low wavenumber and the C-O-C acetate ester shifted to higher wavenumber.

Section 7.6 Adsorption of Organic Macromolecules on CA Thin Films.

Of the 12 organic macromolecules screened (on the Ge substrate), eight were investigated for sorption onto thin films of CA. These compounds were the protein, albumin, the polysaccharides dextran (neutral) and alginic acid (acidic), and the "glycoprotein," gum arabic. These organic compounds served as model EPS. Four surfactants were used Triton X-100 (neutral), benzalkonium chloride (cationic), DBSA (anionic) and Zwittergent 3-16 (zwitterionic). Thin films (1200 to 1500 Å) of CA (42% and 43.9% acetyl) were cast on Ge and ZnSe IREs. Adsorption and desorption phenomena at the aqueous-polymer interface were investigated.

Zwittergent 3-16 Adsorption on Cellulose Acetate (42% acetyl)

Zwittergent 3-16 and DBSA were screened early in the project. Therefore, the thin film consisted of CA (42% acetyl) cast on a 2 mm Ge IRE. The CA film was hydrated with deionized water for 24 hr. A 0.5% solution of Zwittergent 3-16 was pumped through the flow cell. After 4 hr the CA was rinsed with water to the end of an 8-hr experiment. The 1487 cm^{-1} and 1468 cm^{-1} band intensities of the surfactant are plotted as a function of time of flow in Figure 7.6.1. The surfactant sorbed throughout the initial 4-hr period and remained

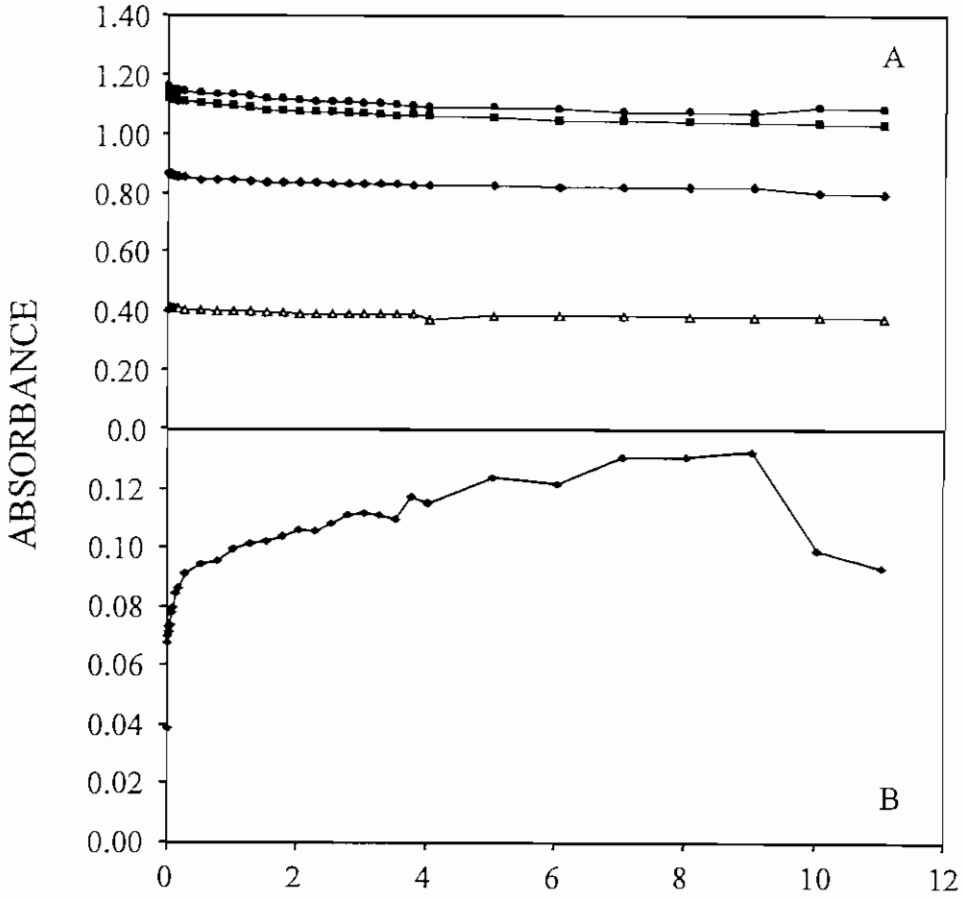

Figure 7.5.1 Plots of the (▪) 1749, (▵) 1369, (•) 1230 and (•) 1049 cm^{-1} band intensities of (A) cellulose acetate (43.9% acetyl) and (B) the 1639 cm^{-1} water band intensity as a function of time of flow.

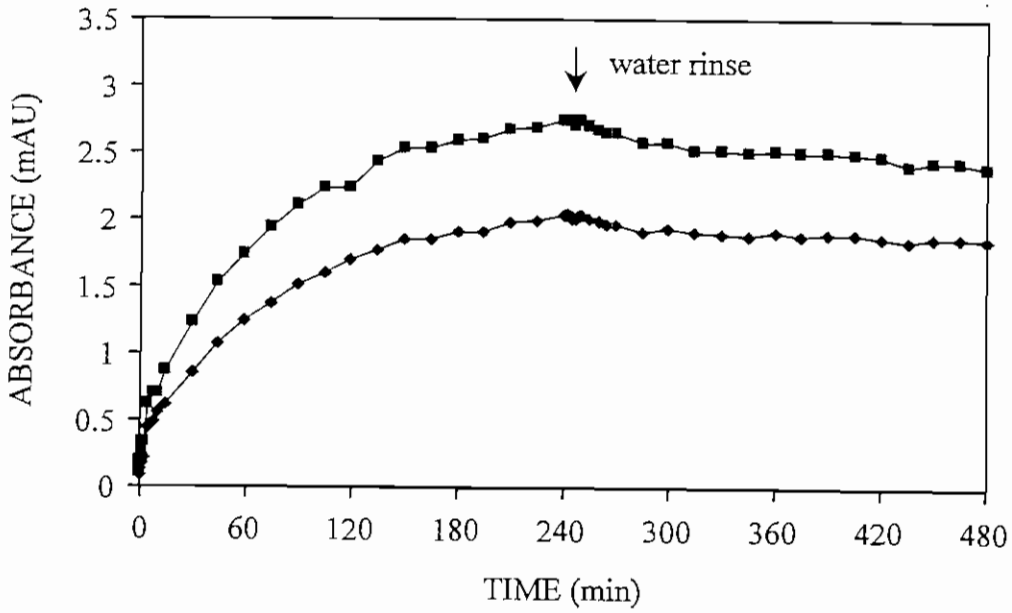

Figure 7.6.1 Zwittergent 3-16 adsorbed on cellulose acetate (42% acetyl) thin film. Plot of the (◆) 1487 cm^{-1} and (■) 1468 cm^{-1} band intensities of Zwittergent 3-16 as a function of time of flow.

firmly adsorbed to the polymer film. A desorption rate of -0.82 x 10^{-3} min^{-1} was calculated, and a layer of Zwittergent 3-16 approximately 23 Å thick was left adsorbed to the CA.

Triton X-100 Adsorption on Cellulose Acetate (43.9% acetyl)

Two CA(43.9% acetyl) films were hydrated with deionized water for 1 hr prior to exposure to Triton X-100. A 0.5% solution was pumped through flow cells containing the CA-coated ZnSe IRE. After 4 hr, MS buffer was pumped through to the end of an 8-hr experiment. Plots of the 1512 cm^{-1} band intensity as a function of time of flow are shown in Figure 7.6.2. Data were normalized to take into account the differences in polymer film thickness. Triton X-100 slowly accumulated at the surface of the CA films over the initial 4-hr period. Adsorption was similar on both CA films. However, slightly more Triton X-100 adsorbed on the thin film in the right AEM flow cell as compared to the CA film in the main bench flow cell. Desorption of the surfactant from the CA was much greater in the right AEM flow cell. Desorption of firmly bound material (between T = 300 and 480 min) occurred at a rate of -24.3 x 10^{-3} min^{-1} (right AEM) as compared to -11.8 x 10^{-3} min^{-1} (main bench). The thickness left on the CA surface varied from 24 Å (right AEM) to 36 Å (main bench) with an average thickness of 30 Å. The differences were attributed to experimental error.

Dodecylbenzenesulfonic Acid Adsorption on Cellulose Acetate

Our primary interest was directed toward DBSA, as it is periodically applied to clean the CA reverse osmosis membranes at Water Factory 21. Studies in our lab have revealed that it is very effective at removing *Mycobacterium sp.* attached to CA thin films.[42] Initially DBSA was run at 0.5% on a CA(42% acetyl)-coated Ge IRE. Later the concentration was dropped to 0.1% to match the concentration used in our fouling composition studies, and adsorption on CA(43.9% acetyl) was investigated.

0.5% DBSA Adsorption on CA(42% acetyl)-Coated Ge IRE. A 0.5% aqueous solution of DBSA was pumped through a flow cell containing a CA-coated Ge IRE that was hydrated with deionized water (pH 7). After 4 hr the polymer film was rinsed with water to the end of an 8-hr experiment. A plot of the 1009 cm^{-1} band intensity as a function of time of flow is shown in Figure 7.6.3. Adsorption of DBSA on CA neared a plateau by the end of 4 hr. DBSA desorbed from the surface of the cellulose acetate film throughout the rinse period. A desorption rate constant of -4.1 x 10^{-3} min^{-1} was calculated for firmly bound DBSA, and a film thickness of 8.6 Å remained after the rinse.

0.1% DBSA Adsorption on CA(43.9% acetyl)-coated ZnSe IRE. Later, the DBSA concentration was dropped to 0.1%, and adsorption on a CA(43.9% acetyl)-coated ZnSe IRE was investigated. Two flow cells were run simultaneously. Plots of the 1180 cm^{-1} and 1009 cm^{-1} band intensities as a function of time flow are displayed in Figure 7.6.4. For clarity, the intensities of the 1138 cm^{-1} were plotted separately. The data were normalized to the 1369 cm^{-1} band of CA to take into account the difference in the thickness between the two thin films. Data points connected by a line represent the average value from the two trials at that given time. Initially adsorption on CA was rapid. After approximately 20 min, the rate of adsorption tapered off; however, DBSA adsorption did not plateau before the end of the

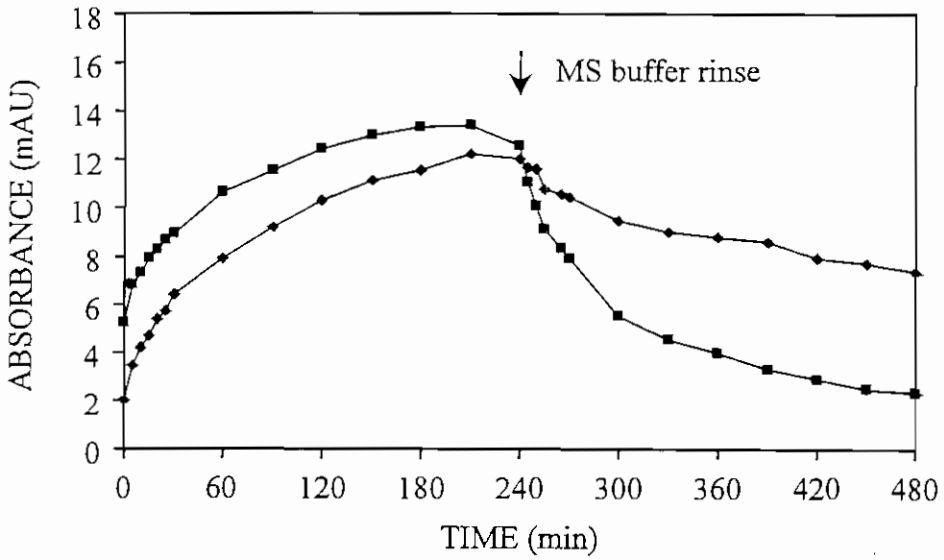

Figure 7.6.2 Triton X-100 adsorbed on cellulose acetate (43.9% acetyl) thin film. Plots of the 1512 cm^{-1} band intensity as a function of time of flow (◆) main bench and (■) right AEM.

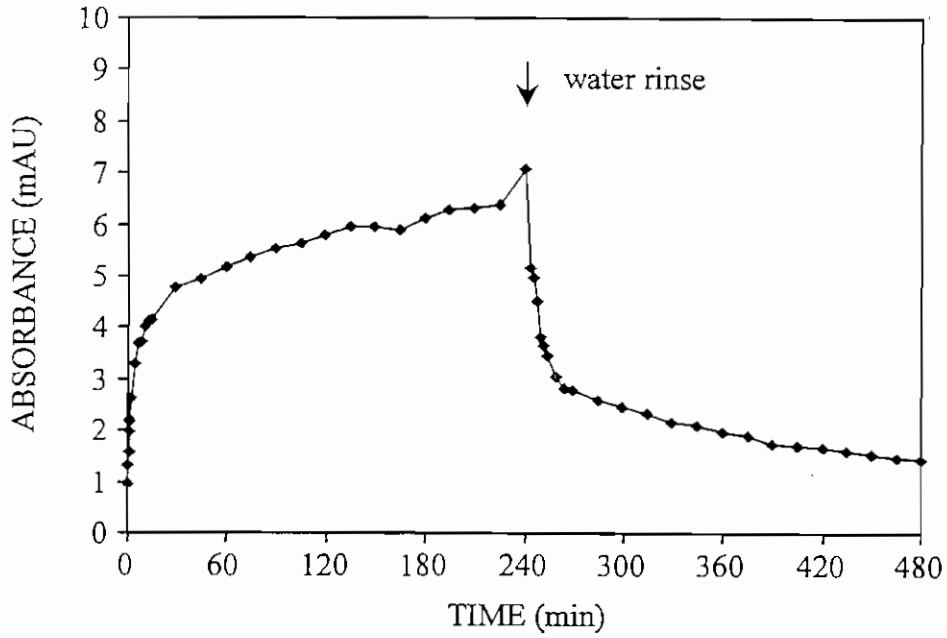

Figure 7.6.3 DSBA adsorbed on cellulose acetate (42% acetyl) thin film. Plot of the 1009 cm^{-1} band intensity as a function of time of flow.

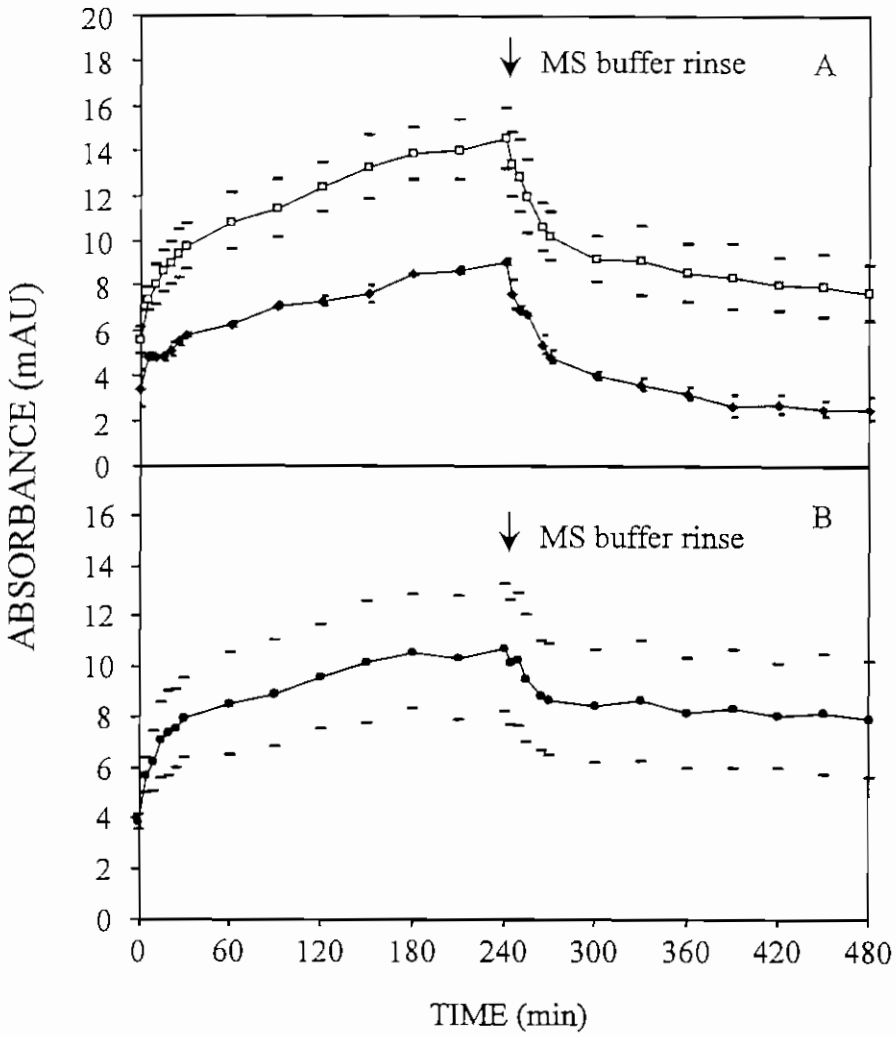

Figure 7.6.4 DBSA adsorbed on cellulose acetate (43.9% acetyl) thin film. Plots of the average (A) (▫) 1180 cm^{-1} and (◆) 1009 cm^{-1} band intensities and (B) 1138 cm^{-1} band intensity as a function of time of flow. Data points connected by line represent the average value from the two trials at the given time.

4-hr period. All three band intensities dropped rapidly at the start of the rinse, then tapered off. However, the 1138 cm^{-1} band, associated with the benzene ring, did not drop at the same rate, nor to the extent of the 1180 cm^{-1} and 1009 cm^{-1} bands. The desorption rate of DBSA (based on the 1009 cm^{-1} band) was -13.6×10^{-3} min^{-1}. The desorption rates of 1138 cm^{-1} (benzene ring) and 1180 cm^{-1} (sulfonate group) were -3.4×10^{-3} min^{-1} and -8.7×10^{-3} min^{-1}, respectively. These results suggest that the benzene ring of the surfactant may be more closely associated with the CA thin film. Similar kinetics were observed when DBSA desorbed from the surface of a Ge IRE (Figure 7.1.12). An estimated DBSA film thickness of 8 Å (based on 1009 cm^{-1} band) was left on the CA film following the buffer rinse.

Effect of DBSA on Organic Conditioning Films on Cellulose Acetate Thin Films

DBSA proved to be so effective at removing adherent cells from CA thin films that more studies were directed toward this surfactant.[§] Bacteria typically produce EPS that anchor the cells to a solid substrate. If the adherent cells are to be removed from the substrate, molecular interactions between the EPS and the substrate must be disrupted. Adsorption of model EPS (albumin, dextran, alginic acid and gum arabic) on CA was investigated, along with the ability of DBSA to displace these organics from the aqueous-polymer interface.

Bovine Serum Albumin Adsorption on CA Thin Film

A 0.5% solution of BSA (in MS buffer) was pumped through a flow cell containing a CA(43.9% acetyl)-coated ZnSe IRE. After 4 hr the polymer surface was rinsed with MS buffer (pH 7). The buffer rinse was followed with 0.1% DBSA solution to the end of a 12-hr experiment. The 1547 cm^{-1} Amide II protein band is plotted as a function of time of flow in Figure 7.6.5. At T = 0 min there is a significant Amide II band intensity, indicating the presence of protein at or near the surface of the CA-coated IRE. Most of the 1547 cm^{-1} intensity at T = 0 min is believed to be primarily bulk aqueous phase protein. Any increase in band intensity after T = 0 min was assumed to be adsorbed material. Little additional protein accumulated at the aqueous-polymer interface after T = 0 min, as compared to BSA adsorption on bare Ge (Figure 7.1.8). The Amide II band intensity rose approximately 2 mAU between T = 0 and T = 60 min, reaching a plateau near 14 AU. BSA ($pK_a = 4.8$) has a net negative charge at pH 7. CA also has a slight negative charge, which may explain BSA's seemingly low affinity for the CA thin film. The 1547 cm^{-1} band dropped rapidly during the first 10 min of the rinse, indicating that most of the Amide II intensity was attributed to bulk (and loosely bound) protein. Some protein did remain firmly bound to the CA film as the Amide II band stabilized near 3 mAU following the 4-hr rinse. An estimated film thickness of 10 Å of BSA was left on the CA surface following the buffer rinse. At T = 480 min, DBSA (0.1%) was pumped through the flow cell. This treatment effectively removed protein at the interface to a level below the detection limit. The 1547 cm^{-1} band

[§] NWRI Final Report Project No. MRDP 669-507-95 Fouling Composition During Membrane Treatment of Secondary Effluent: Microscale Characterization Leading to Fouling Prevention of the Pilot Scale.

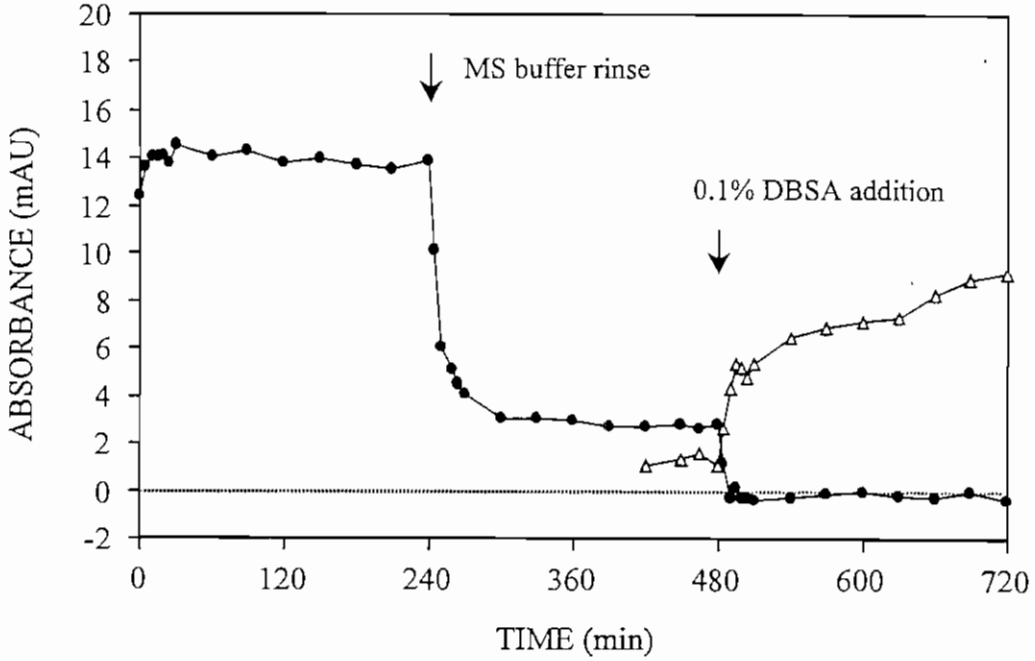

Figure 7.6.5 Albumin adsorbed on cellulose acetate (43.9% acetyl) thin film. Plots of the (•) 1547 cm^{-1} and (▵) 1009 cm^{-1} band intensities as a function of time of flow.

intensity essentially dropped to zero absorbance (Figure 7.6.5) between T = 480 - 720 min. The pump speed was not altered during the switch from buffer rinse to surfactant addition.

Dextran Adsorption on CA Thin Film

A 0.5% dextran solution was pumped through a flow cell containing a CA(43.9% acetyl)-coated ZnSe IRE. The polysaccharide slowly accumulated at the aqueous-polymer interface, as evidenced by the rise in the 1159 cm^{-1} band intensity with time of flow (Figure 7.6.6). During the buffer rinse, dextran desorbed slowly from the interface at a rate of -12.6×10^{-3} min^{-1}. The film thickness was estimated at 29 Å. After the 4-hr rinse, a 0.1% DBSA solution was pumped through the flow cell. The presence of overlapping DBSA and dextran bands made polysaccharide desorption difficult to monitor during DBSA addition (T = 480 - 720 min). In spite of the correction made for overlapping dextran and DBSA bands, the 1159 cm^{-1} band intensity was still offset at the start of the DBSA rinse. However, there did appear to be a rapid displacement of dextran from the interface at the start of DBSA addition (T = 480 min). After 45 min, the desorption rate of dextran dropped to -6.1×10^{-3} min^{-1}, half the rate observed during the buffer rinse. Some dextran still remained adsorbed to the CA film following the 4-hr exposure to DBSA. The film thickness was estimated at 22 Å.

Alginic Acid Adsorption on CA Thin Film

A 0.5% alginic acid solution was pumped through a flow cell containing a CA(43.9% acetyl)-coated ZnSe IRE. At T = 0 min, a 1416 cm^{-1} (COO^- symmetric stretching) intensity of 6.1 mAU was measured, which represented primarily bulk phase alginic acid. Between T = 0 min and T = 30 min, the 1416 cm^{-1} band rose slowly, indicating some accumulation of alginic acid at the aqueous-polymer interface (Figures 7.6.7). Between T = 30 min and T = 4 hr, the rate of adsorption dropped off significantly. When the IRE was rinsed with buffer, this band dropped rapidly (i.e., bulk solution phase algin was washed from the flow cell). However, the 1416 cm^{-1} band did stabilize near 2.5 mAU, indicating that some polysaccharide remained firmly bound to the CA film. The film thickness was estimated at 13Å. When DBSA was pumped into the flow cell, algin was displaced from the polymer surface, as indicated by the immediate drop in the 1416 cm^{-1} band intensity. Less DBSA appeared to adsorb on the algin-pretreated CA film, as the 1009 cm^{-1} DBSA band plateaued near 6.5 mAU, as compared to 9 mAU when adsorbed on an untreated CA thin film. A small amount of alginic acid was left bound at the interface and was estimated at 3 Å thick.

Gum Arabic Adsorption on CA Thin Film

Gum arabic (GA) is an acidic polysaccharide with a closely associated protein component. This plant polysaccharide served as our glycoprotein, although it may not be considered a true glycoprotein. A 0.5% gum arabic solution was pumped through a flow cell containing a CA(43.9% acetyl)-coated ZnSe IRE. The 1080 cm^{-1} C-O stretching band intensity of the carbohydrate component increased rapidly at the start of the experiment,

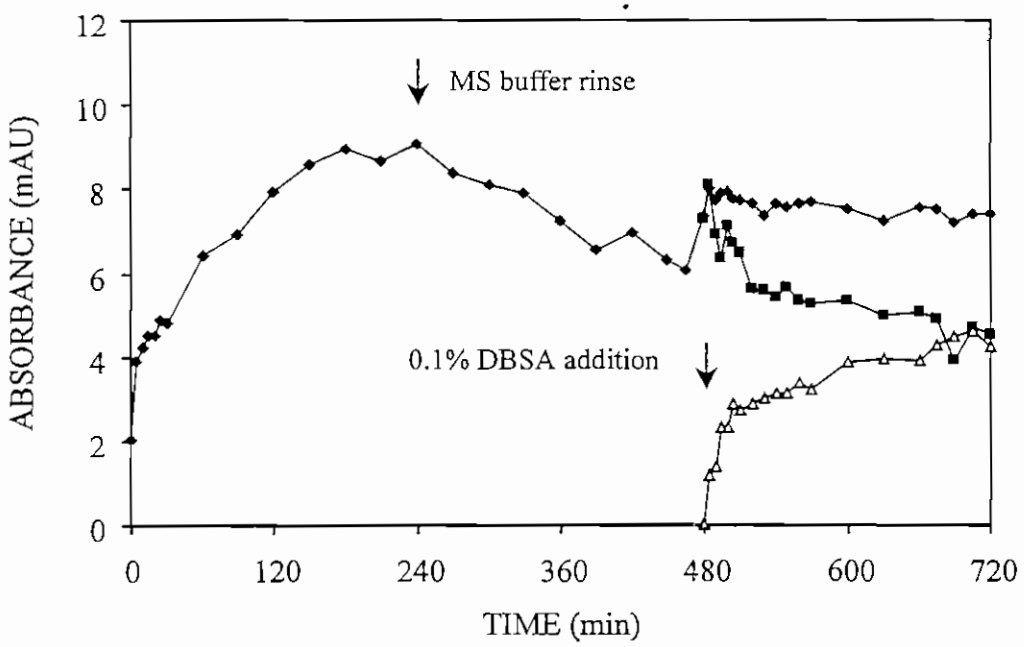

Figure 7.6.6 Dextran adsorbed on cellulose acetate (43.9% acetyl) thin film. Plots of the (◆) 1159 cm^{-1}, (■) 1159 cm^{-1} "corrected" band intensities of dextran and (▵) 1009 cm^{-1} band intensity of DBSA as a function of time of flow.

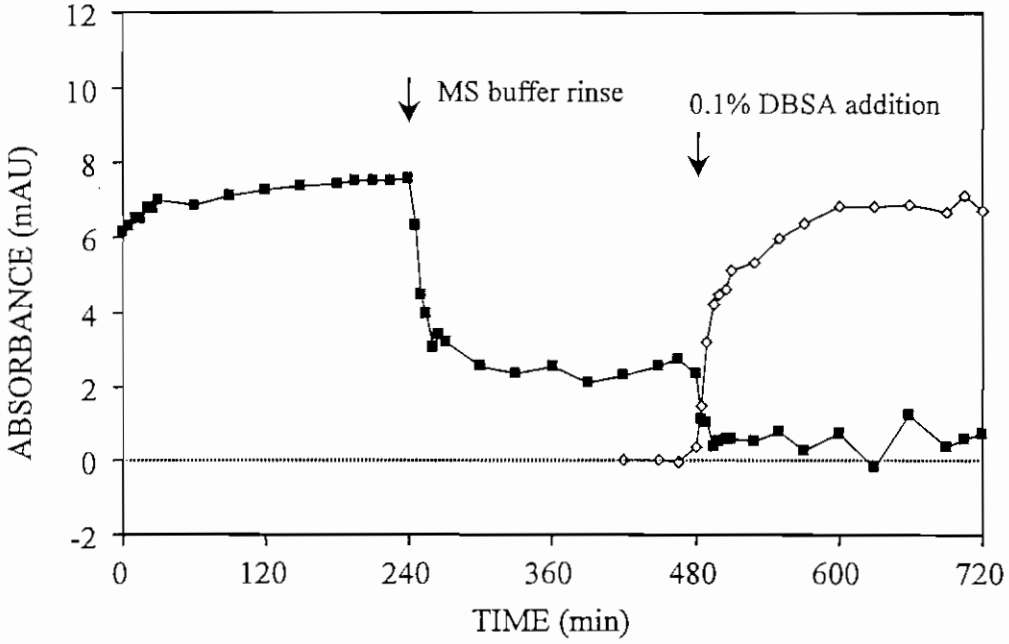

Figure 7.6.7 Alginic acid adsorbed on cellulose acetate (43.9% acetyl) thin film. Plots of (■) 1416 cm^{-1} band intensity of alginic acid and (◇) 1009 cm^{-1} band intensity of DBSA as a function of time of flow.

reaching a maximum near 13 mAU after 30 min (Figure 7.6.8). At the same time, protein adsorbed rapidly at the interface, as indicated by the increase in the 1547 cm^{-1} Amide II band intensity. After 30 min, the rate of protein adsorption dropped but continued to adsorb throughout the 4-hr period, while the 1080 cm^{-1} band associated with the polysaccharide appeared to drop slightly with time. These results suggest that protein slowly displaced polysaccharide at the aqueous-polymer interface. Both the polysaccharide and the protein components desorbed during the buffer rinse but were not completely removed. The film thickness of the polysaccharide component was estimated at 18 Å, and the film thickness of the protein component was estimated at 19 Å. The 1080 cm^{-1} band actually increased during the rinse, between T = 330 min and T = 390 min. However, this increase was attributed to difficulties with the spectral subtractions. DBSA (0.1%) was pumped through the flow cell, and both polysaccharide and protein were rapidly displaced from the CA film. The Amide II band intensity dropped below the detection limit. The polysaccharide component was more difficult to monitor, as the C-O stretching bands of GA overlapped those of CA and DBSA. The 1080 cm^{-1} band dropped 50% during the first 30 min of the rinse. In the last 30 min of the rinse, the C-O stretching band dropped to an intensity near zero absorbance. At the same time, the 1009 cm^{-1} band intensity of DBSA rose rapidly, then the rate of increase dropped (Figure 7.6.8). DBSA adsorption did not plateau before the end of the 4-hr period. A second and final MS buffer rinse was included in this experiment. DBSA desorbed from the CA film, dropping from 8.5 mAU to 3 mAU (T = 780 min), where it remained to the end of the experiment (T = 960 min).

Benzalkonium Chloride Adsorption on CA Thin Film

A 0.5% solution of benzalkonium chloride (BnzCl) was pumped through a flow cell containing a CA(43.9% acetyl)-coated ZnSe IRE. Plots of the 1485 cm^{-1} band intensity of BnzCl, representing adsorption and desorption on CA, are shown in Figure 7.6.9. BnzCl adsorbed on the CA film but did not reach a plateau by the end of the first period. During the buffer rinse, BnzCl slowly desorbed from the interface. The film thickness was estimated at 46 Å. A 0.1% DBSA solution was pumped through the flow cell at T = 480 min. DBSA absorption bands overlap the region of the spectrum used to monitor BnzCl. Therefore, it was necessary to correct for DBSA's contribution to the BnzCl-DBSA spectrum. Taking into account these overlapping bands, BnzCl desorption continued at a constant rate independent of the presence of DBSA (Figure 7.6.9).

The 1009 cm^{-1} band of DBSA did not reach a pleateau after 4 hr. At T = 720 min a final buffer rinse was applied. The adsorbed BnzCl was unaffected by the fmal rinse, while the 1009 cm^{-1} band intensity of DBSA dropped (43%) from 11.7 mAU to 6.41 mAU after 4 hr. More DBSA appeared to remain firmly adsorbed on the BnzCl-pretreated CA film as compared with gum arabic-pretreated CA films (see Figure 7.6.7). In this case, electrostatic forces between positively charged BnzCl and negatively charged DBSA likely played a role in enhancing adsorption. The DBSA left adsorbed on the CA film was estimated at 36 Å.

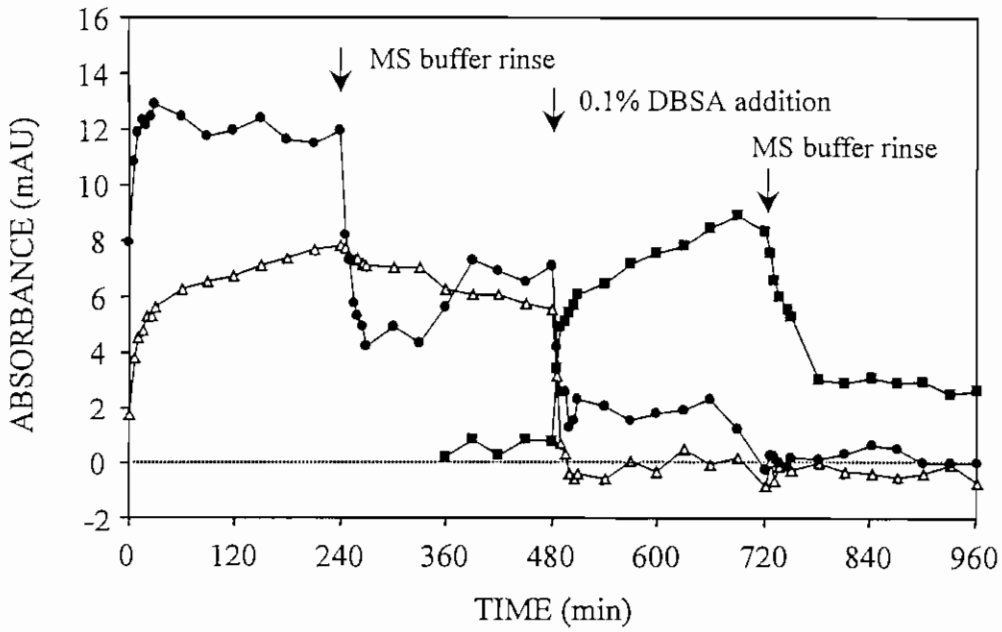

Figure 7.6.8 Gum arabic adsorbed on cellulose acetate (43.9% acetyl) thin film. Plots of (▵) 1547 cm^{-1} Amide II and (•)1080 cm^{-1} C-O band intensity of gum arabic and (■) 1009 cm^{-1} band intensity of DBSA as a function of time of flow.

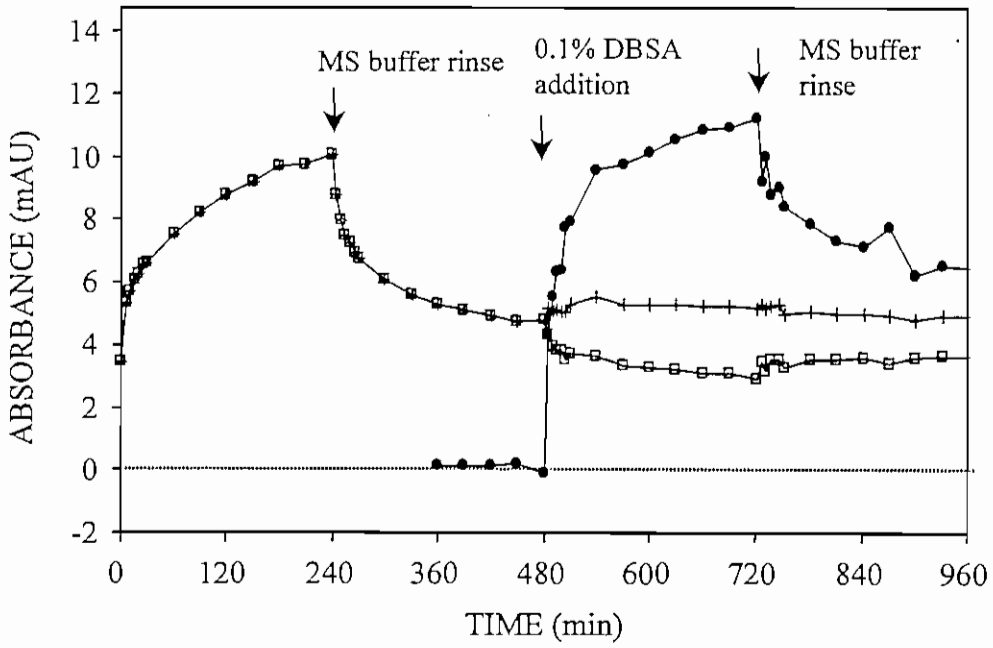

Figure 7.6.9 Benzalkonium chloride adsorbed on cellulose acetate (43.9% acetyl) thin film. Plots of (+) 1485 cm^{-1} and (▫) 1485 cm^{-1} 'corrected' band intensities of benzalkonium chloride and (•) 1009 cm^{-1} band intensity of DBSA as a function of time of flow.

Summary and Discussion

Estimates of the thickness of the organic layer that remained after the buffer rinse are shown in Table 7.6.1. This material was defined as "firmly bound." Adhesion of macromolecules can occur by a number of chemical interactions including electrostatic, hydrophobic, dipole-dipole, Van der Waals and hydrogen bonding. In this limited study with the eight organic compounds (albumin, dextran, alginic acid, gum arabic, dodecyl-benzenesulfonic acid, Triton X-100 and benzalkonium chloride), electrostatic interactions appeared to be a major factor in determining macromolecular adsorption on cellulose acetate thin films. This is especially evident when comparing adsorption of Zwittergent 3-16 and Triton X-100 on films of CA. Once adsorbed, the charged surfactant remained firmly bound, while much of the Triton X-100 was washed from the aqueous-polymer interface.

Table 7.6.1

Film Thickness of Organic Macromolecules
Adsorbed On Cellulose Acetate (43.9% acetyl) Thin Film

Organic Compound	**Properties**	**Film Thickness After Buffer Rinse (Å)**	**Film Thickness After 0.1% DBSA Rinse (Å)**
Triton X-100	nonionic surfactant	50	NA
Benzalkonium Chloride	cationic surfactant	46	36
Dextran	neutral polysaccharide	29	22
Zwittergent 3-16[a]	zwitterionic surfactant	23	NA
Gum Arabic (protein component)	polysaccharide (w/ protein)	19	ND
Gum Arabic (polysaccharide component)	polysaccharide (w/ protein)	18	ND
Alginic Acid	acidic polysaccharide	13	3
Bovine Serum Albumin	acidic protein, $pK_a = 4.8$	10	ND
DBSA	anionic surfactant	8	NA

[a] Adsorption on CA(42% acetyl) thin film cast on Ge IRE.
ND—Not detected
NA—Not applicable

Of the eight organic compounds tested, Triton X-100 appeared to adsorb to the greatest extent based on the film thickness. However, the 1512 cm^{-1} band intensity from the two trials differed greatly following the buffer rinse despite the fact the two films were cast from the same CA solution. Therefore, no strong conclusions were drawn at this time.

Benzalkonium chloride, a cationic quaternary amine, adsorbed to a very high extent on cellulose acetate (43.9% acetyl), presumably binding primarily by attractive electrostatic forces. Asymmetric cellulose acetate used in the manufacture of RO membranes has a reported pK_a near 3.5 and thus is negatively charged at pH 7.[43,44,45] Similar desorption rates were recorded during the MS buffer rinse and during 0.1% DBSA treatment, indicating that the anionic surfactant did not affect benzalkonium chloride desorption from the CA film (Figure 7.6.9). Thus, a large quantity of material remained adsorbed on the CA surface.

The formation of "hemimicelles" at the aqueous-polymer interface may account for the high quantity or firm binding of benzalkonium chloride (and Zwittergent 3-16, see discussion below) on the CA film. The concept of hemimicelles was initially proposed by Gaudin and Fuerstenau.[46] More recently, Childress and Elimelech proposed that dodecyltrimethylammonium bromide forms hemimicelles on negatively charged polymeric membranes.[43] Carboxylate groups in cellulose acetate impart a slight negative charge to polymer. Therefore, the quaternary amine can sorb to the surface by electrostatic interactions, leaving the hydrocarbon tail exposed to the bulk aqueous phase. The bilayer or aggregates form when the aliphatic tail of free surfactant molecules interact with those of the adsorbed layer, thereby minimizing their exposure to the aqueous phase and reducing the free energy of the system (Figure 7.6.10). Benzalkonium chloride, a mixture of C_{12}, C_{14} and C_{16} substituted quaternary amines, is approximately 24 Å in length. The thickness of the adsorbed benzalkonium chloride hemimicelle layer was 46 Å, about twice the thickness, or length, of the molecule. These hemimicelle structures did not form on bare germanium at pH 7 as the adsorbed film was only 6 Å thick.

More DBSA was retained at the CA surface in the presence of an adsorbed film of benzalkonium chloride (see Figures 7.6.4 and 7.6.9). (A final MS buffer rinse was only applied to experiments with gum arabic and benzalkonium chloride.) Electrostatic forces between the positively charged quaternary amine adsorbed on the membrane and the negatively charged sulfonate group likely affect DBSA adsorption.

A large quantity of the neutral polysaccharide dextran also remained firmly bound to the CA film following the buffer rinse. Hydrogen bonding and dipole-dipole interactions presumably contribute to the binding of dextran to the polymer film. DBSA was less effective at removing the neutral polysaccharide as compared to BSA, alginic acid and gum arabic (polysaccharide and protein components). After correcting for overlapping vibrational bands from DBSA, dextran initially appeared to desorb rapidly upon exposure to the surfactant (Figure 7.6.6). However, after 30 min, dextran desorption tapered off to half the rate observed during the MS buffer rinse. The DBSA treatment removed approximately 33% of the polymer material that remained after the buffer rinse. However, a significant quantity of dextran still remained adsorbed to the CA film.

Significantly lower quantities of the negatively charged organic macromolecules alginic acid, albumin and DBSA remained adsorbed to the CA films as compared to dextran

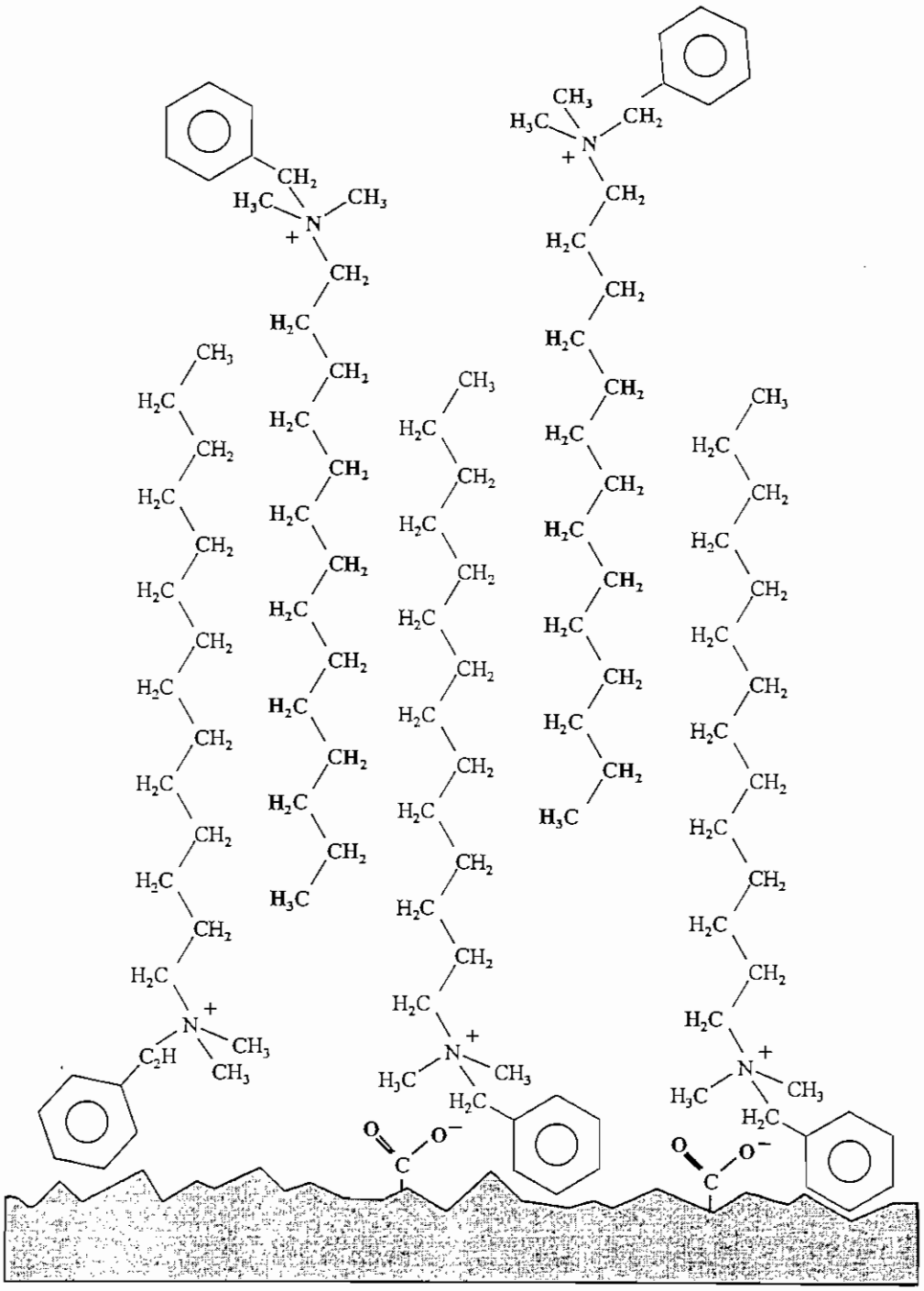

Figure 7.6.10 Diagram of benzalkonium chloride (C_{14}) hemimicelle formed on the surface of cellulose acetate.

and benzalkonium chloride (Table 7.6.1). At low ionic strength ($\mu = 0.05$, MS buffer), charge screening of the double layer is less pronounced. Therefore, electrostatic repulsion between these organics and the membrane surface is greater, presumably leading to less adsorption and retention of these organics on the CA surface following the buffer rinse.[43] Albumin and alginic acid that remained adsorbed on the CA thin film after the MS buffer rinse were rapidly removed upon exposure to 0.1% DBSA (see Table 7.6.1). Protein and polysaccharide are the most prominent components identified in ATR infrared spectra of adsorbed bacterial cells.[24,25,28,47] Application of DBSA to adherent *Mycobacterium* cells resulted in rapid detachment from the surface of a thin film of cellulose acetate.[42] DBSA's effect on adsorbed protein and polysaccharide may account for the desorption or detachment of bacteria from the aqueous-polymer interface. Specifically how the surfactant acts on these macromolecules to cause desorption is not well understood. DBSA may bind to the adsorbed proteins and polysaccharides and reduce the surface tension at the interface, causing the macromolecules to desorb from the surface.

Gum arabic adsorption fell in between the cationic and anionic macromolecules. The polysaccharide contains the acidic sugar, glucuronic acid; however, the composition of the protein component associated with it is not known. Thus, the net charge on gum arabic at pH 7 is unknown. The polysaccharide component of gum arabic was more difficult to remove from the CA surface. The protein component was stripped off immediately, while the polysaccharide was only partially removed when DBSA was first applied. Complete removal of the adsorbed polysaccharide occurred during the last 30 min of the DBSA addition.

DBSA demonstrated an innate ability to remove proteins and polysaccharides adsorbed to thin films of cellulose acetate (43.9% acetyl). Disruption of the chemical interactions between adsorbed organic macromolecules and the polymer surface are key to the development of more effective methods for cleaning membrane surfaces. A better understanding of how these compounds interact and affect desorption is of great interest. Work in the future will continue to be directed toward understanding how surfactants, like DBSA, and other chemicals affect macromolecular interactions at the aqueous-polymer interface.

Section 7.7 Adsorption of Natural Organic Material (NOM) from Reverse Osmosis Feedwater on Ge and Cellulose Acetate Thin Film

Bare Ge and CA-coated ZnSe IREs were exposed to feedwater (Q-22A) to the reverse osmosis elements at Water Factory 21 in Fountain Valley, CA. The feedwater consisted of secondary treated wastewater that had undergone flocculation with lime and an anionic surfactant, recarbonation with CO_2, multimedia sand filtration and chlorination (3 - 4 ppm). The feedwater was filtered at 0.22 μm to remove microorganisms and then analyzed by the Main Laboratory at OCWD. The results of this analysis are shown in Table 7.7.1.

NOM Adsorption from RO Feedwater on Ge IRE

Initially, feedwater was pumped through two flow cells containing Ge IREs. The water was not recirculated. After 21 hr, the Ge surface was rinsed by pumping deionized water through the flow cells to the end of a 36-hr experiment. Material believed to be

Table 7.7.1

Chemical Analysis of
Reverse Osmosis Feedwater (Q-22A)

Chemical Assay	Concentration
Total Organic Carbon (TOC)	8.1 mg/L
Total Dissolved Solids (TDS)	956 mg/L
Total Alkalinity	20.3 mg/L
pH	6.8

associated with protein (1550 cm^{-1} and 1557 cm^{-1}) and carbohydrate (1101 cm^{-1} and 1022 cm^{-1}) were detected at the surface of the IRE. These vibrational bands are plotted as a function of time of flow (Figures 7.7.1A and 7.7.1B, main bench) and (Figures 7.7.2A and 7.7.2B, right AEM). The IR spectra were dominated by vibrational bands associated with plasticizers or monomers from the BUNA O-rings (Figure 7.7.1B and Figure 7.7.2B). Organic material associated with the O-rings continued to adsorb at the Ge interface throughout the water rinse, although the rate of adsorption dropped slightly. Absorption bands near 1502, 1377, and 1240 cm^{-1} were related to compounds leaching from the O-rings. Vibrational bands near 1557 cm^{-1} and 1550 cm^{-1}, and 1101 cm^{-1} and 1022 cm^{-1} also dropped in intensity when the water rinse was initiated. The material believed to be carbohydrate desorbed rapidly from the surface of the IRE, and the two band intensities dropped to near zero absorbance. The protein material desorbed at a much slower rate and remained bound to the Ge surface after the 15-hr rinse.

NOM Adsorption from RO Feedwater on Cellulose Acetate Thin Film

After the problem with leaching plasticizers was resolved, the experiment was repeated with a CA(43.9% acetyl)-coated ZnSe IRE installed in the flow cell. Feedwater was pumped through the flow cell for 24 hr. No absorption bands indicative of organic material at the aqueous-polymer interface were detected. Two possible reasons for the inability to detect organics at the CA interface include (1) insufficient contact time and (2) insufficient sensitivity of the ATR/FT-IR spectrometry methodology (see discussion below).

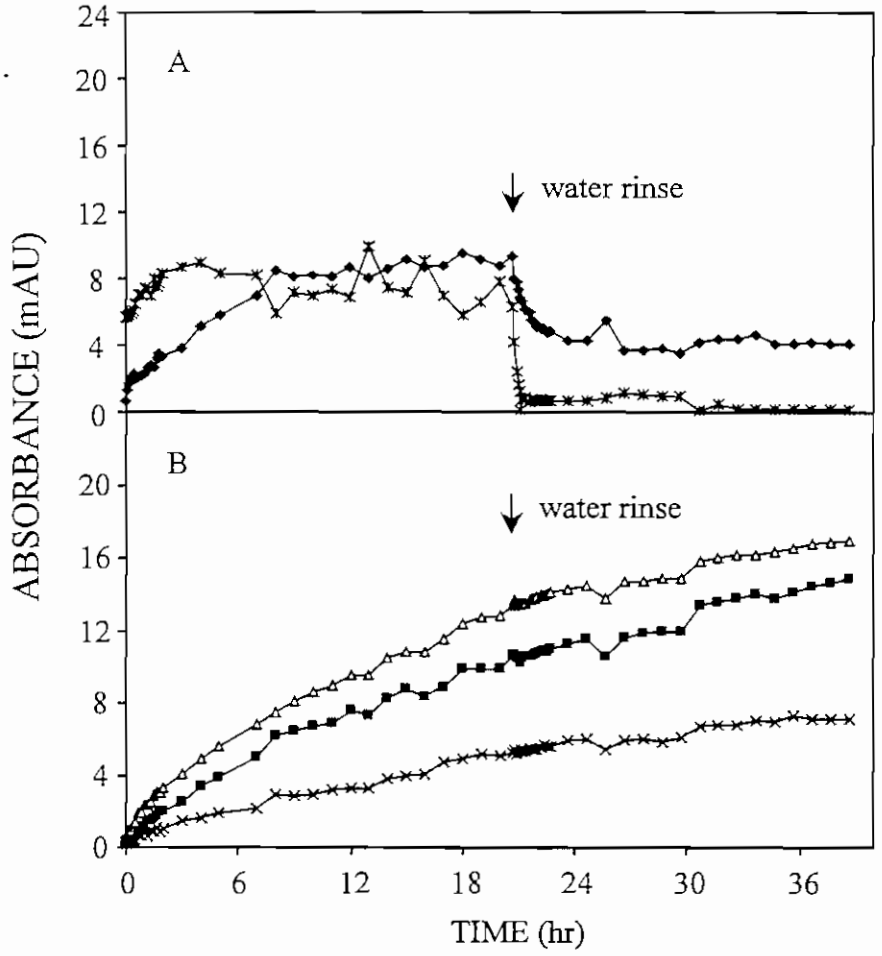

Figure 7.7.1 Reverse osmosis feedwater (Q-22A) adsorbed on Ge IRE. Plots of the (A) (◆) 1550 cm^{-1} and (✱) 1101 cm^{-1}, and (B) (■) 1502, (△) 1377 and (×) 1120 cm^{-1} band intensities as a function of time of flow (main bench).

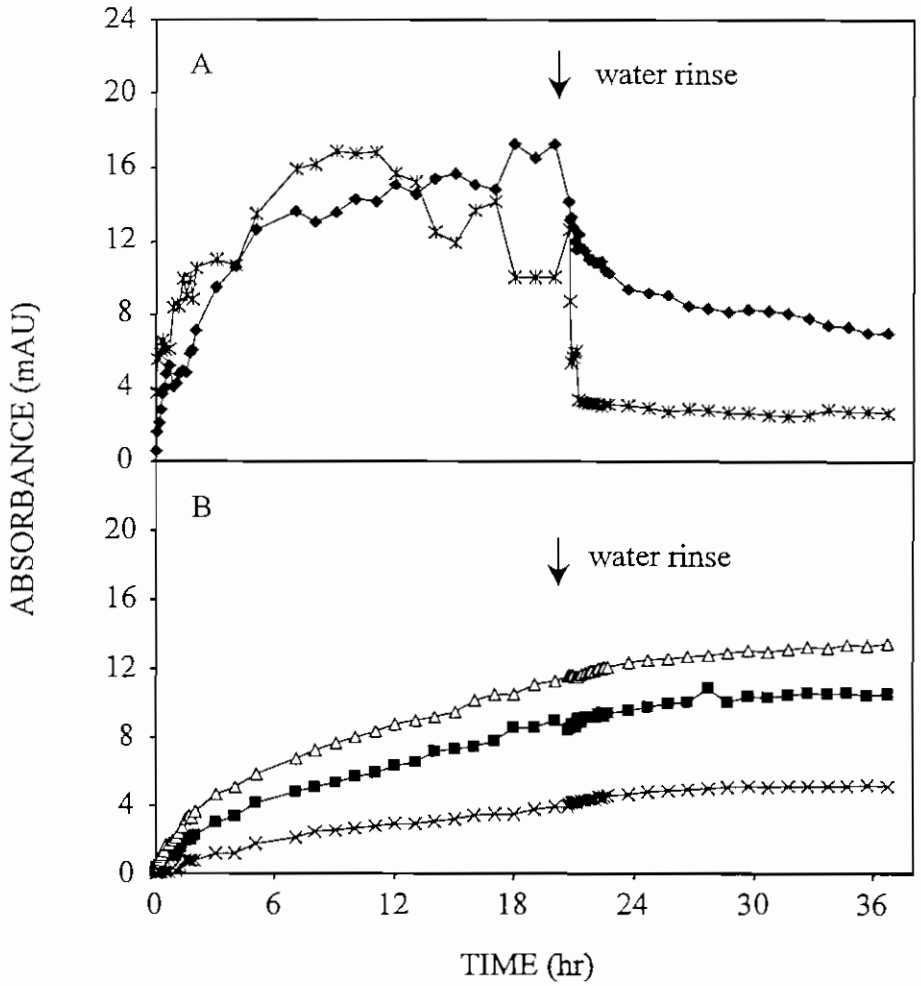

Figure 7.7.2 Reverse osmosis feedwater (Q-22A) adsorbed on Ge IRE. Plots of the (A) (◆) 1557 cm^{-1} and (✳) 1022 cm^{-1}, and (B) (■) 1502, (△) 1377 and (×) 1122 cm^{-1} band intensities as a function of time of flow (right AEM).

Section 7.8 Adsorption of Natural Organic Material from Colored Well Water on Germanium and Cellulose Acetate Thin Film

NOM Adsorption from Colored Well Water on Germanium

Colored water was collected from Deep Well No. 1 (~780 - 880 ft), located at OCWD in Fountain Valley, CA. Initially, unfiltered colored water was pumped through two flow cells, each containing a bare Ge IRE. After 24 hr of flow, the surface was rinsed with deionized water pH 8. Plots of the major absorption bands from adsorbed macromolecules are shown in Figure 7.8.1. Again, the major absorption bands in the IR spectra were associated with plasticizers that leached from the O-rings. These bands included 1500, 1378, 1242, and 1142 cm^{-1}. The 1500 cm^{-1} and 1378 cm^{-1} bands dropped at the start of the rinse but later increased in intensity throughout the remainder of the rinse period (see Figure 7.8.1). No vibrational bands were definitively linked to organic material associated with the colored water.

NOM Adsorption from Colored Well Water on Cellulose Acetate Thin Film

After eliminating the problem associated with O-ring plasticizers, the experiment was repeated. The colored water was filtered at 0.22 μm to remove microorganisms and then pumped through a flow cell containing a CA(43.9% acetyl)-coated ZnSe IRE. The filtered well water was analyzed by the Main Laboratory at OCWD. The results are shown in Table 7.8.1.

Table 7.8.1

Chemical Analysis of
Deep Well No.1 Water
Fountain Valley, CA

Chemical Assay	Concentration
Total Organic Carbon (TOC)	2.4 mg/L
Total Dissolved Solids (TDS)	228 mg/L
Total Alkalinity	156 mg/L
Color Units	60
pH	8.6

After 7 days exposure to the filtered well water, the experiment was terminated. A spectrum collected on Day 1 was digitally subtracted from a spectrum collected on Day 7. It is evident by the derivative band shape (i.e., the low wavenumber side of the band dips below zero) that the carbonyl band shifted to higher frequency upon exposure to the colored water (Figure 7.8.2). At the same time, the C-O-C acetate ester band intensity shifted to lower

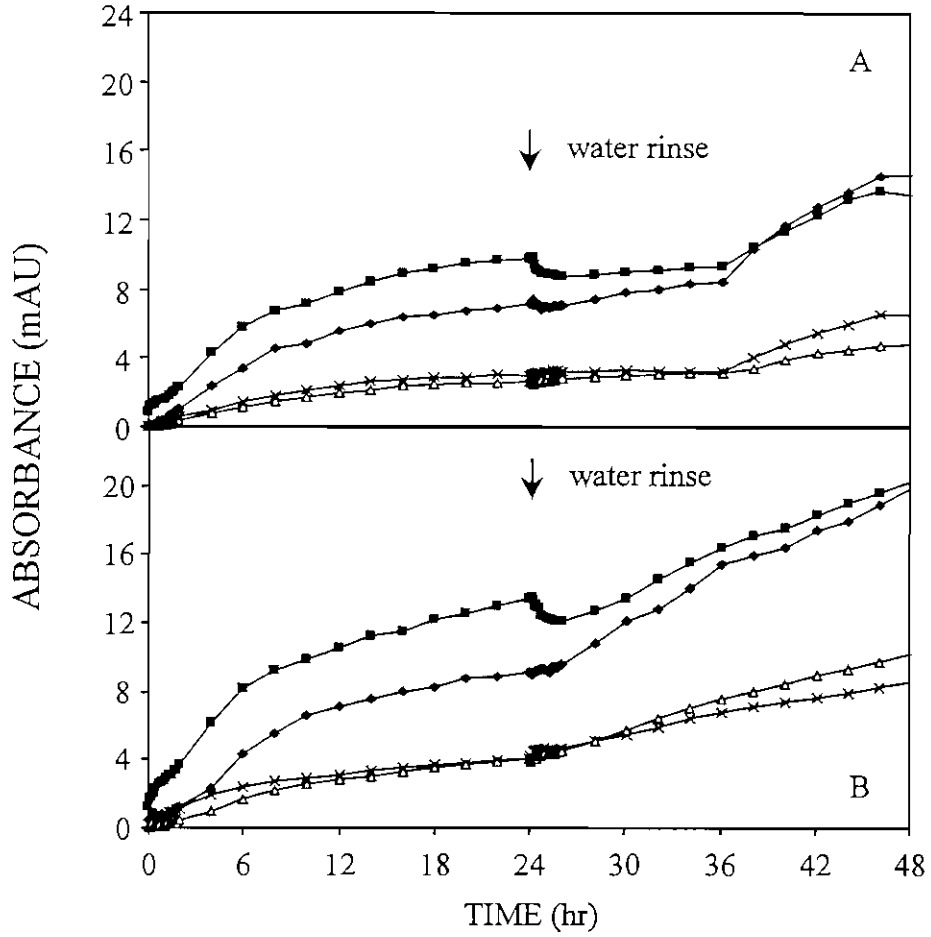

Figure 7.8.1 Ge IRE (A) main bench and (B) right AEM exposed to colored well water. Plots of the (•) 1500, (■) 1378, (▵) 1242 and (×) 1142 cm^{-1} band intensities as a function of time of flow.

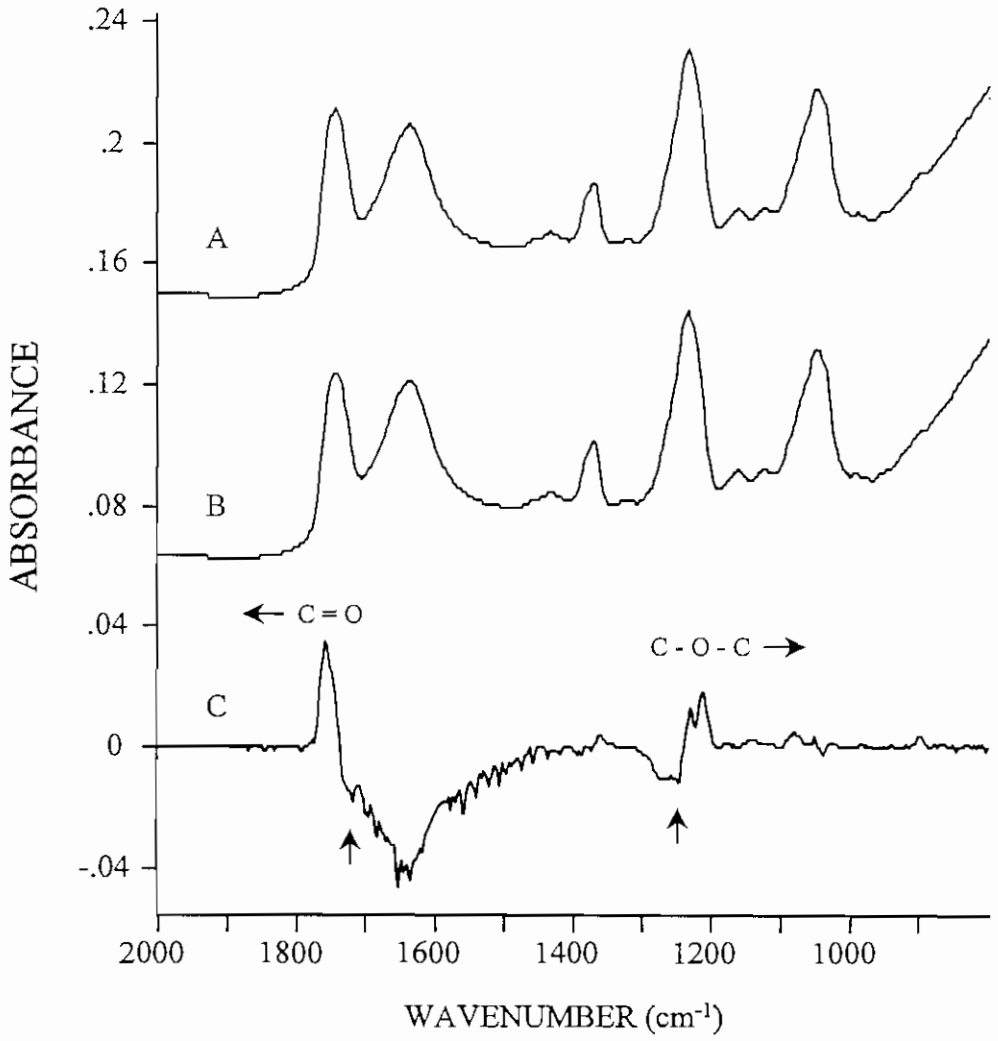

Figure 7.8.2 Spectra of organic material adsorbed on cellulose acetate (43.9% acetyl) thin film from flowing colored well water (A) 7 days (B) 1 day and (C) difference spectrum.

frequency, as this band was also derivative in shape. These shifts are opposite to those observed when the CA was hydrated (Figure 7.8.3). The shifts resulting from exposure to colored water suggest adsorption of material on the CA thin film and loss of the hydrogen bonding. In other words, material adsorbed on the CA film and displaced water from the surface, resulting in the loss of hydrogen bonding. Preliminary results suggest a compound with both aliphatic and aromatic structure (Figure 7.8.4).

Bubble contact angle measurements were made to determine changes in surface hydrophobicity. The height-to-diameter (H:D) ratio was measured for air bubbles captured under the sample substrate. These H:D measurements indicated a slight decrease in the surface hydrophobicity of the CA film, as the H:D ratio shifted from 0.726±0.012 to 0.745±0.008 (Figure 7.8.5). A high bubble H:D ratio is indicative of a hydrophilic surface.

Discussion

The sensitivity of the ATR/FT-IR technique for monitoring the adsorption of natural organic materials was less than anticipated. No organic material was detected at the surface of a CA(43.9% acetyl) thin film exposed to RO feedwater for 21 hr. Insufficient exposure time may also have contributed to the inability to detect adsorbed organic material. A detectable quantity of organic material did adsorb to the surface of a CA(43.9% acetyl) film exposed to colored well water. Preliminary results indicate that the material is both aromatic and aliphatic in nature. Adsorption of this material resulted in the reduction of the surface hydrophobicity of the CA film. This drop in hydrophobicity is opposite to what one would expect if a hydrophobic aliphatic aromatic compound were to adsorb at the surface. However, this increase in surface hydrophilicity is consistent with surface changes observed when humic acids adsorb.[48]

Again, the results are still preliminary and more work needs to be done. Changes are currently being implemented in the laboratory to improve on the sensitivity of the ATR/ FT-IR spectroscopic technique. These improvements are (1) using a thinner 2-mm ZnSe IRE to produce more internal reflections at the aqueous-polymer interface and (2) casting thinner (700-800 Å) films of CA on the IREs to allow more energy to pass through the polymer film.

Section 7.9 Combined ATR/FT-IR Spectrometry and Nomarski DIC Image Analysis of Bacterial Attachment on Cellulose Acetate Thin Films

The original proposal called for measurements of bacterial attachment to be made off-line. The experimental setup consisted of a series of flow cells designed to hold polymer-coated microscope slides (see Figure 7.4.7). Flow cells were connected in series with the ATR flow cell. Slides were periodically removed, stained with DAPI and bacterial cell surface coverage (cells/cm^2) determined as a function of time of flow. After review by the Research Advisory Board, this protocol was discarded in favor of an on-line method where real-time measurements could be made. Immediate implementation of this on-line method for imaging bacteria on CA-coated IREs was not possible. As a compromise, a circular flow cell, containing a CA-coated microscope slide, was placed in series with the ATR flow cell

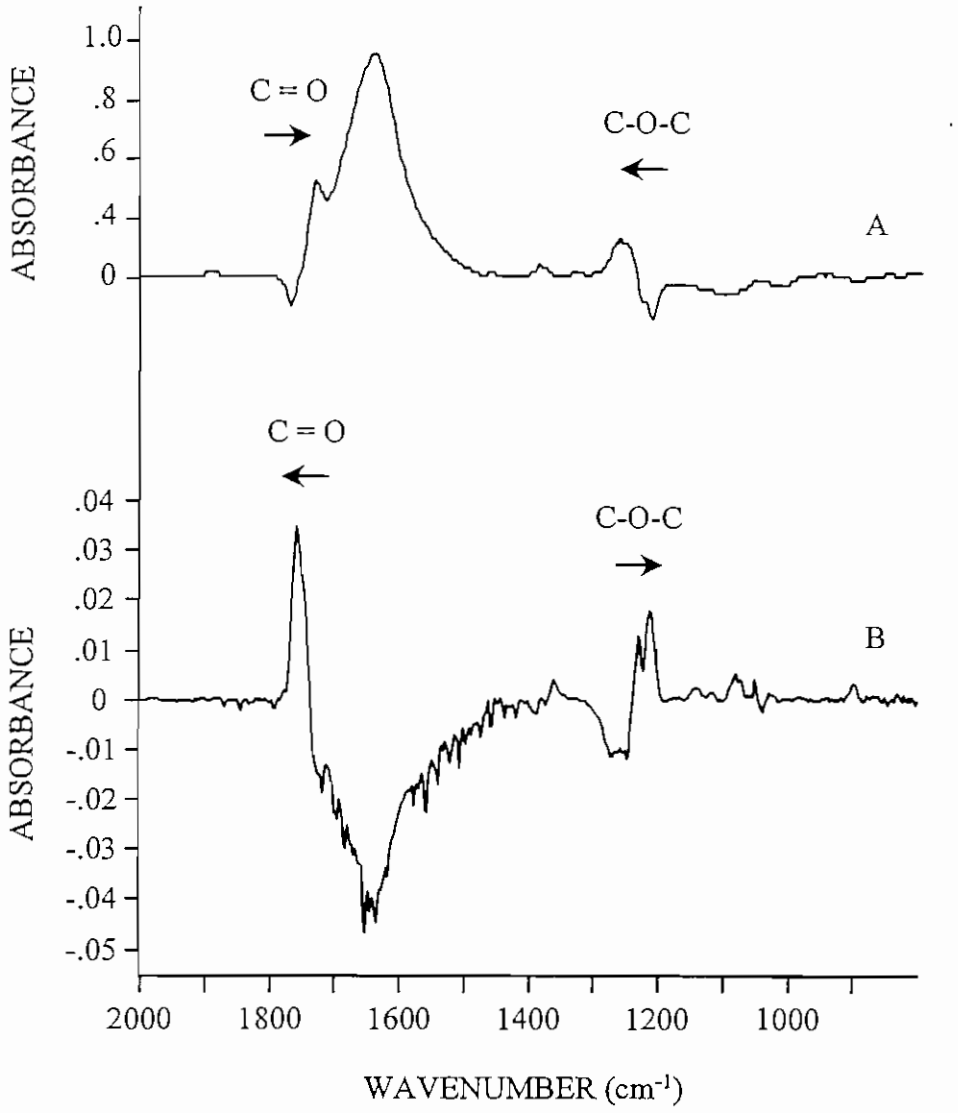

Figure 7.8.3 Difference spectra (A) hydrated CA spectrum less dry CA spectrum and (B) CA thin film exposed to colored well water Day 7 spectrum less Day 1 spectrum.

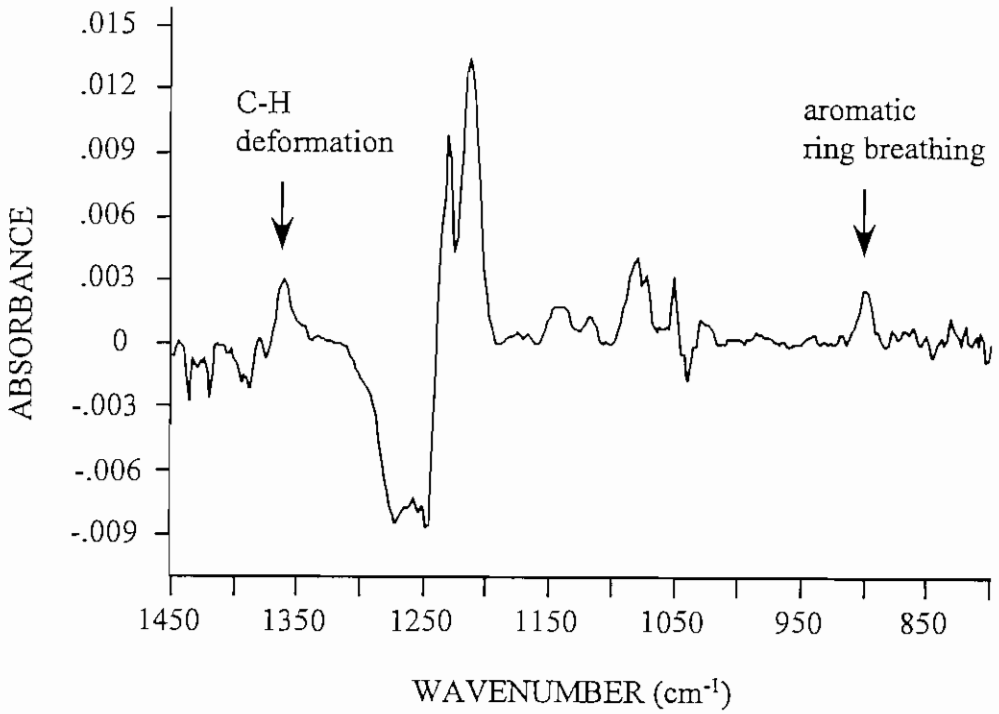

Figure 7.8.4 Difference spectrum (Day 7 less Day 1) of cellulose acetate (43.9% acetyl) thin film exposed to colored well water.

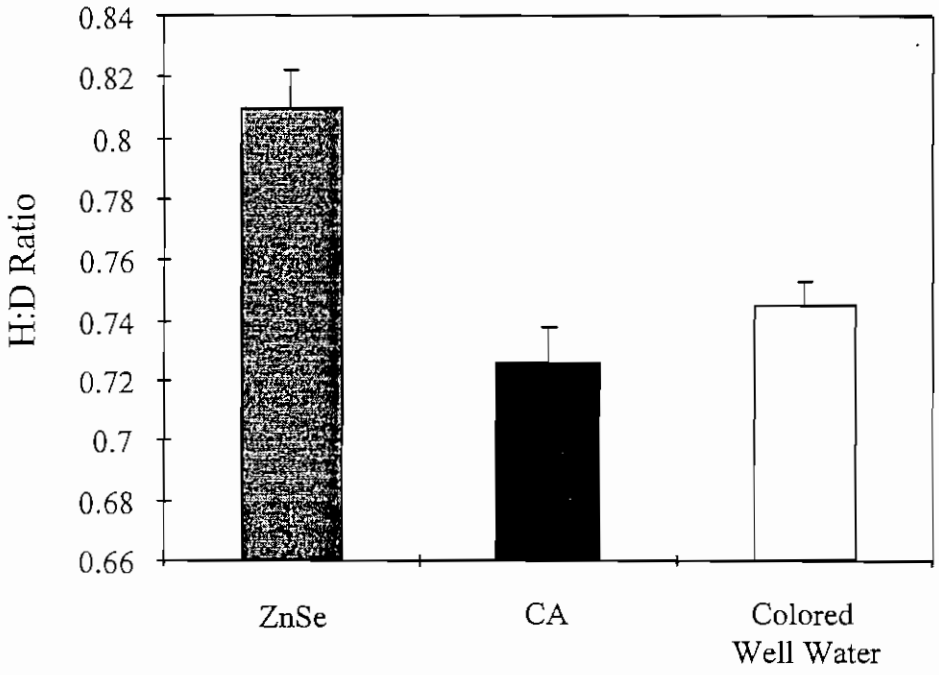

Figure 7.8.5 Captive bubble contact angle measurement. Height:Diameter ratio (± std. dev., n = 10) of air bubble suspended under ZnSe IRE, CA thin film and cellulose acetate (43.9% acetyl) thin film exposed to colored well water for 7 days.

so that images of adherent bacteria could be captured (Figure 6.4 and Figure 7.9.1). Silicone inserts were placed in the imaging flow cell to match the fluid dynamics of the ATR flow cell. Nomarski differential interference contrast microscopy was used to visualize adherent bacterial cells, and images were captured using a CCD camera and framegrabber board.

Effect of Zwittergent 3-16 Pretreatment on *Mycobacterium* BT12-100 Attachment on Cellulose Acetate (43.9% acetyl) Thin Films

The effect of Zwittergent 3-16 pretreatment on bacterial attachment to cellulose acetate (43.9% acetyl) was investigated. At the same time, molecular adsorption at the aqueous-polymer interface was investigated by ATR/FT-IR spectrometry. The CA thin films coated on a ZnSe IRE and glass coverslip were hydrated by pumping MS buffer through the two flow cells. Infrared spectra were collected over a 30-min period. Following hydration of the CA, a 0.25% solution of Zwittergent 3-16 was pumped through the flow cells. After 4 hr the CA films were rinsed with buffer for 2 hr. Finally, a cell suspension (1.0×10^8 cells/mL) of *Mycobacterium* isolate BT12-100 was pumped through the two flow cells. Infrared spectra were collected periodically throughout the 10.5 hr experiment. Visual images were collected during the final 4-hr period, when bacterial cells were pumped through the flow cells. The same cell suspension was also pumped through a circular flow cell containing an untreated CA film, and images were captured over a 4-hr period. The untreated CA film served as the control.

Plots of the four major CA band intensities as a function of time of flow are shown in Figure 7.9.2. The four CA bands and the water band intensity remained unchanged during the short 30-min hydration period. When the Zwittergent 3-16 solution was pumped through the flow cells, the water band rose immediately from 0.851 AU to 1.35 AU, a 57% increase. The intensity of the 1743, 1369 and 1236 cm^{-1} bands of CA also increased but nowhere near in magnitude to the water band (see Table 7.9.1). It is difficult to explain why the intensity of the water band increased so much. The 1743, 1369 and 1236 cm^{-1} band intensities all increased slightly, suggesting that the thin film collapsed on the surface of the IRE when Zwittergent 3-16 was pumped into the flow cell. However, the 1049 cm^{-1} C-O stretching band intensity actually dropped 1.5%, suggesting the opposite. An air bubble may have become trapped in the ATR flow cell when it was filled with buffer during the initial hydration step. When the surfactant solution was pumped through the flow cell, the

Table 7.9.1

Changes in IR Bands Upon Exposure to 0.25% Zwittergent 3-16

Organic Compound	1743 cm^{-1}	1637 cm^{-1}	1369 cm^{-1}	1236 cm^{-1}	1049 cm^{-1}
Zwittergent 3-16	+9.0%	+57%	+5.9%	+3.8%	-1.5%

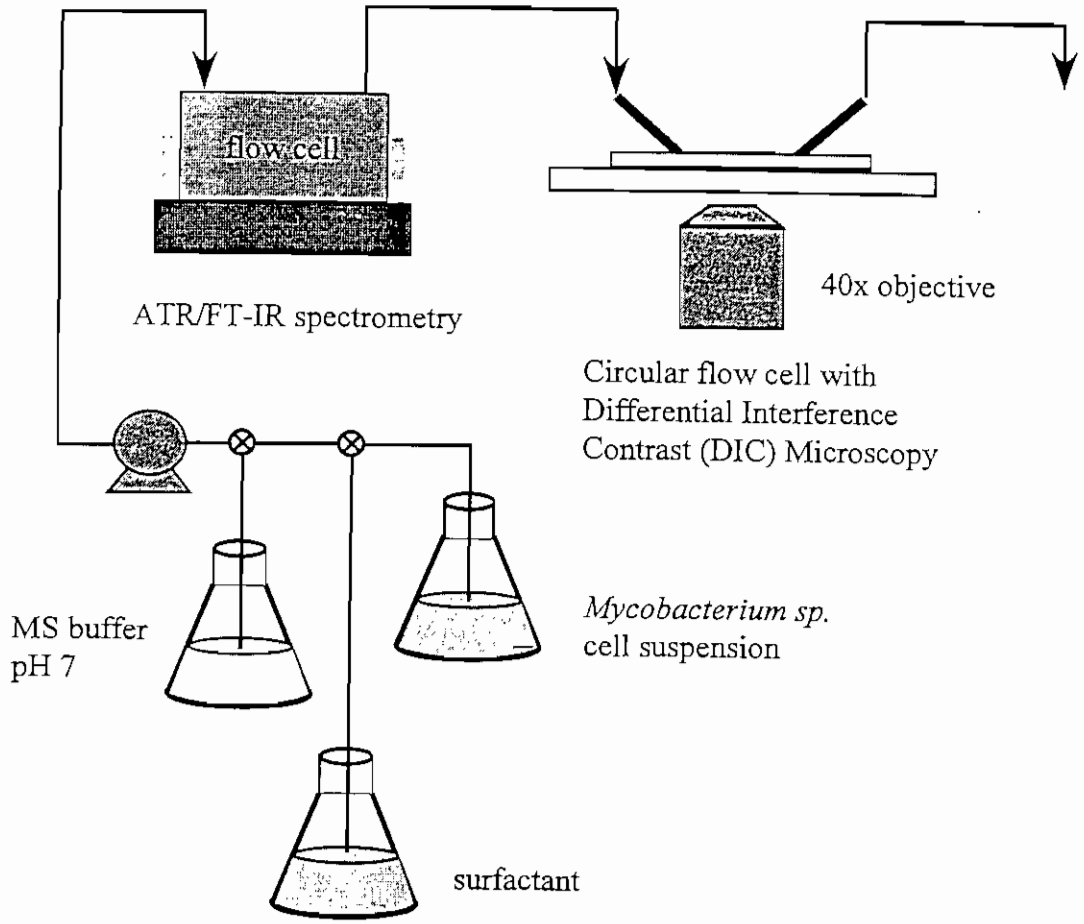

Figure 7.9.1 Schematic diagram of on-line ATR/FT-IR spectrometry/ Normarski differential interference contrast microscopy.

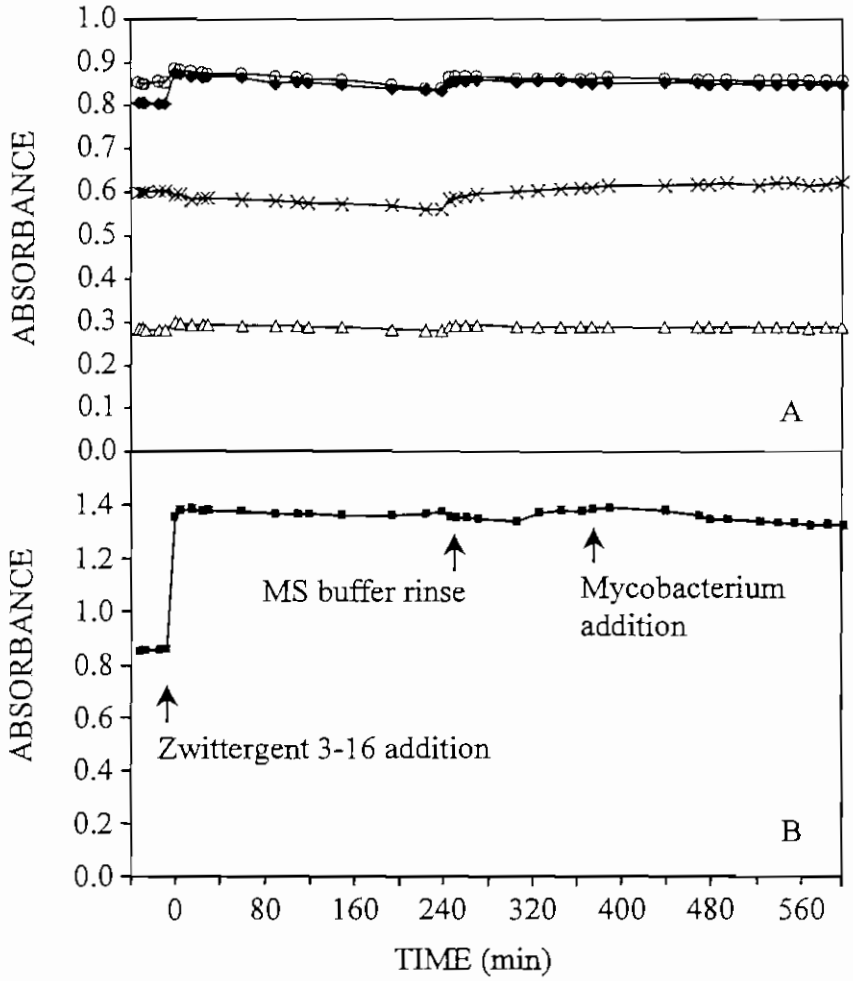

Figure 7.9.2 Plots of the (◆)1743, (△)1369, (○)1236 and (×)1049 cm^{-1} band intensities of (A) cellulose acetate (43.9% acetyl) and (B) the 1637 cm^{-1} water band intensity as a function of time of flow.

bubble was likely displaced, resulting in the observed increase in the 1637 cm^{-1} water band intensity. Aside from the large increase in water band intensity at the start of the Zwittergent 3-16 addition, the CA bands and water band remained essentially unchanged during the 10.5 hr experiment. Again, these CA films on ZnSe demonstrated much greater stability than those cast on Ge IREs (see Figures 7.3.2 and 7.3.3).

A series of ATR/IR spectra of Zwittergent 3-16 adsorbed from flowing solution on CA(43.9% acetyl) is shown in Figure 7.9.3. A plot of the 1487 cm^{-1} band intensity of the surfactant as a function of time of flow is shown in Figure 7.9.4. There was a 15-min delay before a measurable 1487 cm^{-1} band intensity was detected. Some of the delay was attributed to the filling of the flow cell and displacement of MS buffer. The flow cell was not rapidly flushed with surfactant. Instead, it was pumped through at 8 mL/hr, and the data acquisition macro started when surfactant made contact with the CA film. One turnover volume or turnover time takes approximately 7.5 min, assuming plug flow. Therefore, some type of delay was expected. A short delay in Zwittergent 3-16 adsorption on Ge was observed (see Figure 7.1.13). However, this delay was not attributed to filling, as surfactant was rapidly siphoned into the flow cell displacing one volume before the data acquisition was initiated. The surfactant adsorbed at the interface at a constant rate, and the 1487 cm^{-1} band appeared to reach a pleateau of 2.60 mAU after 210 min.

After 4 hr the surface of the CA film was rinsed with MS buffer pH 7. A hydrated CA reference spectrum was subtracted from select sample spectra, revealing the underlying Zwittergent 3-16 spectrum. The 1487 cm^{-1} band did not drop with time, which would have indicated desorption of the adsorbed surfactant. However, the band shape in this region of the spectrum changed significantly, enough that it became difficult to determine whether the difference spectra really represented adsorbed Zwittergent 3-16. Thus, the results from the buffer rinse are inconclusive. In a previous experiment, Zwittergent 3-16 remained firmly adsorbed to CA(42%-acetyl) in spite of a 4-hr water rinse (see Figure 7.6.1). The Zwittergent 3-16 from this experiment presumably remained firmly bound to the CA(43.9% acetyl) film, following the 4-hr buffer rinse.

After the CA thin film was treated with Zwittergent 3-16 and rinsed with buffer, a cell suspension of *Mycobacterium* isolate BT12-100 was pumped through the flow cells. Again, the spectra proved to be difficult to process and the subtracted/difference spectra were difficult to interpret. The typical Amide I (1650 cm^{-1}) and Amide II (1550 cm^{-1}) protein bands, indicative of bacterial attachment, were not clearly visible. A band centered at 1514 cm^{-1} did appear and increased in intensity with time (Figure 7.9.5). This band is about 35 cm^{-1} lower than a typical Amide II protein band. The exact assignment and origin of the 1514 cm^{-1} band is currently in question. A band near 1018 cm^{-1}, assigned to the C-O stretch of carbohydrate/polysaccharide material, also increased with time of flow. A series of ATR/IR spectra in the region near 1018 cm^{-1} are shown in Figure 7.9.6. A plot of the 1514 cm^{-1} and 1018 cm^{-1} band intensities as a function of time of flow are shown in Figure 7.9.7 (top). The 1018 cm^{-1} band appeared to plateau briefly (30 min) near T = 2 hr and then continued to rise, while the 1514 cm^{-1} band intensity rose slowly at a constant rate throughout the 4-hr period. The rate of change of the 1018 cm^{-1} band intensity increase was 2.4 hr^{-1} (between T = 0 min and T = 100 min) as compared to 0.535 hr^{-1} for the 1514 cm^{-1} band, a 4.5-fold difference. The two bands are plotted against each other in Figure 7.9.7 (bottom). The data were fit to a linear regression line with a correlation coefficient (R^2) equal

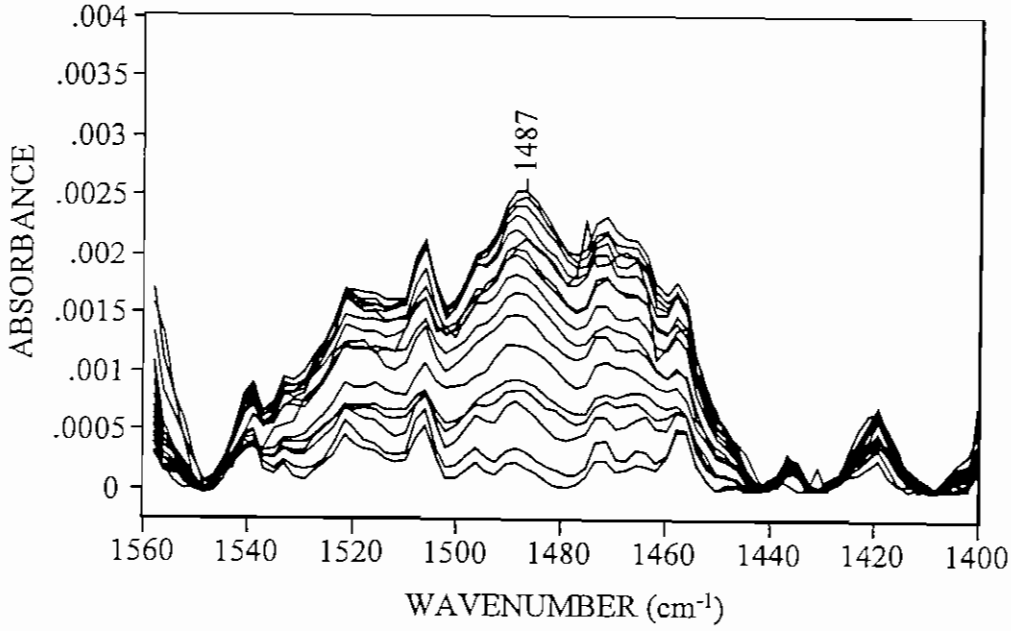

Figure 7.9.3 ATR/IR spectra of Zwittergent 3-16 adsorbed on a cellulose acetate (43.9% acetyl) thin film from flowing solution at pH 7.

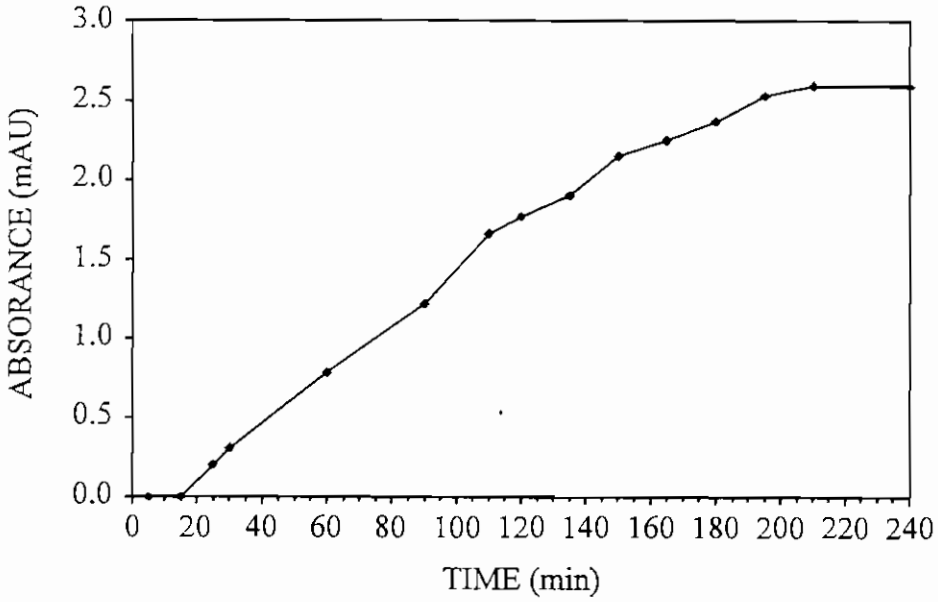

Figure 7.9.4 Zwittergent 3-16 adsorption on cellulose acetate (43.9% acetyl). Plot of the 1487 cm^{-1} band intensity of Zwittergent 3-16 as a function of time of flow.

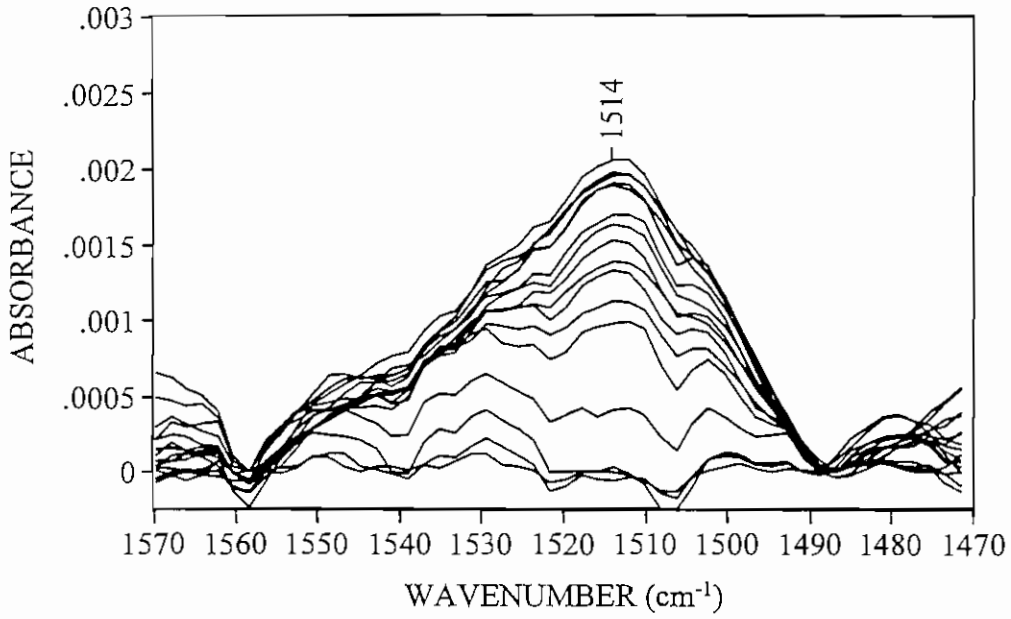

Figure 7.9.5 ATR/IR spectra of Mycobacterium isolate BT12-100 adsorbed from flowing solution on cellulose acetate (43.9% acetyl) thin film.

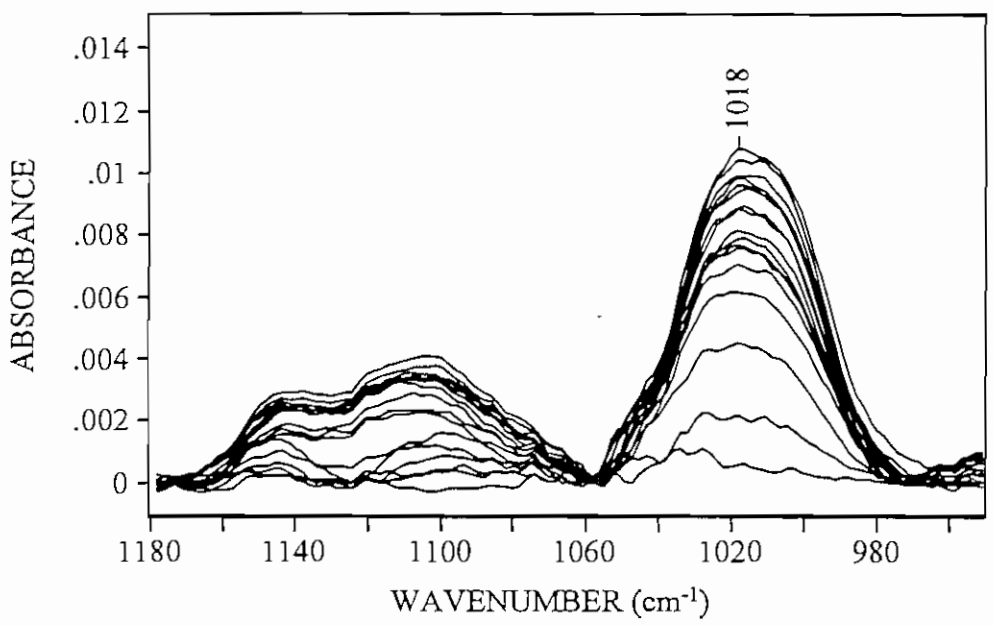

Figure 7.9.6 ATR/IR spectra of Mycobacterium isolate BT12-100 adsorbed from flowing solution on cellulose acetate (43.9% acetyl) thin film.

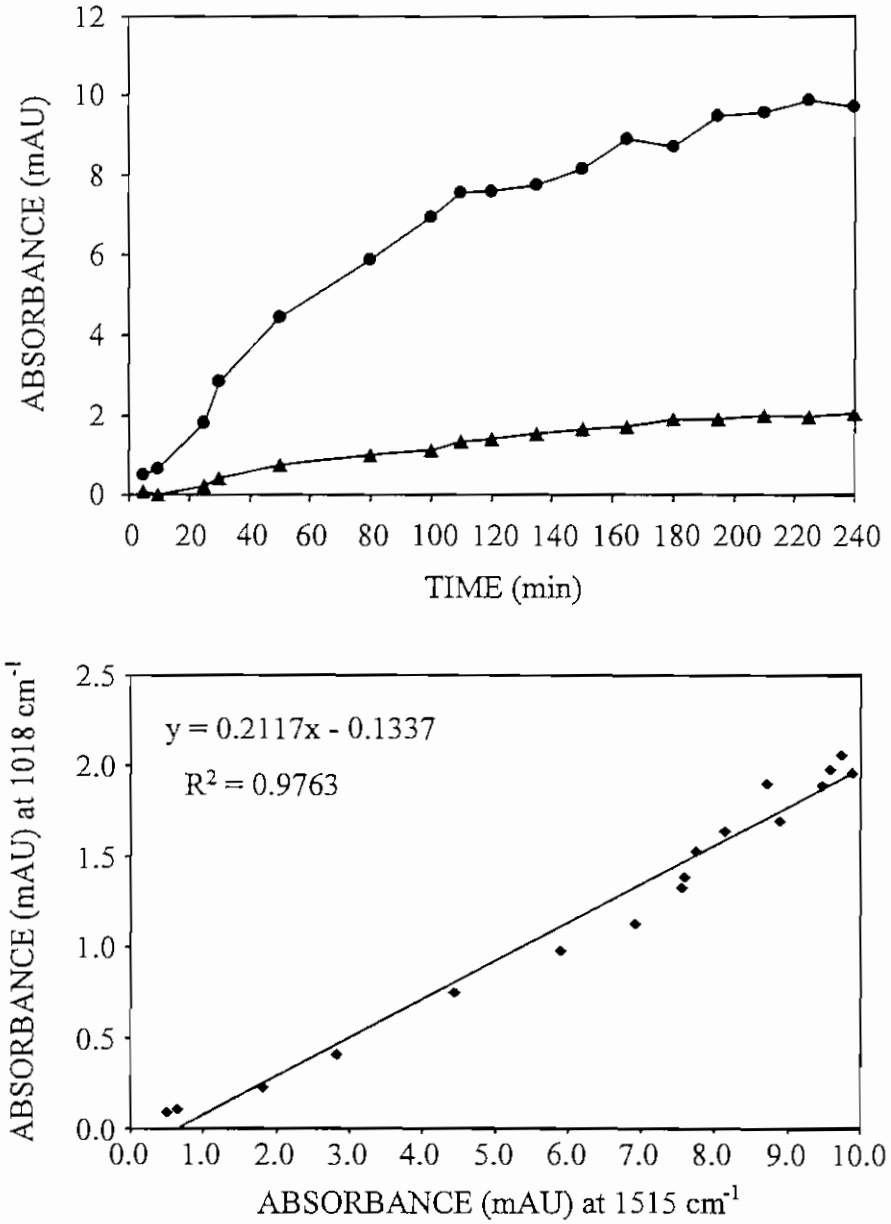

Figure 7.9.7 Plots of the (▲) 1514 cm^{-1} and (●) 1018 cm^{-1} band intensities of Mycobacterium isolate BT12-100 as function of time of flow (top), and plot showing the relationship between the 1514 cm^{-1} and 1018 cm^{-1} band intensities.

to 0.9763. The result indicates that the relative rate of change of these band intensities were constant over the 4-hr period, i.e., the two band intensities increased at two different rates, but the rates at which they changed relative to each other was constant.

Visual images were captured periodically as the *Mycobacterium* cell suspension was pumped through the flow cells. A series of Nomarski DIC images are shown in Figure 7.9.8. Also included are a series of images that show bacterial adhesion on an untreated CA (control) film. Both CA films were exposed to bacterial cells from the same suspension of *Mycobacterium* isolate BT12-100. A plot of the percent surface area occupied by bacteria as a function of time of flow is shown in Figure 7.9.9. Approximately 3-fold less area was covered by *Mycobacterium* cells attached to the Zwittergent 3-16 pretreated CA film as compared to the untreated CA control. Cell adhesion on both films reached a plateau approximately 2 hr into the 4-hr period. Therefore, the rate of adhesion on the pretreated CA film (1.98 hr^{-1}) was also 3-fold less than the rate of adhesion on untreated CA control (5.71 hr^{-1}). While bacterial attachment to the surfactant-treated CA film appeared to plateau near 120 min, the 1018 cm^{-1} C-O stretching band intensity continued to increase with time. However, when bacterial adhesion was correlated with the changes in 1018 cm^{-1} and 1514 cm^{-1} band intensities by plotting the percent surface coverage as a function of IR band intensities, it was apparent that the relationships were linear (Figure 7.9.10). The correlation coefficient (R^2) for the relationship between cell surface coverage and carbohydrate or polysaccharide production was 0.985. Fewer data points were used to determine the correlation than displayed in individual plots, as IR and visual images did not always match with respect to the time of acquisition. The correlation between percent surface coverage and the 1514 cm^{-1} band intensity was not as good ($R^2 = 0.8778$). One could almost argue that the relationship between cell surface coverage and the 1514 cm^{-1} band intensity was linear up to 120 min. After 120 min, the 1514 cm^{-1} band continued to increase while the surface coverage or cell attachment remained unchanged.

Discussion

Zwittergent 3-16 adsorbed onto a CA(43.9% acetyl) thin film, which led to a significant reduction in *Mycobacterium* isolate BT12-100 adhesion as revealed by visual images and calculations of percent surface coverage. Zwittergent 3-16 is a zwitterionic detergent (see Section 7.1) with a terminal sulfonate (SO_3^-) group, quaternary amine and C_{16} hydrocarbon tail. The surfactant is presumed to bind by electrostatic interactions, i.e., via the quaternary amine to carboxylate groups on the surface of the CA film. This would leave the hydrocarbon tail exposed to the bulk aqueous phase, which is not energetically favorable. However, a hemimicelle structure, i.e., a bilayer of surfactant molecules, may form at the surface of the CA film, reducing the free energy of the system (Figure 7.9.11). The 0.5% (12.7 mM) concentration of Zwittergent 3-16 used was well above the reported critical micelle concentration of 0.1 – 0.6 mM. The concept of hemimicelle formation at the surface of synthetic polymer membranes was recently proposed by Childress and Elimelech.[43] A bilayer of dodecyltrimethylammonium bromide (cationic surfactant) was believed to form at the surface of a thin-film composite (TFC) polyamide reverse osmosis membrane at high pH. Similarly, a hemimicelle of sodium dodecylsulfate (anionic surfactant) was proposed to form on TFC polyamide RO, TFC polyamide nanofiltration and cellulose acetate RO membranes

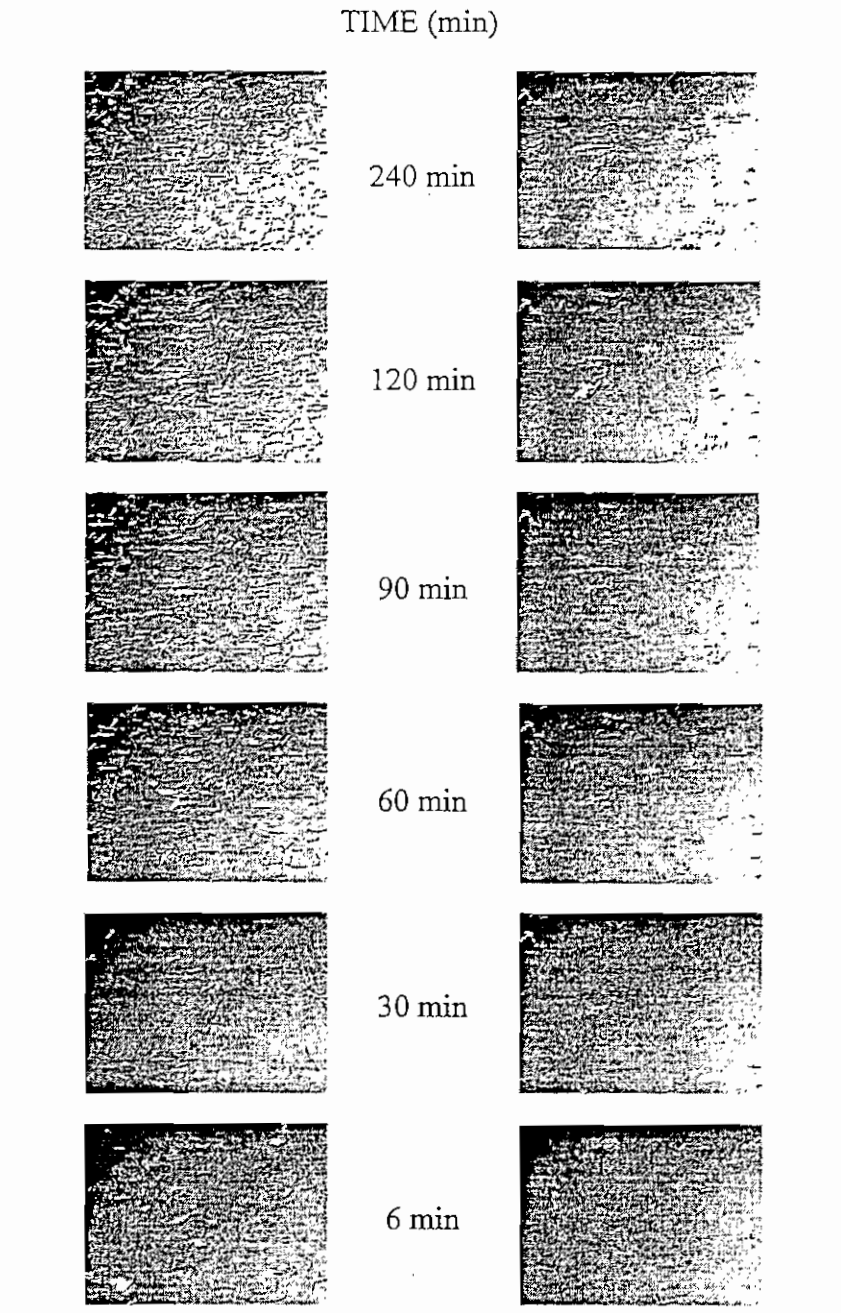

Figure 7.9.8 Nomarski differential interference contrast images of Mycobacterium isolate BT12-100 adsorbed from flowing solution on cellulose acetate (43.9% acetyl) thin film. Each field of view is 117 x 157 microns.

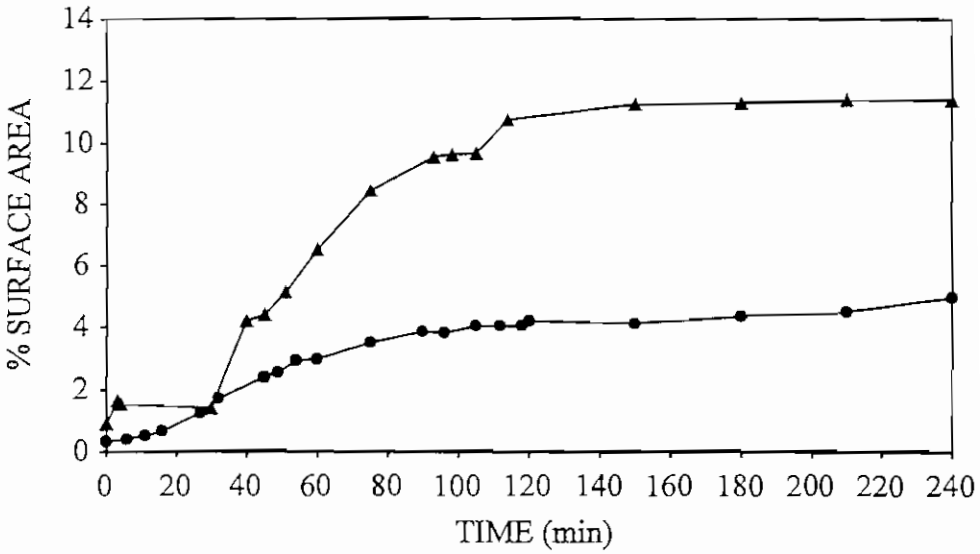

Figure 7.9.9 Plot of the percent surface area covered by Mycobacterium isolate BT12-100 adsorbed on cellulose acetate (43.9% acetyl) (▲) untreated control and (●) pretreated with Zwittergent 3-16 as a function of time of flow.

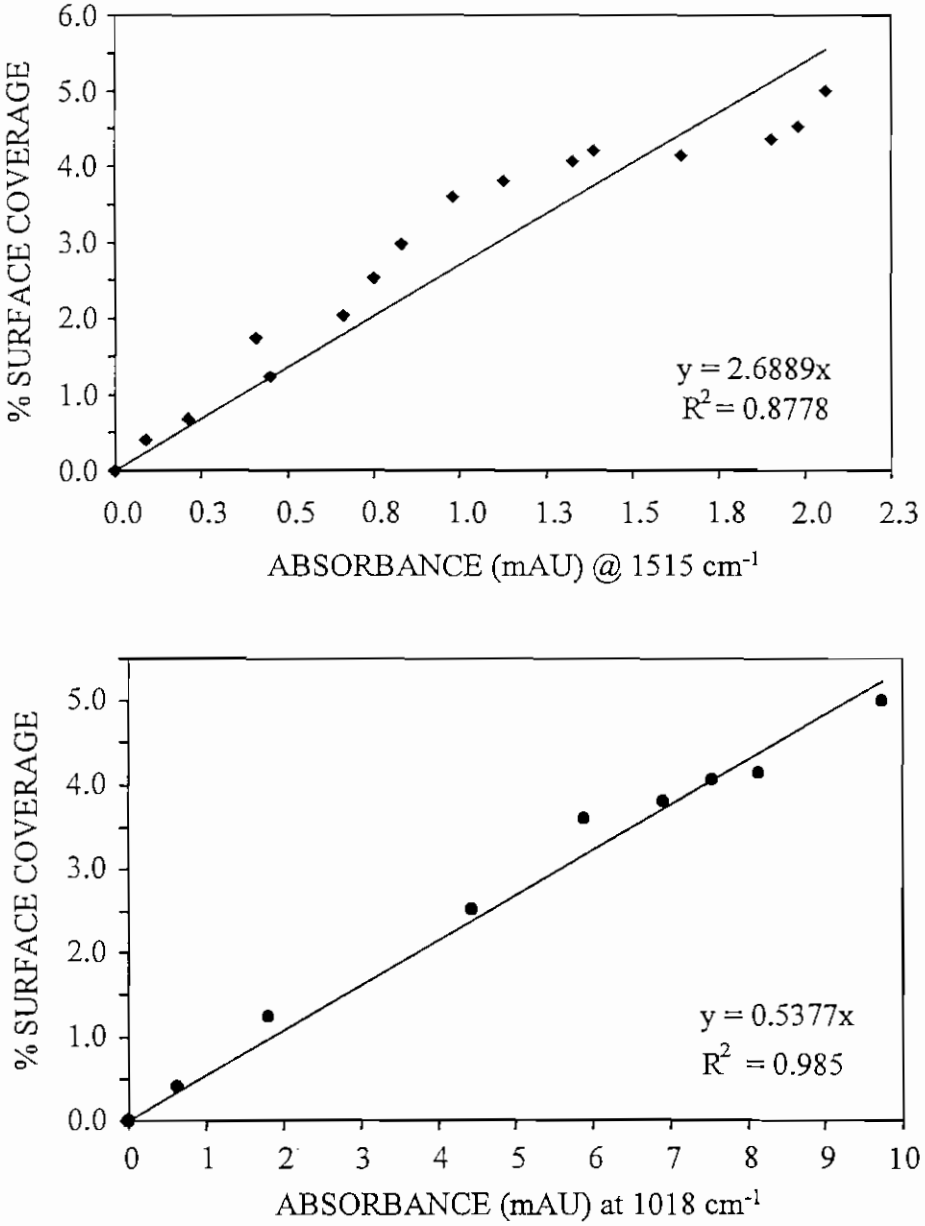

Figure 7.9.10 Plots of the 1514 cm^{-1} (top) and 1018 cm^{-1} (bottom) band intensities of Mycobacterium BT12-100 adsorbed on CA(43.9% acetyl) as a function of percent surface coverage.

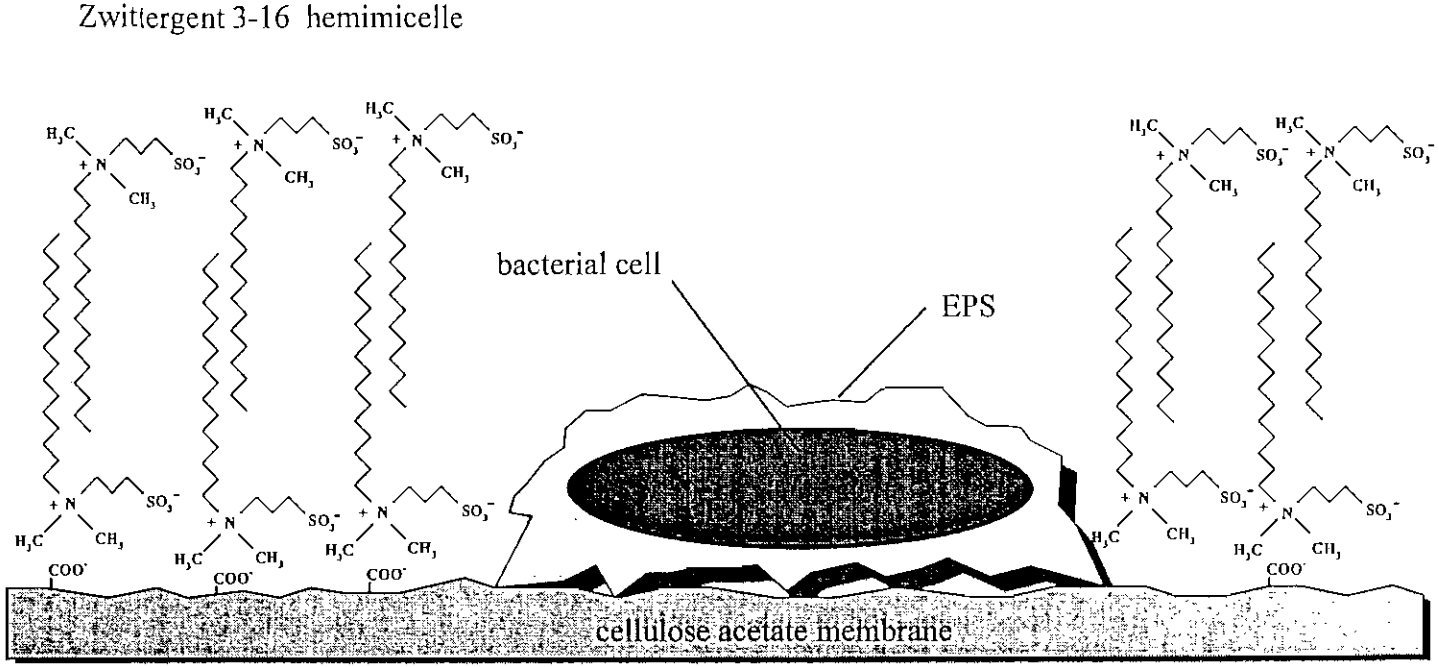

Figure 7.9.11 Bacterial cell adsorbed on the surface of cellulose acetate in the presence of a Zwittergent 3-16 hemimicelle. Diagram not to scale.

at low pH. This adsorbed layer of surfactant alters the chemistry on the surface of CA enough to inhibit attachment of *Mycobacterium* isolate BT12-100. The bacteria that do attach may adhere to areas not covered by Zwittergent 3-16 (see Figure 7.9.11). At no time were the bacteria exposed to bulk phase surfactant, as the flow cell containing the surfactant-treated CA film was rinsed with buffer prior to the introduction of the cell suspension. Therefore, the surface chemistries of the *Mycobacterium* cells exposed to the control and Zwittergent 3-16 treated CA film were the same.

Other studies of bacterial attachment on pretreated CA surfaces by Nomarski DIC microscopy have been reported in our lab.[42] Chloramine, DBSA, DBSA/LiBr, zosteric acid benzalkonium chloride and Zwittergent 3-16 have been used as surface pretreatments with mixed results. A combination of DBSA and LiBr applied to a CA(42% acetyl) thin film effectively reduced *Mycobacterium* isolate BT12-100 attachment. Chloramine, DBSA and zosteric acid pretreatments of CA actually resulted in the promotion of *Mycobacterium* attachment, while pretreatments with benzalkonium chloride and Zwittergent 3-16 did not significantly alter bacterial attachment. A lower concentration of Zwittergent 3-16 (0.1%) and a CA film with a lower acetate (42%) content was used in these experiments, which may explain the difference from our results.

Bacterial attachment is proposed to occur in two steps, an initial weak stage of attachment followed by more firm attachment facilitated by EPS, of which exopolysaccharides are typically a major contributor.[49,7,8,9] Attachment to solid substrates is thought to stimulate extracellular polysaccharide production by bacteria. Vandevivere and Kirchman reported that the addition of sand to shake-flask cultures seemed to induce exopolymer synthesis.[50] At first glance, the 1018 cm^{-1} band associated with carbohydrate/polysaccharide appeared to increase in intensity after adhesion of *Mycobacterium* cells on the Zwittergent-pretreated CA film reached steady state (see Figure 7.9.7 and Figure 7.9.9). This would suggest that polysaccharide production continued after cell attachment had stopped. However, when the two sets of data (surface coverage and IR) were plotted against each other, it became apparent that there is a linear relationship between cell attachment and carbohydrate accumulation at the surface of the cellulose acetate film. Therefore, extracellular polysaccharide production or accumulation of polysaccharide material at the cellulose acetate surface did not occur after bacterial attachment reached a steady state. This can be explained by the fact that the *Mycobacterium* cells were suspended in buffer solution with no nutrients provided for growth. In addition, the time frame of the experiment was limited to 4 hr, and insufficient time elapsed for a detectable amount of growth to have occurred. The plot of 1018 cm^{-1} band intensity against the 1515 cm^{-1} intensity supports this conclusion. Assuming the 1515 cm^{-1} band intensity is a reflection of cell biomass in the form of protein, the relationship is essentially linear with an R^2 value of 0.9763. Therefore, the relative rate of polysaccharide accumulation at the CA interface was equal to the rate of change of the protein adsorption, i.e., cell adhesion at the interface.

How adsorbed surfactants influence cell attachment on membrane surfaces is of great interest. Formation of a stable hemimicelle structure at the aqueous-polymer interface could provide a method by which surface properties, e.g., hydrophobicity or charge, could be altered while maintaining the membrane's innate transport properties. Test studies of membranes operated in reverse osmosis indicate that surfactants, such as Zwittergent 3-16, do not significantly diminish membrane transport properties (data not shown). Similar

studies with zosteric acid indicate very little effect on membrane transport properties.[51] Therefore, surfactants or other chemicals could potentially be applied as a post-production treatment to alter membrane surface properties and to minimize bacterial adhesion. ATR/FT-IR spectrometry work is currently under way to obtain further evidence that these hemimicelle structures form at the aqueous-polymer interface of CA thin films.

The sensitivity of the ATR/FT-IR spectrometric technique used for the detection of natural organic materials and organics associated with bacterial attachment is not what we had hoped. Improvements in our ability to detect these compounds need to be made. The recommended changes are to (1) switch to a thinner internal reflection element to generate more internal reflections at the aqueous-polymer interface—the result is similar to that achieved when the pathlength of a transmission measurement is increased, i.e., greater signal intensity, and (2) cast a thinner (700 – 800 Å) film of cellulose acetate on the IRE, allowing more energy to penetrate into the bulk aqueous phase. These changes are being implemented in the lab.

Our current focus is directed toward the development of the simultaneous ATR/FT-IR spectrometry/fluorescence microscopy technique. This methodology will allow images to be obtained from the same surface on which the IR data is collected. The progress made with this system is discussed below.

Section 7.10 Simultaneous ATR/FT-IR Spectrometry of Adsorbed Organics and Fluorescence Imaging of Adherent Bacteria on Thin Films of Cellulose Acetate

The IR and imaging methodology described above does not allow for the collection of images of adherent bacteria at the same polymer-interface from which the IR radiation internally reflects. A method for making simultaneous real-time measurements of infrared (chemical) data and fluorescent (visual) data was devised. The goal was to manufacture a flow cell that would hold an IRE and also possess a window to accommodate a 40X objective for fluorescence microscopy. The kinetics of bacterial attachment to the polymer film could then be correlated to the IR data collected from that same surface.

Two options were investigated. Both options made use of this special ATR flow cell. Option 1: Place the flow cell on the stage of a microscope. Transmit IR radiation from the spectrometer through fiber optic cables onto the IRE and then off the IRE and onto the detector using more fiber optic cables. Raise the stage-mounted flow cell to the plane of focus of the microscope objective and capture images with a CCD camera. Option 2: Build a fluorescence microscope around the ATR flow cell in the spectrometer. Mount the microscope in a horizontal position and use an x-y-z stage to position the objective on the window of the ATR flow cell.

Mid-IR fiber optic technology has not advanced to the point where it could be successfully implemented to pursue Option 1. Incorporation of a 20-mm wide IRE into the flow cell necessitated the use of large bundles of fiber optic cables to transfer light from the spectrometer onto the end of the IRE. This type of fiber optic bundling was too costly, inefficient and cumbersome. Thus, Option 2 was pursued (Figure 7.10.1).

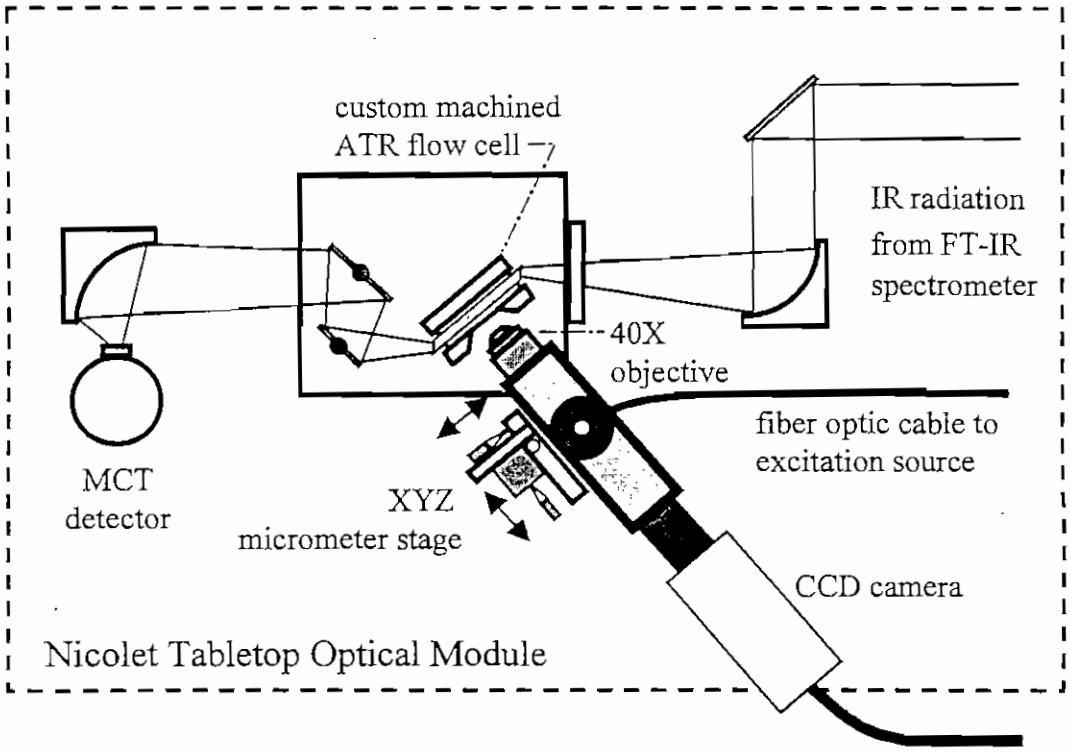

Figure 7.10.1 Schematic diagram of simultaneous ATR/FT-IR spectrometry / fluorescence microscopy experimental setup.

Designs were drawn for a flow cell to accommodate a 50 x 20 mm IRE that would enable collection of visual images of the surface through a coverslip window. Initially, a polycarbonate prototype was manufactured (D-J Engineering, Tustin, CA). Later, a fully operating stainless steel prototype was manufactured and tested (Figure 7.10.2). The flow cell has a 150-μm channel depth and a 170-μm thick window that permits visualization of the polymer-coated IRE surface with a horizontally mounted fluorescence microscope. Further modifications to the stainless steel flow cell still need to be made.

The fluorescence microscope was designed and assembled in-house (Figure 7.10.3). The microscope consists of a 3-dimensional optical bench constructed from C-mount threaded tubular components (Edmund Scientific, Barrington, NJ) and fitted with a Nikon 40X planapochromatic fluorite microscope objective (A. G. Heinze Co. Inc., Melville, NY). The two custom-manufactured dichroic beamsplitter cubes used in the instrument each consist of a dichroic mirror, an excitation filter and a barrier filter (Omega Optical, Brattleboro, VT). The UV cube provides excitation wavelengths from 320 nm to 380 nm and passes emission wavelengths from 430 nm to 500 nm (700+nm without barrier filter). The green filter cube provides excitation energy ranging from 480 nm to 544 nm and passes emission wavelengths >540nm.

A short arc (3 mm) xenon flash lamp (Oriel Instruments, Stratford, CT) provides excitation energy for the microscope. The lamp can be fired at up to 72 Hz by an internal signal generator or sychronized with video frame acquisition via an external trigger control. This flash unit provides up to 2000 mJ at 30 Hz (video real-time frame rate). A liquid light guide (3 mm x 1 m, Oriel Instruments, Stratford, CT) coupled at each end by quartz optics conducts the white light produced by the flash lamp to the microscope's dichroic filter cube.

A modified Gen III proximity focused image intensifier unit is directly coupled to the microscope (B. E. Meyer & Co., Inc., Redmond, WA). A monochrome RS 170-compatible CCD camera optically coupled to the intensifier unit via a relay lens records the intensified microscope images.

The flash and image intensifier limits the energy applied to the bacterial cells or biofilm on the ATR crystal. The pulses of light from the short arc xenon flash employed in this microscope configuration are short in duration (on the order of 100 μsec or less) compared to the video frame width (30 msec). Illumination was only applied during the actual acquisition of data; the ATR crystal remains dark at all other times. Thus, use of the xenon flash and image intensifier insures that the bacteria on the ATR crystal receive the least amount of excitation energy required to obtain a useful image. This method avoids the problems associated with prolonged exposure to short wavelength radiation often encountered during epifluorescent microscopy such as photobleaching of fluorochromes and thermal damage to the specimen, permitting extended time-lapse studies of early bacterial attachment and biofilm formation.

An 8-bit PCI framegrabber board (Flashpoint 128, Integral Technologies, Inc., Indianapolis, IN) in a PC microcomputer digitizes the camera images. This board also provides appropriate synchronization signals to control the xenon flash. Control of image acquisition and further image processing is accomplished using Image-ProPlus image acquisition and analysis software (Media Cybernetics, Silver Spring, MD).

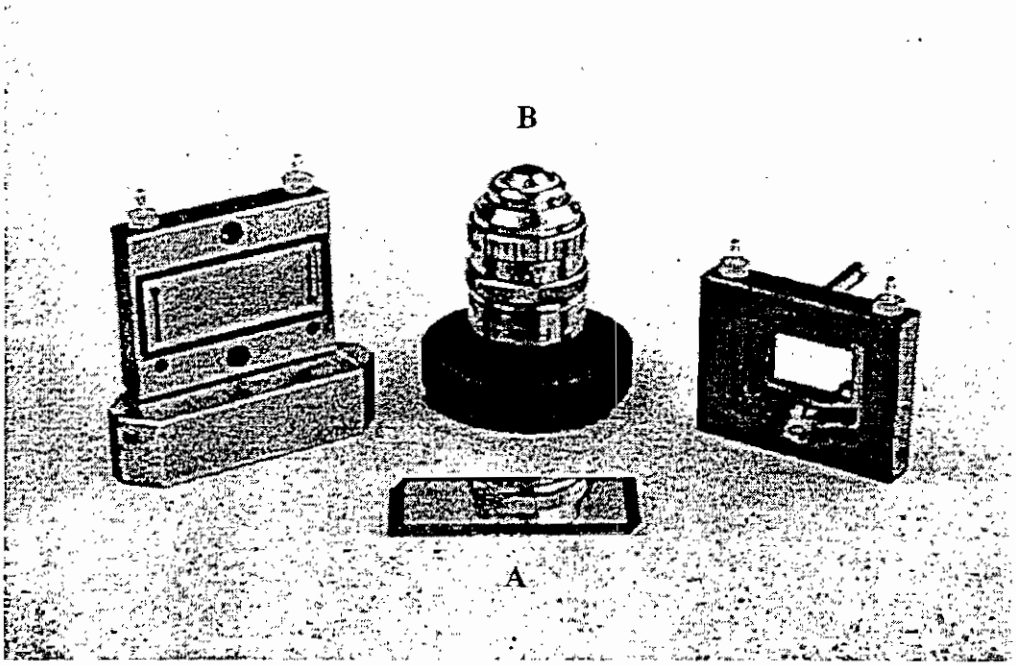

Figure 7.10.2 ATR flow cell for fluorescence microscopy with (A) ZnSe IRE (50x20x2 mm) and (B) 40X objective.

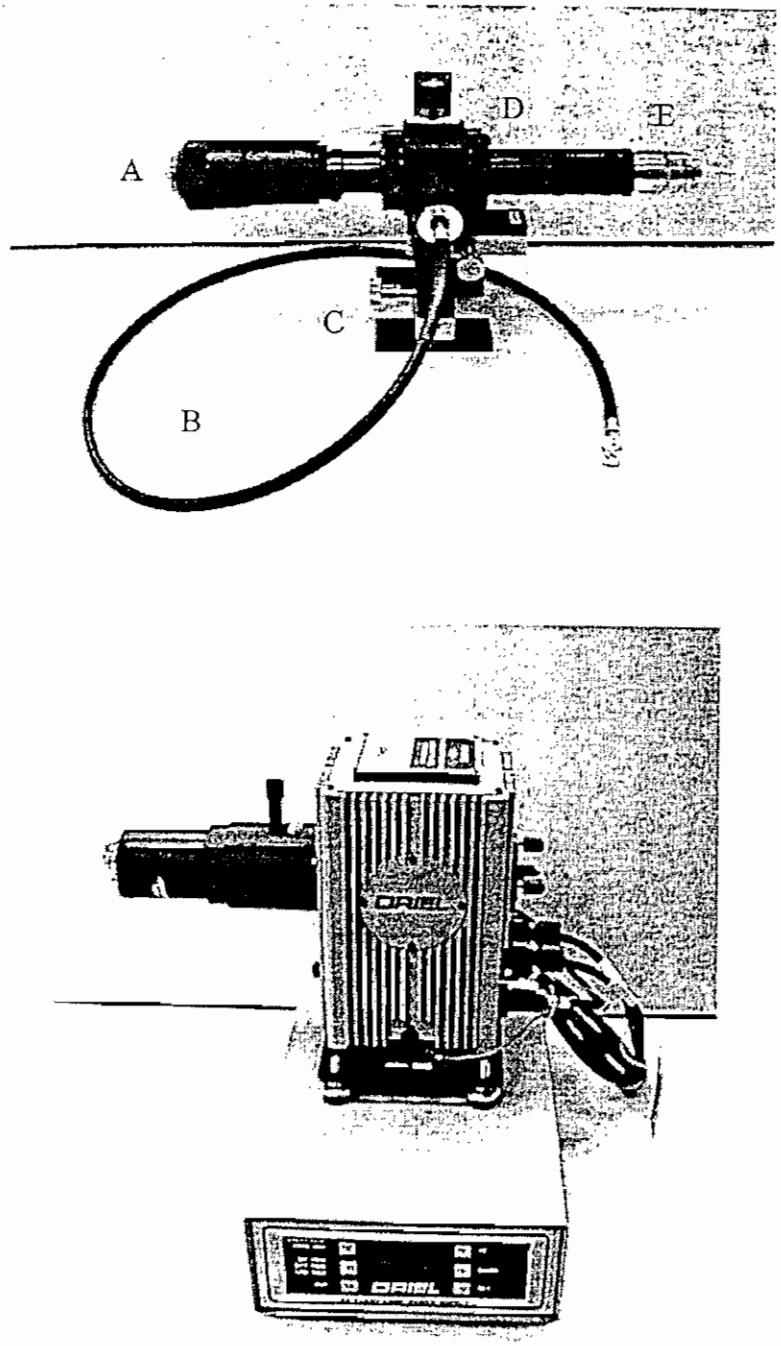

Figure 7.10.3 Epifluorescence microscope (top) with (A) CCD camera mount, (B) fiber optic cable, (C) x-y-z stage, (D) dichroic beamsplitter cube and (E) 40X objective. Xenon excitation source (bottom).

A tabletop optical module (TOM), mirrors (front-end kit) and medium range MCT-A detector (Nicolet Instrument, Madison, WI) were assembled to create a platform on which the ATR flow cell and fluorescence microscope are mounted (see Figure 7.10.4).

Current Status of ATR/FT-IR Spectrometry/Visual Imaging System

The epifluorescence microscope is ready to be tested in conjunction with the flow cell, although the IR optics and flow cell need more work. Alignment of the mirrors and MCT detector needs to be improved. The latest prototype of the ATR flow cell needs to be leak tested and the fluid dynamics assessed. Access to the flow cell window needs to be improved as the microscope objective is not seated properly. The system should be on line in two to three months. This ATR/FT-IR spectrometry/visual imaging system will allow us to obtain visual images of adherent bacteria on polymer surfaces on which dissolved organic material has adsorbed, providing real-time molecular and visual information of adsorption phenomena at the aqueous-polymer interface.

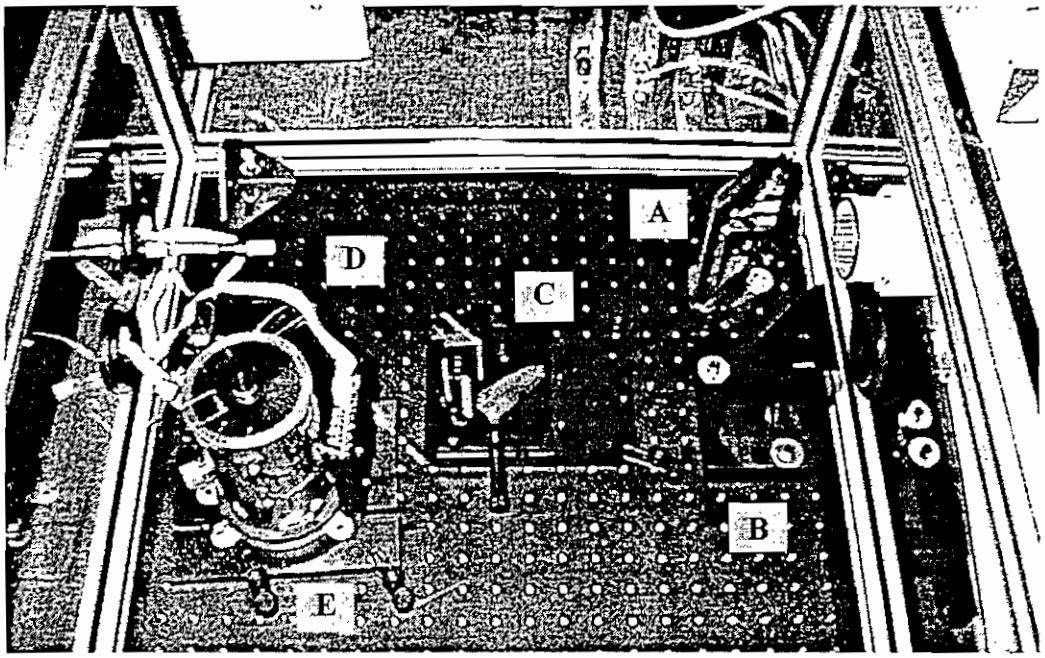

Figure 7.10.4 Tabletop Optical Module (TOM) with (A) flat mirror (B) elliptical mirror, (C) ATR mirror assembly, (D) parabolic mirror and (E) MCT detector.

Section 8.

References

[1] **Fujita, Y., W.-H. Ding and M. Reinhard.** 1995. Identification of wastewater DOC characteristics in reclaimed wastewater and recharged groundwater. Water Environ. Res.

[2] **Argo, David G.** 1980. Evaluation of membrane processes and their role in wastewater reclamation. Vol. I. and II., Final report. Contract No. 14-34-0001-8520. Office of Water Research and Technology, U.S. Department of the Interior, Washington, D. C.

[3] **McCarthy L. Perry, Martin Reinhard, Naomi L. Goodman, James W. Graydon, Gary D. Hopkins, Kristen E. Mortelmans and David G. Argo.** 1982. Advanced treatment for wastewater reclamation at Water Factory 21. Technical Report No. 267; Department of Civil Engineering, Stanford University, Palo Alto, CA.

[4] **Ridgway, H. F., M. G. Rigby and D. G. Argo.** 1985. Bacterial adhesion and fouling of reverse osmosis membranes. J. Amer. Water Works Assoc. **77**:97-106.

[5] **Ridgway, H. F.** 1987. Microbial fouling of reverse osmosis membranes: genesis and control, p.429-481. *In* M. W. Mittelman and G. G. Geesey (ed.), Biological fouling of industrial water systems: a problem solving approach. Water Micro Associates, San Diego, CA.

[6] **Flemming, H. C. and G. Schaule.** 1988. Investigations on biofouling of reverse osmosis and ultrafiltration membranes: Part I: initial phase of biofouling. Vom Wasser **71**:207-223.

[7] **Costerton, J. W. and R. T. Irwin.** 1981. The bacterial glycocalyx in nature and disease. Ann. Rev. Microbiol. **35**:299-324.

[8] **Costerton, J. W., H. M. Lappin-Scott and K.-J. Cheng.** 1992. Glycocalyx, bacterial, p. 311-317. *In* Encyclopedia of microbiology. Vol. 2. Academic Press, Inc., New York.

[9] **Christensen, B. E.** 1989. The role of extracellular polysaccharides in biofilms. J. Biotechnol. **10**:181-202.

[10] **Bryers, J. D.** 1993. Bacterial biofilms. Curr. Opinion Biotechnol. Biochem. Eng. **4**:197-204.

[11] **Characklis, W. G.** 1990. Biofilm Process, p. 195-231. *In* W. G. Characklis and K. C. Marshall (ed.), Biofilms. John Wiley & Sons, New York.

[12] **Baier, R. E.** 1981. Early events of micro-biofouling of all heat transfer equipment, p. 293-304. *In* E. F. C. Somerseales and J. G. Knudsen (ed.), Fouling of heat transfer equipment. Hemisphere Publishing Co., Washington, DC.

[13] **Thurman, E. M.** 1985. Humic substances in groundwater, p. 87-103. *In* G. R. Aiken, D. M. McKnight, R. L. Wershaw (eds.), Humic substances in soil, sediment and water—1985. John Wiley & Sons, New York.

[14] **Amy, Gary L., Raymond A. Sierka, Jim Dedessem, Tim Carey, Chandra Mysore, David Price, Mohamed Siddiqui and Lo Tan.** 1989. Molecular weight "fingerprints" of organic color in Orange County Water District groundwater: implications for treatment process selection and monitoring. Final report. Orange County Water District, Fountain Valley, CA.

[15] **Fletcher, M. and G. I. Loeb.** 1979. Influence of substratum characteristics on attachment of a marine pseudomonad to solid surfaces. Appl. Environ. Microbiol. **37**:67-72.

[16] **Dexter, S. C.** 1979. Influence of substratum critical surface tension on bacterial adhesion. In situ studies. J. Colloid Interface Sci. **70**:346-354.

[17] **Absolm, D. R., F. V. Lambert, Z. Polcova, W. Zingg, C. T. vanOss and W. Newmann.** 1983. Surface thermodynamics of bacterial adhesion. Appl. Environ. Microbiol. **46**:90-97.

[18] **Pringle, J. H. and M Fletcher.** 1983. Influence of substratum wettability of attachment of freshwater bacteria to solid surfaces. Appl. Environ. Microbiol. **46**:881-817.

[19] **Fletcher, M. and G. I. Loeb.** 1979. The influence of substratum characteristics on the attachment of a marine pseudomonad to solid sufaces. Appl. Environ. Microbiol. **37**: 67-72.

[20] **Marshall, K. C., R. Stout and R. Mitchell.** 1971b. Mechanism of the initial events in the sorption of marine bacteria to surfaces. J. Gen. Microbiol. **68**:337-348.

[21] **Fletcher, M. and K. C. Marshall.** 1982. Bubble contact angle method for evaluating substratum interfacial characteristics and its relevance to bacterial attachment. Appl. Environ. Microbiol. **44**:184-192.

[22] **Fletcher, M.** 1976. The effects of proteins on bacterial attachment to polystyrene. J. Gen. Microbiol. **94**:400-404.

[23] **Orstavik, D.** 1977. Acta. Pathol. Microbiol. Scand. **85***:* 47-53.

[24] **Meadows, P. S.** 1971. The attachment of bacteria to solid surfaces. Arch. Mikrobiol. 75:374-381.

[25] **Ishida, K. P. and H. R. Ridgway.** 1995. Analysis of biocide / biofilm interactions by attenuated total reflection Fourier transform infrared spectrometry. Final report. Project No. MRDP 699-503-93. National Water Research Institute, Fountain Valley, CA.

[26] **Bremer, P. J. and G. G. Geesey.** 1991. An evaluation of biofilm development utilizing nondestructive attenuated total reflectance Fourier transform infrared spectroscopy. Biofouling 3:89-100.

[27] **Bremer, P. J. and G. G. Geesey.** 1991. Laboratory-based model of microbiologically induced corrosion of copper. Appl. Environ. Microbiol. **57**:1956-1962.

[28] **Geesey, G. G. and P. J. Bremer.** 1990. Applications of Fourier transform infrared spectrometry to studies of copper corrosion under bacterial biofilms. Mar. Tech. Soc. J. **24**:36-43.

[29] **Suci, P. M., M. W. Mittleman, F. P. Yu and G. G. Geesey.** 1994. Investigation of ciprofloxacin penetration into Pseudomonas aeruginosa biofilms. Antimicrob. Agents Chemo. **38**:2125-2133.

[30] **Harrick, N.J.** 1967. Principles of internal reflection spectroscopy. *In* Internal reflection spectroscopy, p. 13. Harrick Scientific Corporation, Ossining, NY.

[31] **Dluhy, R. A.** 1986. Quantitative external reflection infrared spectroscopic analysis of insoluble monolayers spread at the air-water interface. J. Phys. Chem. **90**:1373-1379.

[32] **Downing, H. D. and D. Williams.** 1975. Optical constants of water in the infrared. J. Geophys. Res. 80:1656-1661.

[33] **Powell, D. A.** 1979. *In* Microbial polysaccharides and polysaccharases. R. C. W. Berkeley, G. W. Gooday and D. C. Ellwood (ed.), p. 117-160. Academic Press, New York.

[34] **Haug, A., B. Larsen and O. Smidsrod.** 1966. A study of the constitution of alginic acid by partial acid hydrolysis. Acta Chem. Scand. **20**:183-190.

[35] **Haug, A., B. Larsen and O. Smidsrod.** 1967. Studies on the sequence of uronic acid residues in alginic aicd. Acta Chem. Scand. **21**:691-704.

[36] **Larsen, B., O, Smidsrod, A, Haug and T. Painter.** 1969. Determination by a kinetic method of the nearest-neighbor frequencies in a fragment of alginic acid. Acta. Chem. Scand. **23**:2375-2388.

[37] **Jang, L. K., N. Harpt, T. Uyen, D. Gransmick and G. G. Geesey.** 1989. An iterative procedure based on the Donnan equilibrium for calculating the polymer-subphase volume

of alginic acid. J. Polym. Sci. **27B**:1301-1315.

[38] **Anderson, D. M. V.** 1988. The structural significance of amino acids in some plant gums, p. 31-37. *In* G. O. Phillips, D. J. Wedlock and P. A. Williams (ed.), Gums and Stabilizers for the Food Industry. Vol. 4. IRL Press, Oxford.

[39] **Oldani, M. and G. Schlock.** 1989. Characterization of ultrafiltration membranes by infrared spectroscopy, ESCA, and contact angle measurements. J. Membr. Sci. **43**:243-258.

[40] **Isner, J. D. and R. C. Williams.** 1993. Analytical techniques for identifying reverse osmosis foulants, Chapter 8, p. 237-275. *In* Zahid Amjad (ed.), Reverse Osmosis, Membrane Technology, Water Chemistry and Industrial Applications. VanNostrand Reinhold, NY.

[41] **Riley, R. L.** Personal communication. Separation Systems Technology, San Diego, CA.

[42] **Toprak, C., J. N. Agar and M. Falk.** 1979. State of water in cellulose acetate membranes. J. Chem. Soc. Faraday I **75**:803-815.

[43] **Ridgway, H. F., G. G. Rodriguez, J. Safarik, T. Cormack and D. W. Phipps.** 1998. Fouling composition during membrane treatment of secondary effluent: microscale characterization leading to fouling prevention on the pilot scale. Final report. Project No. MRDP 669-507-95. National Water Research Institute, Fountain Valley, CA.

[44] **Childress, A. E., M. Elimelech.** 1996. Effect of solution chemistry on the surface charge of polymeric reverse osmosis and nanofiltration membranes. J. Membrane Sci. **119**:253-268.

[45] **Dimisch, H.-U. and W. Pusch.** 1976. Ion exchange capacity of cellulose acetate membranes. J. Electrochem. Soc. **123**:370-374.

[46] **Dimisch, H.-U. and W. Pusch.** 1979. Electric and electrokinetic transport properties of homogeneous weak ion exchange membranes. J. Colloid Interface Sci. **69**:247-270.

[47] **Gaudin, M. and D. W. Fuerstenau.** 1955. Quartz flotation with cationic collectors. AIME Trans. **202**:958-.

[48] **Nichols, P. D., J. M. Henson, J. B. Guckert, D. E. Nivens and D. C. White.** 1985. Fourier transform-infrared spectroscopic methods for microbial ecology: analysis of bacteria, bacteria-polymer mixtures and biofilms. J. Microbiol. Methods **4**:79-94.

[49] **Jucker, C. and M. M. Clark.** 1994. Adsorption of aquatic humic substances on hydrophobic ultrafiltration membranes. J. Membrane Sci. **97**:37-52.

[50] **Marshall, K. C.** 1985. Mechanisms of bacterial adhesion at solid-water interfaces, p. 133-161. *In* D. C. Savage and M. Fletcher (ed.), Bacterial adhesion. Mechanisms and Physiological Significance. Plenum Press, New York.

[51] **Vandevivere, P. and D. L. Kirchman.** 1993. Attachment stimulates exopolysaccharide synthesis by a bacterium. Appl. Environ. Microbiol. **59**:3280-3286.

[52] **Zimmerman, Richard C., David C. White, Gill Geesey and Harry Ridgway**. 1998. Biofouling control through non-toxic means: application of zosteric acid to water treatment systems: a phase I research program. Final report. Project No. TT699-547-97. National Water Research Institute. Fountain Valley, CA.